PhD Dissertation

Effect of sea ice melt on growth and photophysiological performances of sea ice diatoms in the Sea of Okhotsk

オホーツク海における海氷融解が海氷珪藻類の増殖と光合成生理能力に及ぼす影響

by

Dong Yan

Thesis submitted in fulfillment of the requirements for the degree of Doctor in Philosophy in Environmental Science

Course in Geochemistry
Division of Earth System Science,
Graduate School of Environmental Science, Hokkaido University

Contents

Abbreviations

Car, β-Carotene

Cyto*b6f*, cytochrome *b6f* complex

Ddx-Dtx cycle, diadinoxanthin-diatoxanthin cycle

DES, de-epoxidation state index

DMF, *N,N*-dimethylformamide

Ddx, diadinoxanthin

Dtx, diatoxanthin

ETCs, electron transport chains

FCP, Fucoxanthin Chl *a*/*c*-binding Protein

F_v/F_m, maximum photochemical efficiency

Fxn, fucoxanthin

I_k, saturation irradiance for rETR

Lhcx, light-harvesting complex stress-related

NPQ, non-photochemical quenching

PPC, photoprotective carotenoid

PSC, photosynthetic carotenoid

PSI, Photosystem I

PSII, Photosystem II

psbA Photosystem II protein D1

rbcL Ribulose bisphosphate carboxylase large chain

RLC, rapid light curve

rETR, relative Electron Transport Rate

$rETR_{max,}$ maximal relative electron transport rate

RucisCO, Ribulose-1,5-bisphosphate carboxylase/oxygenase

TChl, total chlorophyll

UHPLC, Ultra-High Performance Liquid Chromatography

YII, effective photochemical efficiency in light

Abstract

Sea ice microalgal communities are dominated by diatoms and they play important roles in primary production at high latitudes. Growth of microalgae in ice-covered areas is primarily controlled by the seasonal light climate. In Arctic and subarctic seas, more light penetrates through sea ice in early spring than that during the winter time. This increase in light availability is a key driver of bloom in ice-covered seawaters. During ice melt in spring, ice algae are released from sea ice and could be exposed to changeable temperature, salinity and irradiance levels in surface water. Large variations of those environmental factors are likely to influence photophysiological performance of ice algae. Species with greater flexibility in photoacclimation are afforded a higher chance of survival and seed the following phytoplankton bloom.

The Sea of Okhotsk is the southernmost sea ice zone in the northern hemisphere with a sizeable seasonal ice cover, thus ice algae of the Sea of Okhotsk have a large potential to seed the early spring diatom bloom in the water column. However, little is known about the Okhotsk ice algal communities and their seeding effects. We investigated the dynamics of the composition and the photophysiological performances of an ice algal community in a 6-day laboratory incubation experiment that simulated the natural ice melt conditions. Centric diatoms, especially *Thalassiosira* spp., overwhelmingly dominated the ice algal community throughout the incubation, whereas pennate diatoms, mostly *Navicula* and *Nitzschia*, showed little growth with much higher mortality. The maximum photochemical efficiency of Photosystem II (F_v/F_m) was the lowest at the beginning of the ice melt, suggesting a suppressed photosynthetic functioning by changes in salinity. The cellular pigment contents decreased by 30% due to cellular damage, evidenced by deformed plastids under a microscope. The transcript level of the *rbcL* gene that encodes the large subunit of RubisCO was significantly higher during the ice melt and decreased in the no-ice period, suggesting an urgent need for osmoprotectants under the melt condition. Full recovery of the photosynthesis and growth was also made after complete ice melt. The results indicated high seeding potential of *Thalassiosira* to spring blooms owing to their photophysiological plasticity to dynamic salinity changes.

Saroma Lagoon is an embayment with two inlets leading to the Sea of Okhotsk. There is a

seasonal development of sea ice in this lagoon. To investigate the living and photoprotective strategies of ice algae in such a coastal water system, we grew *Nitzschia* cf. *neglecta*, an ice diatom isolated from the sea ice of this lagoon, under irradiance levels of 30 and 100 µmol photons m^{-2} s^{-1}, and temperatures of 2 and 10 °C. Then the acclimated cells were exposed to high light in order to investigate the plasticity of their photosynthetic functioning. At 10 °C, cells grew faster and showed a weaker susceptibility to high light. Highly efficient photoprotection was achieved through the diadinoxanthin-diatoxanthin cycle-dependent non-photochemical quenching (NPQ). The wide tolerance to both temperature and light changes suggests that the thinning of sea ice and higher temperatures in a warmer climate will lead to more intense blooms in Saroma Lagoon.

Chapter 1

General Introduction

1. Sea ice habitat

Sea ice occurs in both the Arctic and Antarctic. Seasonal sea ice only occurs in winter and melts in summer, such as that in the Sea of Okhotsk. Once the seawater reaches the freezing point, additional heat loss causes supercooling of seawater, thus leads to ice formation (Horner, 1985). During the formation of sea ice crystals, salts in seawater accumulate into droplets called brine. Brine is collected into small pores called brine pockets, and this gives the sea ice a porous structure (Wells and Deming, 2006; Wongpan *et al.*, 2018). Generally, brine pockets are interconnected to form long vertical tubes called brine channels. Some of the brine is released by the sea ice back into the seawater, which makes sea ice much fresher than seawater. Rapid decreases in salt contents in sea ice is mainly contributed by brine expulsion, gravity drainage, and flushing by the surface melt water (Notz and Worster, 2009; Vancoppenolle *et al.*, 2013). Brine channels are important open pathways for brine drainage and material exchange between sea ice and seawater (Vancoppenolle *et al.*, 2010).

Sea ice in the polar and sub-polar regions provides a unique habitat for microorganisms, including numerous algae, bacteria, protists and viruses (Garrison, 1981; Garrison and Close, 1993; Wells and Deming, 2006; Comeau *et al.*, 2013; Arrigo, 2014; Hopes *et al.*, 2017). The microalgae living in sea ice are called ice algae. They form the base of the food web of the sea ice ecosystem and are the only source of fixed carbon for higher trophic levels in the ice cover (Garrison *et al.*, 1987). Algal abundance in sea ice can vary by up to six orders of magnitude, from 10^4 to 10^9 cells L^{-1} (Arrigo, 2016). The highest concentration of ice algae is usually found at the bottom of the ice near the ice-water interface, where the living condition is relatively favorable to cells (Arrigo et al., 1997; Juhl and Krembs, 2010). Since algal cells are incorporated into the sea ice by a variety of mechanisms (Gradinger and Ikävalko, 1998; von Quillfeldt *et al.*, 2003), the biodiversity of the ice algal communities could be very high. Benthic species,

phytoplanktonic species, and brackish or freshwater species all occur in ice algal communities (von Quillfeldt *et al.*, 2003). The diatoms are the most diverse group of ice algae with hundreds of species being found in polar regions (Horner, 1985; Garrison, 1991). Pennate diatoms with large cell size usually contribute more to ice algal communities than centric diatoms (Poulin *et al.*, 2011; Kauko *et al.*, 2018).

In winter, the difference between air and seawater temperature results in a strong vertical gradient of temperature throughout the sea ice (Garrison, 1991; Boetius *et al.*, 2015). For microorganisms living in sea ice, the surrounding salinity of the microhabitat, namely the osmotic environment, also varies as the result of the temperature gradient (Garrison, 1991). Slight decreases in brine temperature can significantly increase the concentration of solutes and particles in the brine due to decreased brine volume fraction (Ewert and Deming, 2013). The average salinity of seawater is usually around 35 for the world ocean. In the Sea of Okhotsk, the average salinity of the surface layer is usually lower due to the large amount of freshwater input from the Amur River (Aota and Ishikawa, 1991). Presence of salts decreases the freezing point of water. For seawater with a salinity of 32, the freezing point would be around –1.8 °C. The salinity of the brine has a large temperature dependency that it varies inversely with temperature (Ewert and Deming, 2013). At the freezing point of –1.8 °C, brine salinity would be similar to that of the seawater. While at –3 °C, the brine salinity would be around 50. And at –5 °C, the brine salinity would be around 85 (Cox and Weeks, 1986). The temperature of sea ice would not be as low as the air temperature owing to the presence of the snow cover that acts as a thermal barrier (Lund-Hansen *et al.*, 2014). However, the ice temperature at 20 cm from the bottom could reach –5 °C in 2 m thick sea ice when air temperatures were around –20 °C (Grant and Horner, 1976). Extreme brine salinity of 173 was found for the Antarctic sea ice in the McMurdo Sound when the air temperature was –16 °C (Arrigo and Sullivan, 1992). Close to the bottom part of the sea ice, the brine salinity would be milder but can still reach 50 in the dense brownish algal layer (Grant and Horner, 1976).

The light conditions in sea ice also significantly affect the photosynthesis and growth of ice algae. Variations in irradiance at the ice bottom was found to largely affect the horizontal distribution of ice algae (Kudoh *et al.*, 1997; Galindo *et al.*, 2016). Light penetrating sea ice is primarily

regulated by the snow cover and ice thickness (Mundy *et al.*, 2005). Variation in the thickness of the snow cover is usually the dominant factor that controls the light transmission into the sea ice due to the high albedo of larger than 85 % of the snow package (Lund-Hansen *et al.*, 2014). The midday photosynthetically active radiation (PAR) beneath the sea ice in summer can be frequently less than 5 μmol photons m^{-2} s^{-1} and is usually below the limit of detection in winter (McMinn and Martin, 2013). The low irradiance level in sea ice is a limiting factor for ice algal growth in winter (Legendre *et al.*, 1992). While irradiance levels may increase by a factor of 20 at the bottom ice from winter to the ice melt season, mainly due to changes of snow conditions (Nicolaus *et al.*, 2012).

2. Sea ice of the Sea of Okhotsk

2.1. Oceanography of the Sea of Okhotsk

The sea of Okhotsk is a semi-closed sea of the western North Pacific Ocean. It is bounded by the Kamchatka Peninsula, Siberia, Sakhalin Island, Hokkaido and the Kuril Islands. In the northern part, there is a broad and shallow continental shelf along the Kamchatka and Siberian coasts, with a depth of less than 200 m. In the southern parts, there is a deep basin called Kuril Basin. The deepest part is deeper than 3000 m (Sea of Okhotsk | Russian Far East | Heritage Expeditions).

The circulation in the Sea of Okhotsk has a general cyclonic feature though there are many complicated local structures (Ohshima *et al.*, 2002). A part of the East Kamchatka Current water flows into the Sea of Okhotsk through the northern passages of the Kuril Islands (Uehara *et al.*, 2012). Among those passages, the Kruzenshtern Strait has a sill depth of around 1900 m and is the primary pathway for the inflow of the Pacific water (Katsumata *et al.*, 2004). Then the relatively warm and high-saline water of the subarctic Pacific Ocean spreads northward along the west coast of Kamchatka peninsula (Favorite, 1976; Martin *et al.*, 1998). The outflow of seawater primarily passes through the Bussol' Strait, which is the deepest one among the straits of the Kuril Islands and has a depth of around 2300 m (Favorite, 1976; Ohshima *et al.*, 2002). The Okhotsk seawater is considerably different from its source water of the western subarctic

north Pacific water that is becomes fresher and more oxygenated (Moroshkin, 1968; Talley and Nagata, 1995). This is because the seawater has been considerably mixed and modified after it flowed in (Talley and Nagata, 1995). The modification includes the effects of the dense shelf water formation in the northern part, the inflow and mix with the high salinity Soya Warm Current, the dilution effect of the fresh water from the Amur River outflow, and the water mixing in the Kuril Island straits (Talley, 1991; Nakamura *et al.*, 2000).

The Sea of Okhotsk is connected to the Sea of Japan through two narrow straits, the Soya Strait and the Tartar Strait. The properties and ventilation of the Okhotsk seawater is profoundly influenced by its connection with the Sea of Japan (Takahashi, 1998). The Soya Warm Current carries the warm and high salinity seawater of the Sea of Japan into the Sea of Okhotsk through the Soya Strait (Takizawa, 1982). Then the warm water gradually mixes with the surrounding seawater as it flows southeastward along the coast of Hokkaido (Aota, 1979). The Soya Warm Current is important in the overall salinity balance of the Okhotsk Sea. It is suggested that the high salinity of the Soya Warm Current water sets the maximum density of ventilation in the Sea of Okhotsk (Talley and Nagata, 1995). Not all of the inflow from the Sea of Japan is warm and with high salinity. The water inflow through the Tartar Strait is cold and fresh. This is because the mouth of the Amur River is located near the northern part of Tartar strait, and almost all of the discharged fresh water flows into the Sea of Okhotsk (Tachibana *et al.*, 2008). The huge freshwater supply from the Amur River accounts for 37% of the total fresh water supply for the Sea of Okhotsk (Aota and Ishikawa, 1991). This significantly contributes to the formation of the low salinity seawater at the surface, which spreads all over the Sea of Okhotsk (Aota and Ishikawa, 1991; Talley and Nagata, 1995).

2.2. Sea ice conditions in the Sea of Okhotsk

2.2.1. Formation and movement of sea ice

The sea of Okhotsk has many of the characteristics of polar seas, though it is located in temperate latitudes (Preller and Hogan, 1998). The most prominent one is the pronounced sea ice cover during the winter time. It is the southernmost sea that has a sizable sea ice cover in the northern hemisphere (Aota and Ishikawa, 1991). The total ice volume was estimated to be 6.3 ×

10^{11} m^3 derived from the ice thickness and the ice concentration from the satellite data (Nihashi *et al.*, 2018). The Sea of Okhotsk is currently undergoing a period of sustained seasonal sea ice loss, putatively due to global warming (Kashiwase *et al.*, 2014; Ohshima *et al.*, 2014).

Polynyas are mainly formed over the north or northwestern shelves and off the eastern Sakhalin coast (Ito *et al.*, 2020). Sea ice begins to form in early November in the northern part of the Sea of Okhotsk. Then it extends southward along the east coast of Sakhalin Island through the winter until 50–90% of the sea is covered in late February or March (Simizu and Ohshima, 2006; Nihashi *et al.*, 2018). The estimated freshwater transport ranges from 12 to 57 km^3, corresponding to 4 to 20% of the annual Amur River discharge (Fukamachi *et al.*, 2006). The northwest shelf polynya of the Sea of Okhotsk is the highest ice production area, contributing to approximately 55% of the total ice production (Martin *et al.*, 1998; Ohshima *et al.*, 2006). Since the surface layer of the Sea of Okhotsk is of low salinity, there is a sharp pycnocline between the surface water and the deeper waters (Ohshima *et al.*, 2001). The winter convection is thus limited within the thin surface layer of 50–100 m which causes rapid cooling down of the upper layer and hence ice formation (Yang and Honjo, 1996). Active sea ice formation is also enhanced by the low air temperature and wind conditions. In winter, the northerly cold offshore winds from Siberia prevail and the air temperature can reach as low as –25 °C at the northwestern coasts (Martin *et al.*, 1998; Nihashi *et al.*, 2009).

Active ice production results in the large amount rejection of brine thus the formation of the dense shelf water (Talley, 1991). The dense shelf water then mixes with the water from the East Kamchatka Current to form the Okhotsk Sea Intermediate Water (OSIW), which is a possible source of the North Pacific Intermediate Water (NPIW) (Talley, 1991; Talley and Nagata, 1995). This water exchange with the North Pacific is important not only for the Sea of Okhotsk itself but makes it an important location for ventilation of the NPIW (Itoh *et al.*, 2003; Shcherbina *et al.*, 2003). Despite the influence on the formation of the NPIW through brine rejection, the sea ice of the Sea of Okhotsk can also directly affect the north Pacific waters. Most of the sea ice melts away by June in the Sea of Okhotsk (Nihashi *et al.*, 2018). Some of the pack ice can flow out of the sea and enter the Pacific Ocean through the southern passages of the Kuril Islands. The melted sea ice can flow into the Pacific Ocean via the Nemuro Strait and the Kunashiri

Strait and become one source of the Coastal Oyashio Water (Ohtani, 1989). The sea ice melted water is characterized by low temperature less than 2 °C and low salinity less than 33.0 (Sakamoto *et al.*, 2010). The influence of the melted sea ice influences the coastal Oyashio from January to April (Katsumata *et al.*, 2004; Oguma *et al.*, 2008).

Sea ice reaches the northern coast of Hokkaido in late January or February (Ohshima *et al.*, 2005). The extension is partly attributed to decreases in temperature. While it is also largely influenced by the prevailing northerly winds and the East Sakhalin Current (Kimura and Wakatsuchi, 1999; Itoh and Ohshima, 2000). The East Sakhalin Current is a western boundary current along the East Sakhalin Shelf. It becomes strong in fall and winter and can extend to the coast of Hokkaido (Itoh and Ohshima, 2000). As mentioned above, the coast of Hokkaido is affected by the Soya Warm Current. However, this current weakens during the winter time, and flows beneath the fresh and cold water of the East Sakhalin Current (Takizawa, 1982; Itoh and Ohshima, 2000). Field observations of the icebreaker P/V *Soya* in early February showed that the thickness of the sea ice in the southern Okhotsk ranges from 19 ± 7 to 55 ± 23 cm with a Poisson Distribution (Toyota *et al.*, 2004). The thickening is mainly achieved through the rafting and ridging as bottom freezing (Toyota *et al.*, 2007). Satellite data showed that the annual mean ice thickness ranges between 30 and 60 cm along the Hokkaido coast (Shirasawa 2005; Nihashi 2018). The thickness of thermally grown ice in the northern part of the sea is around 110 cm (Shirasawa 2005). The large variation in the thickness of sea ice near Hokkaido is due to mechanical processes during the complex experience of migration and growth of the drift ice (Toyota *et al.*, 2004, 2007).

2.2.2.Nutrient status in sea ice

The vast majority of salts and nutrients in sea ice is dissolved in the brine inclusions (Light *et al.*, 2003). The microenvironment of the brine is usually characterized by low concentrations of CO_2, high concentrations of dissolved organic matter, low concentrations of nutrients, and high NH_4^+, which are resulted from active biological activity within the confined system (Thomas and Dieckmann, 2002). The fluid transport between brine and seawater is the dominant factor controlling dissolved nutrient supply to sea ice (Vancoppenolle *et al.*, 2010; Wongpan *et al.*, 2018).

The mechanism is that the brine with little nutrients was mixed with fresh and nutrient-rich seawater by convection (Vancoppenolle *et al.*, 2010). Ice algae also plays a role in the nutrient transportation due to active uptake of the nutrients flowed in (Vancoppenolle *et al.*, 2010). The macro-nutrients including NO_3^-, NO_2^-, PO_4^{3-}, and $Si(OH)_4$ in the Okhotsk sea ice mainly come from seawater (Kanna *et al.*, 2014). Concentrations of those macro-nutrients were found to be lower in sea ice than that in the surface water in the ice-covered area, while high concentrations of NH_4^+ was found in sea ice (Kanna *et al.*, 2014).

Iron (Fe) is the most abundant metal in phytoplankton cells (Ho *et al.*, 2003), with more than 50% of intracellular Fe located in the photosynthetic system, mainly in photosystems I and II (PSI and PSII) and cytochrome *b6f* (Cyt *b6f*) (Strzepek and Harrison, 2004). It is the most important micronutrient for marine phytoplankton growth (Raven *et al.*, 1999). Two processes of Fe supply are assumed to be important to sustain the high primary productivity in the Sea of Okhotsk. One of them is Fe loadings from the Amur River and transport by the East Sakhalin Current. The other is the transportation via the intermediate water (Nishioka *et al.*, 2007, 2014). The concentration of Fe in the sea ice in the southern Sea of Okhotsk is greater than that in the surrounding seawater (Kanna *et al.*, 2014). Kanna et al., (2018) found that Fe supply to the near surface water of the southern Sea of Okhotsk mainly came from sea ice melt water but not the deep water. Fe stored in sea ice of the Sea of Okhotsk is mainly in particulate form (Kanna and Nishioka, 2016). It is bio-available and may contribute to phytoplankton growth when it is released into surface waters in spring (Sugie *et al.*, 2013).

2.3. Microalgal communities of the Sea of Okhotsk

Marine production in the Arctic and subarctic primarily comes from microalgae, including phytoplankton in the water column and ice algae associated with sea ice (Sakshaug, 2004). The Sea of Okhotsk is characterized by high biological productivity (Kim, 2012). The average primary productivity was estimated to be around 450 g C m^{-2} per year and the total annual production was estimated to be around 720×10^6 g C (Kim, 2012). Shipboard investigation on the primary production of the phytoplankton in the Sea of Okhotsk was mainly conducted in

summer. The primary production in the central area of the sea and the eastern shelf of Sakhalin Island varied and ranged between 0.002 to 0.27 g C m^{-3} day^{-1} in the surface layer. The values for the water column ranged between 0.03 to 2.73 g C m^{-2} day^{-1} (Sorokin and Sorokin, 1999). In particular, primary production was high at stations near Sakhalin Island with diatom bloom dominated by the centric diatom *Thalassiosira nordenskioeldii*, reaching 5 g C m^{-2} day^{-1} (Sorokin and Sorokin, 1999). The growth and the primary production of the phytoplankton in the Sea of Okhotsk is largely affected by nutrient status. Liu et al., (2009) investigated the primary production on the continental shelf along the east coast of Sakhalin Island and the area close to the Bussol' Strait. They found that the phytoplankton growth in the studying area was strongly affected by nutrient availability, with the phytoplankton growth significantly suppressed under nutrient-depleted conditions. Data from the same cruise showed that phytoplanktonic communities in nutrient-depleted waters were dominated by picoplankton less than 2 μm, while phytoplankton lager than 10 μm was more abundant in nutrient-rich coastal waters (Suzuki *et al.*, 2011). Shiomoto (1997) investigated the size-fractionated Chl *a* and primary production in surface waters of the southern part of the Sea of Okhotsk in late fall and winter (October-November). The cell number and primary production of large phytoplankton gradually increased during the period of investigation. The possible reason is the gradually deepening of the mixed layer down to the dichothermal water, which supplies abundant nutrients to the surface (Shiomoto, 1997). In the southwestern part of the Sea of Okhotsk near Hokkaido, the primary productivity in the surface layer showed clear seasonality and a large dependency on light conditions (Kasai and Hirakawa, 2015).

Previous studies demonstrated that diatoms play a major role in the phytoplanktonic communities of the Sea of Okhotsk (Ohwada, 1956; Sorokin and Sorokin, 1999; Orlova *et al.*, 2004; Suzuki *et al.*, 2011; Kasai and Hirakawa, 2015). Diatoms (Bacillariophyceae) are unicellular microalgae with cell sizes ranging from 2 μm to 2 mm (Tomas, 1997). Approximately 20 % of the global photosynthetic fixation of carbon on Earth, or 40% of the carbon sequestration in the oceans, is achieved by diatoms (Nelson *et al.*, 1995; Falkowski and Raven, 2013). They are possibly the most important eukaryotic group of phytoplankton (Guiry, 2012). One distinctive feature of diatom is that their cell wall contains silica. The name diatom is derived from the

Greek *diatomos*, meaning 'cut in half', because the cell wall is constructed by two parts. And one part (the epitheca) overlaps the other (the hypotheca) like the lid of petri-dish (Sakshaug, 2004) (Fig.1.1). The brownish color of the cells comes from the algal pigments Chl *c* and fucoxanthin (Kuczynska *et al.*, 2015). Diatoms are divided into centric or pennate diatoms that usually have radial and bilateral symmetry, respectively (Tomas, 1997; Sakshaug, 2004). The majority of the important marine planktonic diatoms are centric diatoms, including *Chaetoceros* and *Thalassiosira* (Medlin and Priddle, 1990; Tomas, 1997; Hoppenrath *et al.*, 2007; Park *et al.*, 2016). While some pennate diatoms may also be common sometimes, such as *Fragilariopsis*, *Navicula,* and *Pseudo-nitzschia* (Hasle and Booth, 1984; Medlin and Hasle, 1990; Fritz *et al.*, 1992). In the Sea of Okhotsk, the most frequently observed diatom genera were *Thalassiosira* and *Chaetoceros* (Orlova *et al.*, 2004; Zhang *et al.*, 2006; Suzuki *et al.*, 2011; Kasai and Hirakawa, 2015).

There is a large amount of ice algae in the Okhotsk Sea ice. Brownish sea ice was commonly observed at the bottom of Okhotsk sea ice, especially in spring (Leonov *et al.*, 2007). The brownish color is from the algal cells and therefore is an indicator of high ice algal abundance. Chlorophyll *a* (Chl *a*) concentrations in the Okhotsk sea ice ranged between 0.2 to 3.5 mg m^{-2}, and was up to an order of magnitude higher than that in the under-ice seawater (Granskog *et al.*, 2015). McMinn et al. (2008) reported an extremely high Chl *a* concentration of 1.6×10^3 mg Chl *a* m^{-3} in the pack ice near Shiretoko with an average thickness of around 70 cm. Despite the high biomass of the ice algal communities living in the Okhotsk sea ice, detailed research on the ice algal communities in the Sea of Okhotsk is sparse. Taguchi et al., (2000) first reported the community composition of ice algal communities inside and outside the Mombetsu Harbor of the Sea of Okhotsk. They found that in addition to *Thalassiosira* and *Chaetoceros*, pennate diatoms of *Fragilariopsis*, *Nitzschia* and *Navicula* also contributed largely to the microalgal community. McMinn et al., (2008) found the ice algal communities of the pack ice from Shiretoko in northern Hokkaido were mainly dominated by the centric diatoms *T. nordenskioeldii* and *T. punctigera* and proposed that the domination by *Thalassiosira* was quite unusual for sea ice algal communities.

3. The sea ice in Saroma Lagoon

3.1. Sea ice conditions of the Saroma Lagoon

Saroma Lagoon is a semi-closed embayment and is connected with the Sea of Okhotsk through two channels. Sea ice usually begins to develop in early January, covers the entire surface of the lagoon for an average of two to three months, and melts away at the beginning of April (Kudoh, 1993; Nomura *et al.*, 2009). Sea ice in Saroma Lagoon is land-fast ice. The hydrochemical characteristics of this lagoon are similar to that of the coastal Okhotsk seawater due to active water exchanges (Takeuchi and Fujiyoshi, 1989; Shibanuma *et al.*, 1995). The water temperature varies largely throughout the year, ranging from around –1.5 °C when there is ice cover to a maximum of larger than 20 °C in summer. The sea ice temperature can be very low in winter, reaching less than –3 °C or even lower depending on the air temperature and the depth of the snow cover (Kudoh, 1993). The primary production in water column, integrated from the surface to the depth with 1% surface light ranged between 298 and 786 mg C m^{-2} day^{-1} during the spring bloom season (Shiomoto *et al.*, 2012). The lagoon is influenced by freshwater discharge from rivers, so the water salinity is usually less than 32 (Michel *et al.*, 1997). Nomura et al., (2009) suggested that the freshwater discharge from rivers supplies chemical components into sea ice through brine channels, which is a key process influencing the biogeochemical cycle in the lagoon.

3.2. Microalgal communities of the Saroma Lagoon

A dense layer of ice algae develops at the bottom of the ice by early spring (Taguchi *et al.*, 1997). Sea ice algal biomass ranged between 0.1 to 250 mg Chl *a* m^{-2} (Kudoh *et al.*, 1997; McMinn A. *et al.*, 2005; McMinn *et al.*, 2008). The ice algal community of Saroma Lagoon bear a resemblance to that of the Arctic sea ice and is overwhelmingly dominated by diatoms. The two most important representatives in the Arctic, *Nitzschia frigida* and *Melosira arctica* (Obrezkova *et al.*, 2014; Leu *et al.*, 2015), also exist in Saroma sea ice and the latter was usually among the top three abundant species since 2007 (Hattori, unpublished data). One prominent character of the Saroma ice is the dominance of the chain-forming centric diatom *Detonula confervacea* (Kikuchi-Kawanobe and Kudoh, 1995; Michel *et al.*, 1997; Taguchi *et al.*, 1997; Kashino *et al.*, 1998;

McMinn A. *et al.*, 2005; McMinn *et al.*, 2008). The species has a distribution not only in the sea ice of Arctic and subarctic but also in temperate waters without winter ice cover (Smayda, 1969; Okolodkov, 1992). Its occurrence in Saroma Lagoon has only been acknowledged since 1992 (Kikuchi-Kawanobe and Kudoh, 1995). Regardless of the dominance in sea ice, it had a remarkably low abundance both in the contagious seawater as well as the drift sea ice of the Sea of Okhotsk during the ice covered season (Taguchi *et al.*, 2000; McMinn A. *et al.*, 2005; Kasai *et al.*, 2014; Yan, unpublished observation).

4. The seeding effect of ice algae

Fig. 1.2 demonstrates a seasonal cycle of freeze and melt of sea ice. The bloom of diatoms after the melt of sea ice is a common phenomenon in the Sea of Okhotsk (Smirnova, 1959). In spring, a shallow pycnocline is formed due to the warming up of the melted sea ice at the surface. It is suggested that both the sufficient light and the stable vertical structure contributed to the beginning of the phytoplankton bloom in the Sea of Okhotsk (Sorokin and Sorokin, 1999). Spring bloom usually begins in late April to May in the southern part and June to July in the northern part (Sorokin and Sorokin, 1999). Accordingly, the time of termination is also different. In the central part of the sea, they may proceed until the end of June and in the colder parts of the northern shelf, they may last until July or August (Sorokin and Sorokin, 1999, 2002; Shuntov, 2001). The annual primary production in the Sea of Okhotsk is largely derived from spring diatom bloom following sea ice melt (Ohwada, 1956; Zhang *et al.*, 2006). When ice breakup begins in spring, ice algae are rapidly washed out of the ice and dispersed into the water column, causing a significant increase in the downward flux of ice algal cells under the Okhotsk sea ice (Leonov *et al.*, 2007; Hiwatari *et al.*, 2008). In the northeast coast of Hokkaido, a spring peak of Chl *a* concentration is usually found after sea ice retreats. Diatoms larger than 10 μm were found to be dominant (Hamasaki *et al.*, 1998). The magnitude of the spring peak was correlated with the length of the period of sea ice growth (Taguchi *et al.*, 2000). The initial concentration of phytoplankton biomass was larger when there is a longer period of sea ice cover (Mustapha and Saitoh, 2008).

Previous studies suggested that the release of ice algae into the water column initiated the spring development of phytoplankton (Garrison *et al.*, 1987; Garrison and Close, 1993). This release is enhanced toward the end of the melt season and some released ice algae may continue their growth in the water column to become the seed of the phytoplankton bloom after ice retreat, which is known as the seeding effect of ice algae. Taguchi et al., (2000) investigated whether the large amount cells in the phytoplankton bloom after ice retreat comes from ice algae. They found that some ice algae showed fast sedimentation and made little contribution to phytoplankton bloom. While the planktonic circular large cells of *Thalassiosira* grew rapidly in the water column.

5. Photosynthesis of microalgae

5.1. Basic knowledge of photosynthesis

Photosynthesis is the biological conversion of light energy to chemical bond energy that is stored in organic carbon compounds (Falkowski and Raven, 2013). In other words, photosynthesis is the process that light energy is absorbed by photosynthetic pigments and its transfer to chemical energy. The oxygenic photosynthesis in phytoplankton is catalyzed by four multi-subunit membrane-protein complexes, Photosystem II (PSII), Photosystem I (PSI), cytochrome *b6f* complex (Cyto*b6f*), and F-ATPase (Nelson and Yocum, 2006).

Photosynthesis begins with the light absorption by photosynthetic pigments and the energy transfer to the special paired Chl *a* molecules in reaction centers of PSII (Nelson and Yocum, 2006; Vinyard *et al.*, 2013). When a photon is absorbed, the electron of the Chl *a* molecule is transferred to a higher energy orbital and this results in the formation of excited state, which is unstable. In order to return to the stable ground state, the excitation energy has to go into either of the following ways. The first is that the excited state may decay directly. This means the excited electron falls back to its original, stable orbital. During this process the excess energy of the absorbed photon must be returned. This occurs either by dissipation through molecular vibrations (heat) or by giving off fluorescence (Maxwell *et al.*, 1994; Olaizola *et al.*, 1994; Havurinne and Tyystjärvi, 2017). It can also be given up to another molecule, a pheophytin that serves as the first electron carrier in the electron transfer pathway of PSII (Beardall, 1989). This electron transfer results in the charge separation between the special pair of excited chlorophyll

molecules of reaction centers and pheophytin and this initiates the photosynthetic chemistry. The chlorophyll molecule that lost its electron is very oxidative that it oxidizes water, leading to the generation of O_2, and returns to the stable ground state.

If the absorbed photons are in excess of that can be used in photochemical reactions of photosynthesis, there will be an accumulation of excited Chl *a* molecules in reaction centers. This raises the probability of the formation of oxygen species in cells (Rijstenbil, 2005). Oxygen species cause damage in its local environment by destroying cellular components such as lipids, nucleic acids, and proteins (Mallick and Mohn, 2000). This photooxidative damage leads to a dramatic depression of photochemical efficiency, and is termed as photoinhibition. The D1 protein in PSII is known as the primary target of this damage (Kanervo *et al.*, 1997; Andersson and Aro, 2001). Damaged D1 proteins must be removed and replaced by newly synthesized molecules for PSII to recover. If repair cannot catch up with damage, there will be less functional D1 protein and this exacerbates photoinhibition (Li *et al.*, 2017).

Not all light absorbed is used for photosynthesis. Ideally, all the absorbed photons are converted into energy that can be used for carbon assimilation, ultimately promoting growth. The imbalance between the absorbed light energy (photons) and the photosynthetic performance is caused by alterative electronic pathways. This includes the Mehler reaction, the cyclic electron transport of around PSI, and the cyclic electron cycle around PSII (Miyake, 2010; Shikanai, 2014; Curien *et al.*, 2016; Wagner *et al.*, 2016). These processes can be considered as additional electron sinks that can dissipate energy. This usually increases the non-photochemical quenching (NPQ), an effective photoprotective strategy in algal cells (Olaizola *et al.*, 1994; Lavaud and Lepetit, 2013). Through those photoprotective mechanisms, algal cells can minimize the oxidative photodamage generated by excess excitation energy. This is especially important to maintain effective PSII photochemistry.

5.2. Survival of ice algae under ice melt condition

As mentioned in Section 1, the living conditions in sea ice is not very comfortable. The ice temperature could be much lower than seawater, and at the same time the surrounding brine

salinity could be much higher than that in seawater. Ice algae have to cope with not only the low metabolic rate caused by the low temperature but the osmotic stress caused by the extremely high brine salinities. This probably resulted in the lower rates of primary production by sea ice algae compared to their phytoplankton counterparts (Arrigo *et al.*, 1997; Arrigo, 2016).

Dramatic changes can occur in the microenvironment surrounding algal cells in sea ice, which includes gradients in light, temperature and salinity (Garrison, 1991; Manes and Gradinger, 2009; Lund-Hansen *et al.*, 2014). Some ice algae do not maintain a phytoplankton population after ice melt. Their disappearance is a result of fast cell sedimentation, as well as cell death caused by predation or the rapid environmental change as ice melts (Grant and Horner, 1976; Michel *et al.*, 1997; Taguchi *et al.*, 1997; Różańska *et al.*, 2009; Rajanahally *et al.*, 2014). For example, *N. frigida* and *M. arctica* quickly sink out from the water column and do not have a seeding effect on the phytoplankton bloom in spring (Haecky *et al.*, 1998; Kauko *et al.*, 2018). While some other species, such as *T. nordenskioeldii* and *Fragilariopsis*, continue their growth in the water column and sustain for a longer time (Taguchi *et al.*, 2000). For some pennate ice diatoms, photobehavioral strategies are also used in order to maintain photosynthesis under changing environmental conditions. This mainly refers to the vertical migration in pennate diatoms (Aumack and Juhl, 2015).

A fast acclimation would be quite essential for a species to survive the low salinity lens beneath the melting sea ice (Taguchi *et al.*, 1997). Changes in salinity possibly cause severe osmotic stress to the algal cells as ice melts. Laboratory experiments found that some ice diatoms are capable to maintain a relatively high growth rate within a wide range of salinity of 10 to 50 (Smayda, 1969; Grant and Horner, 1976). In the most extreme cases, some ice diatoms can grow exponentially in brine that has a salinity of 105 at –6°C (Aletsee and Jahnke, 1992). However, it is worth noting that after being exposed to extreme salinities, there was a lag period before normal growth can be reached. The lag period, which varies among species, is when ice algal cells rearrange the metabolism to protect themselves from the acute osmotic shock. In other words, ice diatoms can acclimate to the harsh living conditions in sea ice, but if the salinity is changing so fast, the cells may die of osmotic stress before they can acclimate to the new salinity. Some ice algal species might not be able to survive a higher temperature due to a narrow thermal tolerance range. The acclimation to salinity of diatoms was found to be temperature-dependent

that the capacity to tolerate extreme salinities increased at optimal growth temperatures (Smayda, 1969; Krawiec, 1982).

Ice diatoms can possibly tolerate a temperature as high as 8 °C (Fiala and Oriol, 1990; Mock and Valentin, 2004; Coello-Camba *et al.*, 2015). A low tolerance to much higher irradiance levels in water after the ice melt may cause severe photoinhibition and cell death. In the Calvin-Benson Cycle, CO_2 fixation is catalyzed by the rate-limiting enzyme RubisCO (Ribulose-1, 5-bisphosphate carboxylase/oxygenase) that requires CO_2 as the only inorganic substrate for carbon fixation (Cooper *et al.*, 1969). Similar to many enzymes, RubisCO has a turnover rate that significantly decreases with temperature. Organisms including diatoms usually up-regulate the abundance of this enzyme to compensate for the slow rates at chilling temperatures (Morgan-Kiss *et al.*, 2006). Young et al., (2015) suggested that in psychrophilic diatoms, all RubisCO must be active and that the active sites are nearly saturated with substrate for growth.

Light is a major resource for phytoplankton (Litchman and Klausmeier, 2001). Light availability significantly alters the growth status of all photosynthetic organisms. The underwater light condition in seawater could be very different from that in sea ice that it is characterized by extreme temporal and spatial variability (Dubinsky and Stambler, 2009; Falkowski and Raven, 2013). Light conditions in sea ice depends on the snow depth, the ice thickness and ice algal biomass (Arrigo, 2014). The bottom of sea ice is usually of low light intensity (Section1). Since most ice algae proliferate near the bottom of sea ice, acclimation to low irradiance would be needed for more efficient photosynthesis. Therefore, ice algae have long been considered to be shade-adapted and photosynthesis usually saturates at low irradiance levels. Hancke *et al.* (2018) recently revealed that the initial growth of ice algae began at extremely low irradiance of less than 0.17 μmol photons m^{-2} s^{-1}. The low-light acclimated algal cells can suffer from sever photoinhibition and photodamage if there is a sudden increase in light intensity. Growth is the net impact of assimilation and consumption. To maximize growth in a variable light environment, cells must be able to achieve balanced growth by modulating bioactivity (MacIntyre and Cullen, 2005). Diatoms contain light-harvesting pigments such as Chl *a*, Chl *c*, and fucoxanthin. The main carotenoid is fucoxanthin (Fxn). It absorbs in the green range of the spectrum, and is highly abundant in the light harvesting complex of diatoms, presenting in a 1:1

stoichiometry with Chl *a* (Owens *et al.*, 1980; Owens and Falkowskit, 1982; Gundermann and Büchel, 2012). Besides, there is a group of carotenoids that play important roles in photoprotection. This includes β-carotene and xanthophylls (Kuczynska *et al.*, 2015). The xanthophylls are involved in the diadinoxanthin-diatoxanthin cycle (Ddx-Dtx Cycle) (Demers *et al.*, 1991; Goss and Jakob, 2010). This cycle is the de-epoxidation of Ddx to Dtx, and the reverse reaction of the epoxidation of Dtx to Ddx. This cycle is basically under the control of light conditions. The de-epoxidation is activated under acidified conditions of the thylakoid lumen, which usually occurs when there is excess excitation energy in the electron transport chain (Goss and Jakob, 2010; Goss and Lepetit, 2015). The fast accumulation of Dtx showed a strong correlation with NPQ, suggesting the important role of Dtx in photoprotection under high light conditions (Lavaud, 2002; Ruban *et al.*, 2004; Ruban, 2017).

6. Aim of the study

My PhD work investigated the survival and growth of ice algae under changing environmental conditions. Ice algal cells of the Sea of Okhotsk are released into seawater every spring as sea ice melts. The released ice algae are capable to seed the spring phytoplankton bloom. Despite the large biomass of the Okhotsk ice algae, the ecology and their seeding roles toward the spring bloom are not fully understood. Chapter 2 describes the investigation of the fates of ice algae during and after ice melt in the Sea of Okhotsk. A laboratory experiment simulating the field ice melt was conducted to measure the changes in the community composition during and after complete ice melt. The algal photosynthesis in the seawater was also measured to see the correlations with the dynamics of the community. Knowing the fate of ice algae under the ice melt condition improves our understanding on the community dynamics and primary production of the Sea of Okhotsk in the changing climate. Chapter 3 describes an incubation work using a strain of the pennate diatom *Nitzschia* cf. *neglecta* isolated from the sea ice of Saroma Lagoon. Global warming poses a serious challenge to marine ecosystems (Petrou *et al.*, 2010). The multi-year ice in the Arctic is declining, specifically through changes in sea-ice thickness, the timing of advance and retreat, and associated shifts in overlying snow (Stroeve and Notz, 2018).

Over the past five decades, there is a declining trend in the formation of sea ice in the Sea of Okhotsk due to global climate change (Ohshima *et al.*, 2014; Nihashi *et al.*, 2018). There exist conflicting views of how increased temperature affects microalgal productivity in sea ice-covered waters. The culture temperature and irradiance level were increased to investigate whether an ice alga can survive such conditions significantly different from that of sea ice. Then the cultured cells were exposed to high light to investigate the photoprotective strategies.

The results of the experiments give us a better understanding of how ice algae survive under changing environments when sea ice melts and how the related ecological effects.

7. Figures

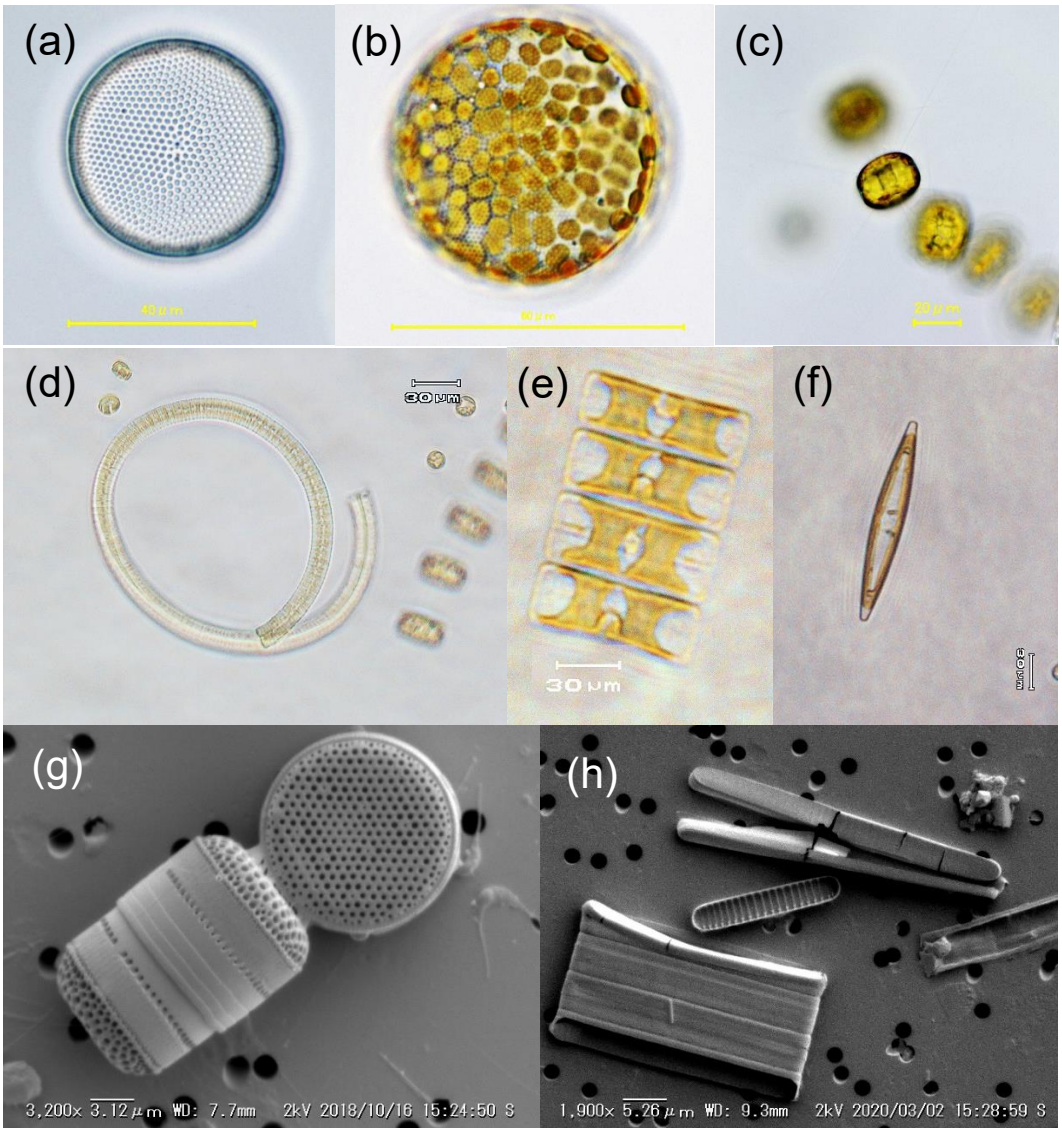

Fig. 1.1 microscopic photos of diatoms. (a) an empty frustule of a single cell of *Shionodiscus* sp.; (b) a living cell of *Thalassiosira* sp. with plastids and chloroplasts; (c) a chain of living cells of *Thalassiosira* sp.; (d) a long chain of living cells of *Fragilariopsis* sp. (central); (e) a short chain of four cells of *Navicula* sp.; (f) a single living cell of *Navicula* sp.; (g) two cells of *Shionodiscus* sp., one in valve view, another in girdle view; (h) short chains of *Fragilariopsis cylindrus*. Light microscope: (a) to (f); Scanning electron microscope: (g) and (h). Centric diatoms: (a), (b), (c), and (g); Pennate diatoms: (d), (e), (f), and (h). All species comes from the sea ice of the Sea of Okhotsk, except (g), which comes from seawater of Sanriku of the northwestern Pacific.

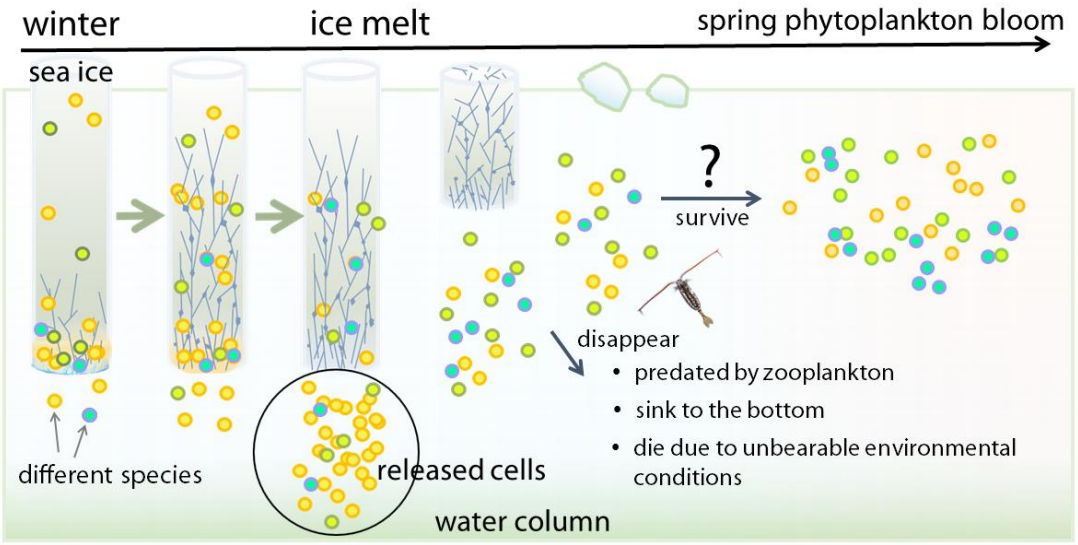

Fig. 1.2 Schematic of the dynamics of the microalgal community during the seasonal transition of winter-spring in a seasonal ice-covered area.

Chapter 2

Response to sea ice melt of an ice algal community from the Sea of Okhotsk

1. Abstract

Phytoplankton communities in seasonal ice-covered areas are largely affected by ice algae. The Sea of Okhotsk is the southernmost sea ice zone in the northern hemisphere with a sizeable seasonal ice cover. Therefore, ice algae of the Okhotsk sea ice have a large potential to seed the early spring bloom. Little is known about the Okhotsk ice algal communities and their seeding effects. We investigated the dynamics of the composition and the photophysiological performances of an ice algal community from the Okhotsk sea ice in a 6-day laboratory incubation experiment that simulated the natural ice melt conditions. Centric diatoms, especially *Thalassiosira* spp., overwhelmingly dominated the ice algal community throughout incubation, whereas pennate diatoms, mostly *Navicula* and *Nitzschia*, showed little growth with much higher mortality. The maximum photochemical efficiency of Photosystem II (F_v/F_m) was the lowest at the beginning of the ice melt, suggesting a suppressed photosynthetic functioning by changes in salinity. The cellular pigment contents decreased by 30% due to physical damage of the cellular membrane, evidenced by deformed plastids under a microscope. The transcript level of the *rbcL* gene that encodes the large subunit of RubisCO was significantly higher during ice melt and decreased in the no-ice period, suggesting an urgent need for carbon fixation under the melt condition. Full recovery of photosynthesis and growth was also made after complete ice melt. Our results indicated high seeding potential of *Thalassiosira* to spring blooms owing to their photophysiological plasticity to dynamic salinity changes.

2. Introduction

Sea ice algae can form a large fraction of sea-ice biomass (Tedesco *et al.*, 2019). Previous studies suggested that the release of ice algae into the water column initiated the spring development of phytoplankton (Garrison *et al.*, 1987; Garrison and Close, 1993), which is known as the seeding effect of ice algae. There is a substantial standing stock of ice algae in the Okhotsk Sea ice. Dense ice algal communities have commonly been observed at the bottom of Okhotsk sea ice, especially in spring (Leonov *et al.*, 2007). Chlorophyll *a* (Chl *a*) concentrations in the Okhotsk sea ice ranged between 0.2 to 3.5 mg m^{-2}, and was up to an order of magnitude higher than the under-ice seawater (Granskog *et al.*, 2015). McMinn et al. (2008) reported an extremely high Chl *a* concentration of 1.6 $\times 10^3$ mg Chl *a* m^{-3} in the pack ice near Shiretoko with an average thickness of around 70 cm. Granskog et al. (2015) also found considerable excess protein-like compounds in the Okhotsk Sea ice relative to the under-ice seawater, suggesting active biological production within the ice.

The annual primary production in the Sea of Okhotsk is largely derived from spring diatom blooms following the sea ice melt (Ohwada, 1956; Zhang *et al.*, 2006). The spring blooms usually continue until the end of June in the central areas and mid-July or early August in the colder eastern and northern parts (Sorokin and Sorokin, 1999; Shuntov, 2001). When ice breakup begins in spring, ice algae are rapidly washed out of the ice and dispersed into the water column, causing a significant increase in the downward flux of ice algal cells under the Okhotsk sea ice (Leonov *et al.*, 2007; Hiwatari *et al.*, 2008). Spring phytoplankton communities in coastal southern Okhotsk waters off Hokkaido, Japan can also be directly affected by ice melting. High Chl *a* concentrations of around 30 and 60 mg m^{-3} have been observed in the southern part of the Sea of Okhotsk and the coastal waters of Mombetsu Harbor during the ice melt season (Taguchi *et al.*, 2000; Kanna *et al.*, 2018). Such high Chl *a* concentration could be attributed to the released ice algal cells. Longer periods of ice cover corresponded to larger magnitudes of the spring Chl *a* peak of the ice edge blooms in the Southern Okhotsk because this condition would favor algal growth and accumulation at the surface water (Kudoh, 1993; Mustapha and Saitoh, 2008). Besides, there are possibilities that the Okhotsk sea ice algae also contribute to the phytoplankton growth in the Oyashio waters of the western North Pacific. Pack ice often flows out into the

North Pacific through the southern passes of the Kuril Islands, indicating the pack ice could be one of the sources of the highly productive coastal Oyashio waters and influences ocean conditions off the southeast coast of Hokkaido, Japan (Ohtani, 1989; Talley and Nagata, 1995). It is thus likely that ice algae in the Okhotsk sea ice have a seeding effect on the spring phytoplankton bloom of subarctic waters near Japan (Kuroda *et al.*, 2019).

Not all of the algal cells would remain active after leaving the sea ice habitat. The released ice algae may either continue to grow in seawater to become the seed of the phytoplankton bloom after ice retreat or disappear from the water column over time (Haecky *et al.*, 1998; Mundy *et al.*, 2011; Kauko *et al.*, 2018). Their disappearance would be results of fast cell sedimentation (Michel *et al.*, 1997; Haecky *et al.*, 1998), cell death caused by predation, or necrosis due to rapid environmental changes as ice melts (Grant and Horner, 1976; Taguchi *et al.*, 1997; Różańska *et al.*, 2009; Rajanahally *et al.*, 2014). Ice algae live in brine of sea ice. The brine salinity is determined by the ice temperature (Assur, 1960; Horner, 1985). At extreme temperatures in winter, brine salinity can be 6–7 times higher than that of typical seawater at the upper part of the sea ice (Ewert and Deming, 2013). Brine salinity would be milder at the bottom part of the sea ice but can still reach 50 in the dense brownish algal layer (Grant and Horner, 1976). During the ice melt season, the brine in sea ice is generally washed out by the nearly fresh surface meltwater (Zhang *et al.*, 1999; Notz and Worster, 2009). Ice algae thus can experience significant changes in salinity when ice melts. The ice temperature usually ranges from −4.5 to −1.8 °C from the upper to the bottom part in the southern Sea of Okhotsk (Toyota *et al.*, 2007), which corresponds to brine salinities ranging from around 75 to 32 (Assur, 1960; Horner, 1985). The average salinity of the surface seawater in this region is around 32.4 in winter. While the salinity drops to values < 29 if there is a layer of melted sea ice in surface waters (unpublished data).

Salinity change during ice melt could cause drastic changes in the physiology of ice algae as they are flushing out of sea ice (Arrigo and Sullivan, 1992; Taguchi *et al.*, 1997; Ralph *et al.*, 2007; Ryan *et al.*, 2011). Laboratory experiments found that ice diatoms are capable of maintaining a relatively high growth rate within a wide range of salinity of 10 to 50 (Smayda, 1969; Grant and Horner, 1976; Baars, 1982). In the most extreme case, some ice diatoms were able to grow exponentially in brine with a salinity of 105 at –6°C (Aletsee and Jahnke, 1992). However, there

was usually a lag period before normal growth can be reached after being exposed to extreme salinities. The lag period, which varies among species, could occur when ice algal cells rearrange the metabolism to protect themselves from the acute osmotic shock. In other words, algal cells may die of osmotic stress before they can acclimate to the new salinity. Salinity changes severely disturb the cellular homeostasis caused by differences between the internal and exogenous concentration of inorganic ions (Guillard and Ryther, 1962). This could lead to photosynthesis and growth inhibition, respiration increase, and cell deformation in diatoms (Qasim *et al.*, 1972; Jahnke and Baumann, 1983; Rijstenbil *et al.*, 1989; Yoshida *et al.*, 2020). Indirect damages mediated by the liberation of reactive oxygen species also causes additional oxidative stress (Hernando *et al.*, 2015). Krell et al. (2007) demonstrated that the dominant ice organisms need to be well adapted or acclimated to a dynamic salinity regime coping with both hypersaline stress during ice formation and hyposaline stress during ice melt. Physiological acclimation of released ice algae is thus needed in order to grow and survive in the seawater.

The Sea of Okhotsk is a marginal sea of the subarctic North Pacific and is the southernmost sea in the northern hemisphere with a sizeable seasonal sea ice cover (Ohshima *et al.*, 2005). Sea ice is primarily produced on the northwestern shelf of the Sea of Okhotsk and off East Sakhalin, and then advected southward due to the transportation of the prevailing northwesterly winds and the East Sakhalin Current (Martin *et al.*, 1998; Fukamachi *et al.*, 2009). The formation of the dense shelf water and the Okhotsk Sea intermediate water, which become a source water for the North Pacific Intermediate Water, is also driven by this wintertime brine rejection associated with the ice formation (Shcherbina *et al.*, 2003). Sea ice develops southward, reaches a maximum in February or March by covering 50–90% of the sea, and melts away in late May or early June (Ohshima *et al.*, 2006). According to Japan Meteorological Agency (2019), the maximum sea ice extent in the Sea of Okhotsk from 1971 to 2019 has declined by 0.062×10^6 km^2 per decade, corresponding to a loss of 3.9% of the total sea area per decade. Despite the large biomass of the Okhotsk ice algae, the ecology and their seeding roles toward the spring blooms are not fully understood. We conducted a laboratory experiment simulating the field ice melt and measured the changes in the community composition during and after complete ice melt. We investigated the ice diatom composition of the Okhotsk sea ice using both light microscopy and the high-

throughput sequencing method in order to get a more complete picture of the community. Since the survival and growth is directly related to the photosynthesis of algal cells, we also measured algal photosynthesis in the seawater, including the maximum photochemical quantum efficiency of Photosystem II (PSII, F_v/F_m), pigment composition, and the transcript levels of *rbcL* gene. The *rbcL* gene encodes the large subunit of the Ribulose-1,5-bisphosphate carboxylase/oxygenase (RubisCO) and was used as an indicator of carboxylation activity. We hypothesize that fast photophysiological acclimation to changing salinities provides competitive advantage during ice melt.

3. Materials and methods

3.1. Experimental set-up

A sea ice core was collected from the southeastern part of the Sea of Okhotsk (44.83 °N, 144.52 °E) aboard the icebreaker Patrol Vessel *Soya* (Japan Coast Guard) on February 9, 2019. During the sea ice expedition, the day time air temperature was around –8 °C. The average surface seawater temperature was around –1.84 °C. The ice core used was 27 cm in length and 14 cm in diameter. The sea ice temperature ranged from –4.7 °C at the surface to –1.90 °C at the bottom. The sampled ice core was immediately covered with semi-transparent polyethylene bags and stored in a –5 °C freezer in the dark for three weeks until further analysis.

For the melt experiment, the bottom 5 cm of the ice core with dense yellow-brown color was cut off with a stainless saw in dim light. Then the bottom was further equally divided into four pieces of around 200 g. Each piece of ice was kept in an acid-cleaned 2 L glass beaker filled with 200 mL Okhotsk seawater with a salinity of 32.2 in a freezer incubator for two days for recovery and acclimation to the incubation environment. The beakers and the seawater were autoclaved at 121 °C for 20 min before use. The seawater used in this study was filtered through Whatman GF/F glass fiber filters (nominal pore size 0.7 μm, Whatman, UK) before sterilization. During the acclamation of two days, the freezer was set at –3°C to minimize ice growth and ice melt. The light was provided by a white LED light source (LMGA1WG21K50A4-10F, Prince Industry Inc., Japan) specially designed for freezing environments placed at the upper part of the

incubator. The irradiance level was measured by a 4 π sensor (QSL-2100, Biospherical Instruments Inc., USA) and was around 50 μmol photons m^{-2} s^{-1}. After the two-day acclimation, 1.5 L sterilized *in situ* seawater was added to each 2 L beaker with the ice piece, and the temperature was adjusted to around 0°C to simulate the ice melt condition. Water samples were taken at the time of 0, 1, 2.5, 10, 24, 31, 55, 79, 103 and 127 h, hereafter t_0, t_1, $t_{2.5}$, t_{10}, t_{24}, t_{31}, t_{55}, t_{79}, t_{103} and t_{127}, respectively. During the melting process, the water temperature was monitored using a digital thermometer with its sensor soaked in one of the beakers. Water temperature and salinity were measured and recorded before each sampling using a digital salinometer with a conductivity temperature sensor (TetraCon® 325, Wissenschaftlich-Technische Werkstätten GmbH, Germany) (Fig. S2.1). Cell suspensions in beakers were stirred three times a day using a stainless rod to prevent settling. Because almost all of the ice has completely melted out after an incubation of 31 h, the whole incubation was divided into two parts: the ice melt period and the no-ice period by t_{31}.

3.2. Light microscopy

To avoid a rapid change of salinity in the beakers caused by ice melt, there was a limitation on the volume of water that can be taken during each sampling. Each time we took around 25 mL water from the beaker before ice was completely melted. This resulted in a final water salinity of around 29 at the end of the incubation. A small fraction of around 5 g from the ice core bottom was also sampled and melted with 20 mL seawater for species identification. These water samples were stored in the dark at 4°C before analysis under an inverted light microscope (CKX41-FI, Olympus, Japan). Diatoms in the water samples were identified and counted within a few days after each sampling. Taxonomic identification followed Tomas (1997). Identifications were to the species level if possible but to the genus in most cases. To calculate the growth rate, cell abundance was natural log transformed before plotting against the day of incubation and the specific growth rate (μ, day^{-1}) was calculated as the slope of the linearly fitted curve.

3.3. Cell viability

To distinguish between live and dead cells, cells in water samples of 5 mL were stained with the LIVE/DEAD™ *Bac*Light™ stain (Thermo Fisher Scientific, Inc., USA) for 30 min

in the dark. Then the sample was filtered onto black 25 mm polycarbonate membrane filters (0.2 μm in pore size, Whatman Nuclepore™, UK) and stored at –80 °C until analysis with an epifluorescence microscope (BZ-9000, KEYENCE, Japan) following Agusti et al. (2015).

3.4. Pigments

Samples of 5 or 10 mL were filtered onto GF/F glass fiber filters (25 mm in diameter, nominal pore size 0.7 μm, Whatman, UK) under gentle vacuum pressure (< 0.013 MPa). The filter samples were immediately frozen in a deep freezer at –80 °C for later analysis. Pigment extraction and analysis were conducted according to Suzuki et al. (2015) using the *N*,*N*-dimethylformamide (DMF) bead-beating technique and Ultra-High Performance Liquid Chromatography (UHPLC). The identified pigments were grouped into photosynthetic carotenoids (PSC = fucoxanthin (Fxn)), photoprotective carotenoids (PPC = diadinoxanthin + diatoxanthin + β-carotene (Car)) and total chlorophyll (TChl = Chl *c* + Chl *a*) (Roy *et al.*, 2011).

3.5. qPCR and RT-qPCR of rbcL

For the DNA and RNA analysis, water samples were filtered onto polycarbonate nucleopore filters (pore size 2 μm, Whatman, UK) with gentle vacuum pressure (0.013 MPa). Then the filters were stored in a deep freezer at –80 °C until extraction. DNA and RNA extraction and the qPCR and RT-qPCR of the *rbcL* gene were conducted following Endo et al. (2013) and Endo et al. (2015), respectively.

3.6. Metabarcoding of diatom-derived 18S rRNA gene

The diatom-derived 18S rRNA gene (rDNA) including the V4 region was amplified and sequenced using the Ion Torrent sequencing technique following Endo et al. (2018). The target 18S fragment of the extracted DNA was amplified using the *TaKaRa Ex Taq*™ Hot Start Version (TaKaRa). Each DNA sample was amplified in triplicates. The amplicon was checked by 1.2% agarose gel electrophoresis, purified using AMPure XP magnetic beads (Beckman Coulter) and quantified with an Agilent 2100 Bioanalyzer using a high sensitivity DNA Kit (Agilent Technologies). The PCR templates were then diluted to a final concentration of 13 pM and mixed for the emulsion PCR using the Ion OneTouch™ 2 system with the Hi-Q™ OT2 Kit

(Thermo Fisher Scientific). The products of emulsion PCR were enriched using an Ion OneTouch™ ES (Thermo Fisher Scientific) and then loaded onto an Ion 318™ v2 chip. Sequencing of the amplicon libraries was performed using an Ion Torrent PGM system with the Ion PGM™ Hi-Q™ sequencing kit (Thermo Fisher Scientific).

Signal processing, base calling, and quality filtering were conducted using the Torrent Suite™ (Thermo Fisher Scientific). Sequences with polyclonal and no match against the A-adapter were initially filtered. Further quality control was conducted using the FASTX-Toolkit (http://hannonlab.cshl.edu/fastx_toolkit/). The reads without the trP1 adapter or the reverse primer sequence were removed. The remaining reads that have at least 75% of bases with a quality score of 26 were kept and trimmed so that only the V4 part between 18 and 270 bp of each read was used for further analysis. Ten thousand reads for each sample were used for the taxonomic assignment. The reads were aligned and classified on the SILVAngs web interface (https://www.arb-silva.de/ngs/) using a local nucleotide BLAST search against the non-redundant version of the SILVA SSU Ref dataset (release 132; http://www.arb-silva.de). Identical reads were clustered into OTUs of >98% identity. Reads of each OTU were used for taxonomic assignments. Singletons and the taxonomic assignments other than diatoms were not used for the taxonomy analysis.

3.7. Maximum photochemical efficiency of Photosystem II (F_v/F_m)

The maximum photochemical efficiency of Photosystem II (PSII) (F_v/F_m) was measured at each sampling time using a pulse amplitude modulated fluorometer (Water-PAM, Walz, Germany). Before measurement, samples need to be placed in the darkness for a period of time to make all PSII reaction centers open. The measurement is initiated by switching on the measuring light. This gives a measurement of a minimum fluorescence, F_o. Then a high intensity, short duration flash of light, also called a saturation pulse is applied. This allows the contribution of photochemical quenching to be transiently reduced to zero because it transiently close all PSII reaction centers. Provided that this flash is short enough, no increase in heat dissipation occurs. Then we get the maximum fluorescence F_m. The maximum photochemical efficiency of PSII was calculated as $F_v/F_m = (F_m - F_o)/F_m$. F_v is the variable fluorescence. F_v/F_m reflects the

proportion of efficiently working PSII among the total PSII population. Cell suspensions were placed in a quartz cuvette during the measurement. The saturating pulse was provided by a red-LED with a peak illumination at 620 nm and set at 4,000 μmol photons m^{-2} s^{-1} and lasted for 400 ms for all measurements (Yan *et al.*, 2019).

3.8. Statistics

Differences among different incubation time and periods were tested using one-way analysis of variance (ANOVA) and *t*-test after Levene's test for the homogeneity of variances. Multivariate analysis was conducted using the package "vegan" of R (Dixon, 2003). We used Principle Component Analysis (PCA) to investigate the differences in community composition among different periods of incubation-the bulk ice, the ice melt period, and the no-ice period. Hellinger distance was used for the ordination. The significance of the differences among groups was tested using Permutational-multivariate analysis of variance (PERMANOVA) with 999 permutations. For the cluster analysis, the cell abundance data was $\log_{10}2$ transformed, and Euclidean distances among different diatom groups were used. The clustering method was unweighted arithmetic average (UPGMA). The significance level was set at 0.05.

4. Results

4.1. Growth rate

The specific growth rates of the whole diatom community, the centric and pennate diatoms during the melt or no ice periods were calculated (Fig. 2.1). The specific growth rate for the no-ice period from day 2 to day 6 (μ_w) showed that the community growth (0.18 ± 0.02 day^{-1}) was mainly contributed by centric diatoms (0.18 ± 0.03 day^{-1}).While the growth rate of pennate diatoms was 3.5 times slower than that of the centric diatoms during the no ice period ($p < 0.01$) and the cell abundance of pennate diatoms remained low throughout the incubation. To simplify the calculation of the algal growth during the ice melt period, we assumed that the algal cells remaining in sea ice and those released into the seawater had the same growth rate, μ_i. By doing this we can imagine that all the algal cells were staying in sea ice until the moment ice had melted out (t_{31}) when all cells were released into the seawater. Then the total cell number at t_0 plus the increased cell number due to cell growth in sea ice would equal to the total cell number

in seawater at the moment when all ice disappears.

$N_{ice}(t_{31}) = N_{sw}(t_{31})$,

where $N_{ice}(t_{31})$ and $N_{sw}(t_{31})$ are the cell number in sea ice and seawater at t_{31}, respectively. The total cell number in sea ice at t_{31} is

$N_{ice}(t_{31}) = N_{ice}(t_0) \times \exp(\mu_i t_{31})$. (equation1)

$N_{ice}(t_0) = c_{ice}(t_0) \times V_{ice}(t_0)$, (equation2)

where $c_{ice}(t_0)$ is the cell concentration in the bulk ice and $V_{ice}(t_0)$ is the original volume of the sea ice used. Both of them are known. And the total cell number in seawater after all cells were released is

$N_{sw}(t_{31}) = c_{sw}(t_{31}) \times V_{sw}(t_{31})$, (equation3)

where $c_{sw}(t_{31})$ is the cell concentration in the seawater and $V_{sw}(t_{31})$ is the total volume of the seawater plus the water volume used for water sampling. Both of them are known.

Then we can calculate μ_i by solving the above three equations. Results showed that despite the large difference in μ_w between centric and pennate diatoms, the calculated μ_i for the two groups were similar, around 0.05 day^{-1}, and very close to that of the μ_w of pennate diatoms in the no-ice period.

4.2. Cell viability and cell structure

The percentages of dead cells in the diatom community were low (Fig. 2.2). The highest percentage was around 5.89 ± 0.71% in the pennate diatoms under the ice melt condition. This percentage dropped to < 2% after ice melt ($p < 0.01$). The average percentage of dead cells of centric diatoms was 0.50 ± 0.17% during ice melt and increased to 1.68 ± 0.64% in the no-ice period ($p < 0.05$).

We tracked changes in the structure of some large diatom cells with a light microscope during the incubation periods (Fig. 2.3). Most of the observed cells during ice melt looked quite different from those normal healthy-looking cells in the laboratory culture. Obvious signs of salt stress include (a) loss of all or a large part of the pigments, so the chloroplasts became pale;

(b) chloroplast pellets not evenly distributed or spread in a single layer close to the cell wall in the cytoplasm like that in healthy cells. Instead, chloroplast pellets formed small aggregates inside the cell; (c) visible adhesive sticky gel attached to the stressed centric diatom cells. Most of the stressed cells recovered with time during the incubation. The color of the chloroplast became brighter and darker. The mucilage around the cells became invisible. At the end of the incubation, the cells in the beakers looked similar to the normal healthy-look cells in the laboratory culture under a microscope.

4.3. Diatom community composition

To make better comparisons of the results between microscopy and metabarcoding, the diatom genus or groups that shown in the figure need to meet the following two standards (Fig. 2.4). (1) The top ten abundant ones (i.e. abundance of cells or gene fragments) during the whole incubation. (2) Genus or groups that were found at each time of sampling. Other genus or groups were added up to groups of other pennates and other centrics. The complete run 302 files of the 18S rDNA sequences have been deposited in the DDBJ Sequence Read Archive 303 under accession number PRJDB9641. Both the light microscopy (LM) and the 18S rDNA data showed that centric diatoms dominated the communities. Genus or group contribution to the total was averaged. The top five abundant genus (groups) were *Thalassiosira* (74.7%), *Chaetoceros* (9.9%), *Porosira* (3.5%), *Nitzschia* (3.4%) and *Navicula* (2.6%) for the LM-based communities, whereas *Thalassiosira* (75.8%), *Navicula* (7.4%), *Porosira* (7.1%), the total other pennate diatoms (5.6 %) and the total other centric diatoms (2.1%) for the 18S rDNA-based communities. There was an overwhelming dominance of *Thalassiosira* of >70% revealed by both methods. *Chaetoceros* was the second most abundant genus in terms of cell number, around 10%, while it was much less abundant in the 18S rDNA community (0.3%). Overall, pennate diatoms were slightly more abundant in terms of 18S rDNA sequences (14.7%) than LM cell counts (8.9%).

Unweighted arithmetic average clustering (UPGMA) was used to investigate the possible associations of the identified diatom groups (Fig. 2.5). The identified diatoms formed 3 major clusters based on their abundance for both LM and 18S rDNA communities. Cluster 1 contains only the dominant genus *Thalassiosira*. The LM and 18S communities shared some relatively

abundant genus for Cluster 2, including *Chaetoceros, Porosira*, *Navicula* and *Nitzschia*. Cluster 3 contained diatoms with low abundance. The other pennates or centrics were included in Cluster 2 for 18S rDNA metabarcoding, while in Cluster 3 for LM. PCA results showed that the first component, most likely to be related to the time of incubation, explained 45.42% and 66.65% of the variance in LM and 18S rDNA metabarcoding, respectively (Fig. 2.6). The biplots showed that *Thalassiosira* was more commonly found in the samples from the no-ice period for both LM and 18S communities. For the LM community, *Thalassiosira, Chaetoceros*, and *Detonula* were more related to the samples from no-ice period. Other diatoms showed various patterns in their abundance with the incubation time and were more commonly found in the ice-melt samples. For the 18S rDNA communities, *Porosira* and *Navicula* were found to be more abundant in the bulk ice than the samples that have undergone incubation. *Nitzschia* and the total other pennates were abundant at the beginning of the incubation (t_0) while decreased in number after that.

To see the changes in community composition at the species level, we constructed an 18S rDNA library for a local BLAST using the diatom isolates from the sea ice and seawater of the Sea of Okhotsk, the Saroma Lagoon adjacent to the sea, and the coastal Oyashio seawater. Species that were not successfully isolated but were abundant in the algal community in the results of LM and SILVAngs were also included in the library. In that case we used the best hit 18S rDNA sequences of the OTUs in the NGS data with 97% in similarity downloaded from the NCBI database. To make simple comparisons, the most abundant 100 OTUs in the results were used for annotation. Like the results of the PCA based on the 18S rDNA of SILVAngs database, our local BLAST also showed a significant decrease in the number of OTUs of *Navicula* and *Nitzschia* after incubation (Fig. 2.7). Despite the increase in the contribution of *Thalassiosira* to the total after incubation, the relative abundance of different *Thalassiosira* species also changed. *T. nordenskioeldii* was the most abundant one in the bulk ice, while three other *Thalassiosira* species including *T. antarctica, T. hyalina and Thalassiosira.* sp. showed faster increases and became dominant in the community at the end.

4.4. Photophysiological performance

The cellular pigment contents showed a decreasing trend until each minimum value was reached

after 10 h of incubation (Fig. 2.8), and then they increased until the end. The PSC and TChl showed similar trends that the minimum values at t_{10} were around 70% of the original ones at t_0 and the final content at t_{127} was twice than that at t_0. For the PPC, the decreasing trend was more significant than the increase. The decrease in PPC was >50% at t_{10} and the recovery, with a much slower rate than the other pigment groups, was finally completed at the end of the incubation.

The sea ice melt significantly suppressed F_v/F_m (Fig. 2.9). The variation of F_v/F_m was large during the ice melt period when the cell concentrations were lower. Though being suppressed, the lowest F_v/F_m was 0.39 ± 0.05 at t_0 which means the PSII was still functional under the salt stress. F_v/F_m then increased and reached the maximum of 0.62 ± 0.01 at t_{79} and stayed at the same level until the end of the incubation.

The transcript levels of the *rbcL* gene were significantly higher during the ice melt period than that of the no-ice period (Fig. 2.10). After the melt of 5 h, the gene expression began to decrease and then kept a relatively steady state until the end of the incubation. Overall, the transcript levels of the *rbcL* gene during the first 5 h were 8 times higher than the average level of the steady state from t_{79} to t_{127} ($p < 0.01$).

5. Discussion

Pennate diatoms such as *Fragilariopsis, Nitzschia* and *Navicula* usually dominate sea ice algal communities (Poulin *et al.*, 2011; Szymanski and Gradinger, 2016). While the diatom community composition of the Okhotsk Sea ice used in our study showed different patterns (Fig. 2.4). Most of the abundant *Thalassiosira* found in the Okhotsk sea ice were also reported from the sea ice of the Arctic, which includes the Chukchi Sea, the East Siberian Sea, the Laptev Sea and the Barents Sea, though their dominance was much less frequent than pennate diatoms (Hegseth, 1992; Okolodkov, 1992). The Okhotsk sea ice could be unique that the discoid chain-forming centric diatoms *Thalassiosira* often occur with high abundance (McMinn et al. 2008; Ohwada 1956). We analyzed other sea ice samples taken during the same cruise and found that the dominance of *Thalassiosira* spp. in the Okhotsk Sea ice was not a single case (data not shown).

The dominance of *Thalassiosira* during the no-ice period in our laboratory experiment is in consistence with that in the field that the early spring blooms of *Thalassiosira* is a common

phenomenon occurring in the Sea of Okhotsk and the western subarctic Pacific, including the Oyashio region and the northwestern Sea of Japan near Russia when the water temperatures were still < 5°C (Ohwada 1956; Sorokin and Sorokin 1999; Motylkova and Konovalova 2010; Suzuki et al., 2011; Yoshida et al. 2018). In particular, *T. nordenskioeldii* usually dominates the spring phytoplankton bloom in the shelf surface waters of the Sea of Okhotsk with water temperatures of 2–5°C and salinities of 20–27 (Sorokin and Sorokin, 1999), a condition that is quite similar to our laboratory work. Yoshida et al. (2018) reported that the spring phytoplankton communities of the shelf coastal Oyashio water differentiated from other Oyashio water masses by the presence and the dominance of *Thalassiosira*, suggesting a sea ice origin since the coastal Oyashio water is derived from sea ice meltwater within the Sea of Okhotsk (Ohtani, 1989). The pack ice even extends its influence to the Funka Bay of the southwestern Hokkaido that the seed populations of the *T. nordenskioeldii* bloom in spring was from the coastal Oyashio water and was transported southward by the lateral advection (Shinada *et al.*, 1999). We thus suggest that the Okhotsk sea ice could be a source of those early spring blooms of *Thalassiosira* spp. in the coastal northwestern Pacific areas, indicating the seeding effect of the Okhotsk ice algae. And interestingly, we found a succession of *Thalassiosira* species during the no-ice period (Fig. 2.7). *T. nordenskioeldii* was the most abundant one in the bulk ice, while it was gradually outcompeted by *T. antarctica, T. hyalina* and *Thalassiosira* sp. In nature, *T. nordenskioeldii* is known to develop early in the growth season and disappears from the plankton community as the season advances along the northern coasts (Paasche, 1975). Zooplankton grazing might contribute to the succession in the field, while in this study it played a minor role because very few zooplankton were observed under the microscope. The mechanism of this succession is possibly related to the competition for nutrients and need to be studied in the future work.

Pennate diatoms had a larger abundance in the community of the bulk ice and at the beginning of the incubation (Fig. 2.4 and 2.6). The decrease in the contribution during the later stage of the incubation was probably caused by the lower growth rate compared to that of the centric diatoms (Fig. 2.1). The growth rate of pennate diatoms remained low in both the ice-melt and the no-ice periods. While the growth rate of centric diatoms increased by four-fold after the complete ice melt. The community growth rate during the no-ice period, around 0.18 day^{-1}, was

mainly contributed by the centric diatoms and was slightly lower than the maximum growth rate of ice diatom isolates or communities under similar temperature, salinity and light conditions reported in previous studies (Gilstad and Sakshaug, 1990; Hegseth, 1992; Juhl and Krembs, 2010; Aslam *et al.*, 2012, 2018; Olsen *et al.*, 2017; Kulk *et al.*, 2019). In those studies, the maximum growth rates of *T. antarctica*, *T. nordenskioeldii*, and *P. glacialis* under similar conditions were consistent and around 0.3 day^{-1} (Gilstad and Sakshaug, 1990; Kulk *et al.*, 2019). While reported maximum growth rate for pennate diatoms were around 0.2 day^{-1} and was mainly collected from *Fragilariopsis cylindrus* and *Nitzschia frigida,* two representative pennate diatoms of the polar regions (Hegseth, 1992; Juhl and Krembs, 2010; Aslam *et al.*, 2012, 2018). This indicates that pennate diatoms have the potential to grow while the intrinsic growth rate might be slower than centric diatoms under similar environmental conditions. We also suggest that the much slower growth rate of the pennate diatom of around 0.06 day^{-1} in this study could be partly due to the difference in the species composition of different communities investigated between our study and others. In our study, *Navicula* and *Nitzschia* were the most abundant pennate species in the bulk ice algal community (Fig. 2.4 and 2.6), while the most well-investigated *F. cylindrus* by previous studies was seldom observed. *Navicula* and *Nitzschia* usually occur in large abundance in the benthic algal communities (Chen *et al.*, 2019). There is evidence that growth of such pennate species that occur in both the benthic zone and sea ice could be inhibited under changing salinity conditions. A study on the distribution and abundance of benthic epipelic diatoms along an estuarine gradient found that *Navicula* were more closely associated with the haline part of an estuary (Underwood *et al.*, 1998). An Arctic *Navicula* species showed much more significant decrease in growth rates under changing salinities compared with centric diatoms (Grant and Horner, 1976). We thus suggest that such ice diatoms are possibly characterized by strong stenohalinity. In consistence with those findings, we found larger percentage of dead cells in pennate diatoms during ice melt (Fig. 2.2). The results suggest that besides a lower intrinsic growth rate at a chilling temperature, the susceptibility to the osmotic stress caused by ice melt is a more likely reason for the low growth rate of the pennate diatoms. On the other hand, the ecological success of *Thalassiosira* under stressful ice melt conditions could partly be attributed to their wide tolerance to salinity changes. In nature, *Thalassiosira* blooms are commonly observed in estuaries

and coastal waters (Rijstenbil, 1987), suggesting their tolerance to mesohaline environments. Laboratory studies found some *Thalassiosira* species can tolerate salinities spanning 15-60 and had broad peaks spanning 25-45 for growth (Grant and Horner, 1976; Brand, 1984). Some species showed extreme euryhalinity and could even grew in freshwater medium (Brand, 1984).

The seeding of ice algae is dependent on the survival and sedimentation of algal cells (Haecky *et al.*, 1998; Tedesco *et al.*, 2012). Fast sinking results in a shorter residence time thus less contribution to the phytoplankton bloom (Haecky *et al.*, 1998). Indeed, many pennate ice diatoms are characterized by rapid sedimentation during the ice melt season (Taguchi *et al.*, 2000; Kauko *et al.*, 2018; Selz *et al.*, 2018). The sinking behavior of pennate diatoms is first due to their preference for benthic habitats (Gradinger and Ikävalko, 1998). Additionally, there is evidence that diatom sinking is under direct metabolic control and is closely related to the cell size and energy availability, hence photosynthesis and respiration (Waite *et al.*, 1992; Gemmell *et al.*, 2016). High sinking rates are more often observed at low growth rates and in senescent cells when the energy becomes less sufficient (Smetacek, 1985; Waite *et al.*, 1992; Durkin *et al.*, 2016). Our data suggests that the low energy availability and cell death due to inefficient photosynthesis under melt stress also contributed to the fast sedimentation of some pennate ice diatoms, hence reducing their seeding effect to the open-water bloom.

The salt stress caused a 30% decrease in the cellular content of PSC and TChl after 10 h of incubation (Fig. 2.8). We attribute this decrease to cell damage rather than acclimation due to the fact that abnormal cells were commonly observed at the beginning of the ice-melt period (Fig. 2.3). Similar cell deformation was also found in the large marine centric diatoms *Ditylum brightwellii* and *Corethron hystrix* when the cells were exposed to low salinities (Rijstenbil *et al.*, 1989; Aizdaicher and Markina, 2010). For both species, lower salinity caused significant shrinkage of cytoplasm. Cytoplasm strands and chloroplasts moved to the center or edge of the cells in *D. brightwellii* (Rijstenbil *et al.*, 1989). For *C. hystrix*, decreasing the medium salinity to 20 caused granular cellular contents and concentrated chloroplasts (Aizdaicher and Markina, 2010). Meanwhile, photosynthetic performance and cell division were severely inhibited (Rijstenbil *et al.*, 1989). In our study, lower F_v/F_m at the beginning of the ice-melt indicated the malfunction of PSII (Fig. 2.9). However, it appears that the functioning of photosynthesis of the investigated

Okhotsk algal ice community was quite robust. Signs of F_v/F_m recovery have already appeared when sea ice was still in culture during the first day, and F_v/F_m showed a continuous increasing trend until day 4. It is worth noting that nearly half of the PPC pigments had been lost at t_{10} and the recovery progressed much slower than the other pigment groups. PPCs, especially diadinoxanthin (Ddx) and diatoxanthin (Dtx) are directly related to the non-photochemical quenching of chlorophyll fluorescence (NPQ) to dissipate excess excitation energy in diatoms through the diadinoxanthin-diatoxanthin cycle (the Ddx-Dtx Cycle) (Goss and Jakob, 2010; Lavaud and Lepetit, 2013). The Ddx-Dtx Cycle could be a common photoprotective strategy by ice diatoms to protect themselves against high light after being released to water columns (McMinn *et al.*, 2010; Petrou *et al.*, 2010, 2011; Reeves *et al.*, 2011; Yan *et al.*, 2019). The results of this study indicate that PPCs play a minor role in the acclimation to salinity fluctuations in the Okhotsk ice diatom communities.

We found sticky mucilage around diatom cells during the ice melt period (Fig. 2.3). The mucilage is referred to as extracellular polymeric substances (EPS) (Hoagland *et al.*, 1993). Sea ice diatoms are known to produce polysaccharide-rich EPS (Krembs *et al.*, 2002; Abdullahi *et al.*, 2006). They function as cryoprotectants and osmoprotectants in sea ice by changing the physical structure of the ice pores to impede the desalination process while enhancing retention of organisms within the ice where light levels support substantial algal activity (Krembs *et al.*, 2011). Under stressful conditions, the enhanced production of EPS is usually accompanied with increased transcript levels of genes related to carbon metabolism. Bussard et al. (2017) found an up-regulation of the genes related to carbon concentrating mechanisms (CCMs) in the model diatom *T. weissflogii* in response to lower salinities down to 20. Decreased temperature and increased salinity induced a significant up-regulation of the genes involved in carbohydrate metabolism of the ice diatom *F. cylindrus* in order to protect themselves from the stress caused by the freezing condition (Aslam *et al.*, 2018). RubisCO catalyzes the first step of CO_2 fixation in photosynthesis. Due to the significant decrease in the turnover rate with temperature, high yield of this enzyme has been proposed as an adaptive mechanism under cold environments to the offset poor catalytic efficiency at low temperatures (Devos *et al.*, 1998; Morgan-Kiss *et al.*, 2006). Indeed, we also found an 8-fold higher transcript levels of the *rbcL* gene during the ice

melt period (Fig. 2.10). The transcript levels under the ice melt condition was higher than that of the no-ice period for the samples taken at the similar time of the day ($p < 0.05$). This suggests that the cells made great efforts to do carbon fixation during the ice-melt period in need of protection and repairing.

6. Conclusion

The diatom *Thalassiosira* was a major component of the Okhotsk sea ice diatom community and has a great potential to seed the spring phytoplankton bloom in the Sea of Okhotsk. The fast acclimation to salinity changes ensured the ecological success of *Thalassiosira*. Pennate diatoms of *Navicula* and *Nitzschia* were abundant in sea ice while their contribution decreased and became negligible as the incubation progressed. Besides the inherently lower growth rates of *Navicula* and *Nitzschia*, the growth was hindered by the osmotic stress, indicated by higher mortality during the ice melt period. The inefficient photosynthesis and cell death under the melt stress possibly reduced their seeding potential.

7. Figures

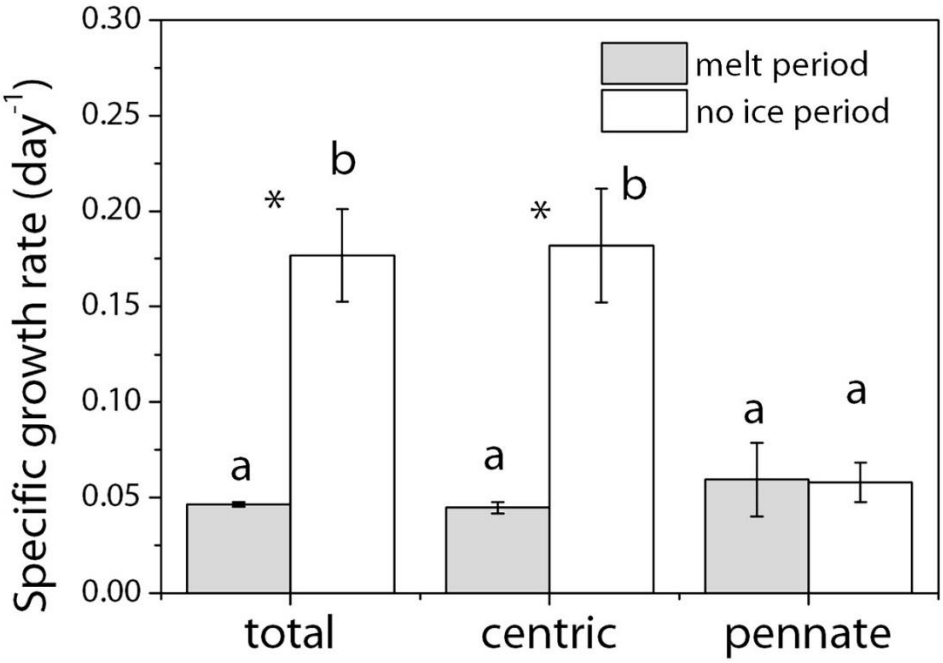

Fig.2.1 Specific growth rate (μ, day^{-1}) of different diatom groups. Gray, melt period; white, no-ice period. Mean values (± SD) are the average of four independent measurements. Alphabets indicate significant difference among different diatom groups. Stars indicate significant difference between the two incubation periods. ANOVA was used for comparisons. The significance level was 0.05.

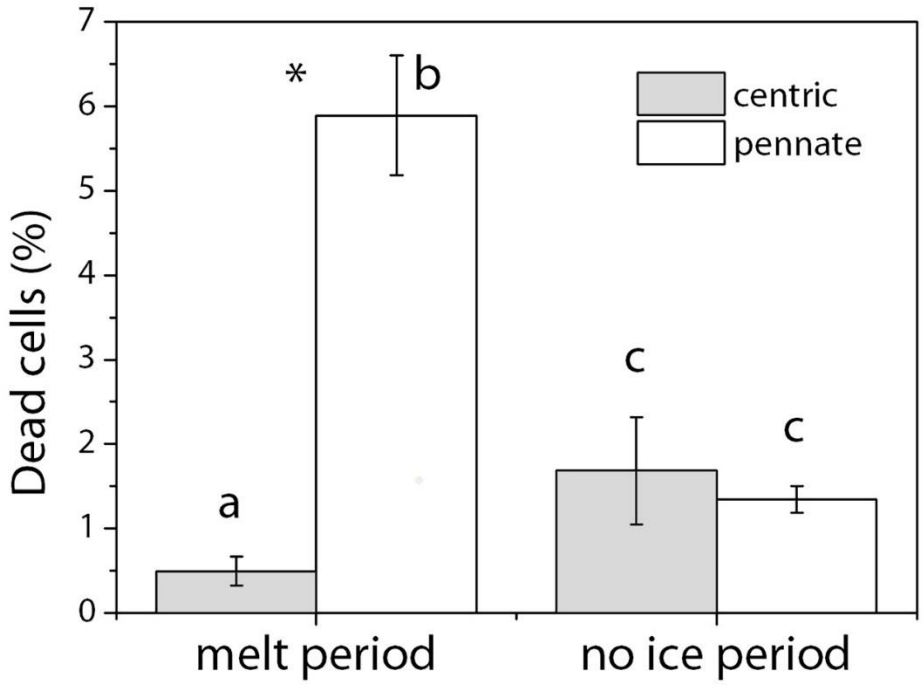

Fig.2.2 Percentage of dead cells (%) in the diatom community during the melt period and the no-ice period. Grey, centric diatoms; White, pennate diatoms. Mean values (± SD) are the average of four independent measurements. Alphabets indicate significant difference among different diatom groups. Stars indicate significant difference between the two incubation periods. ANOVA was used for comparisons. The significance level was 0.05.

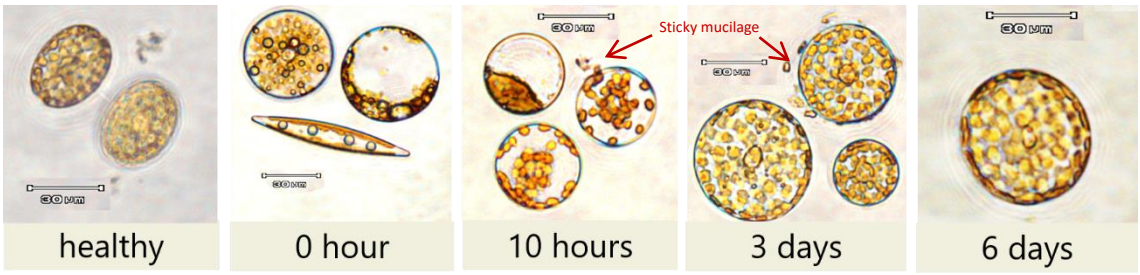

Fig. 2.3 Some typical-look cells under the light microscope during the incubation.

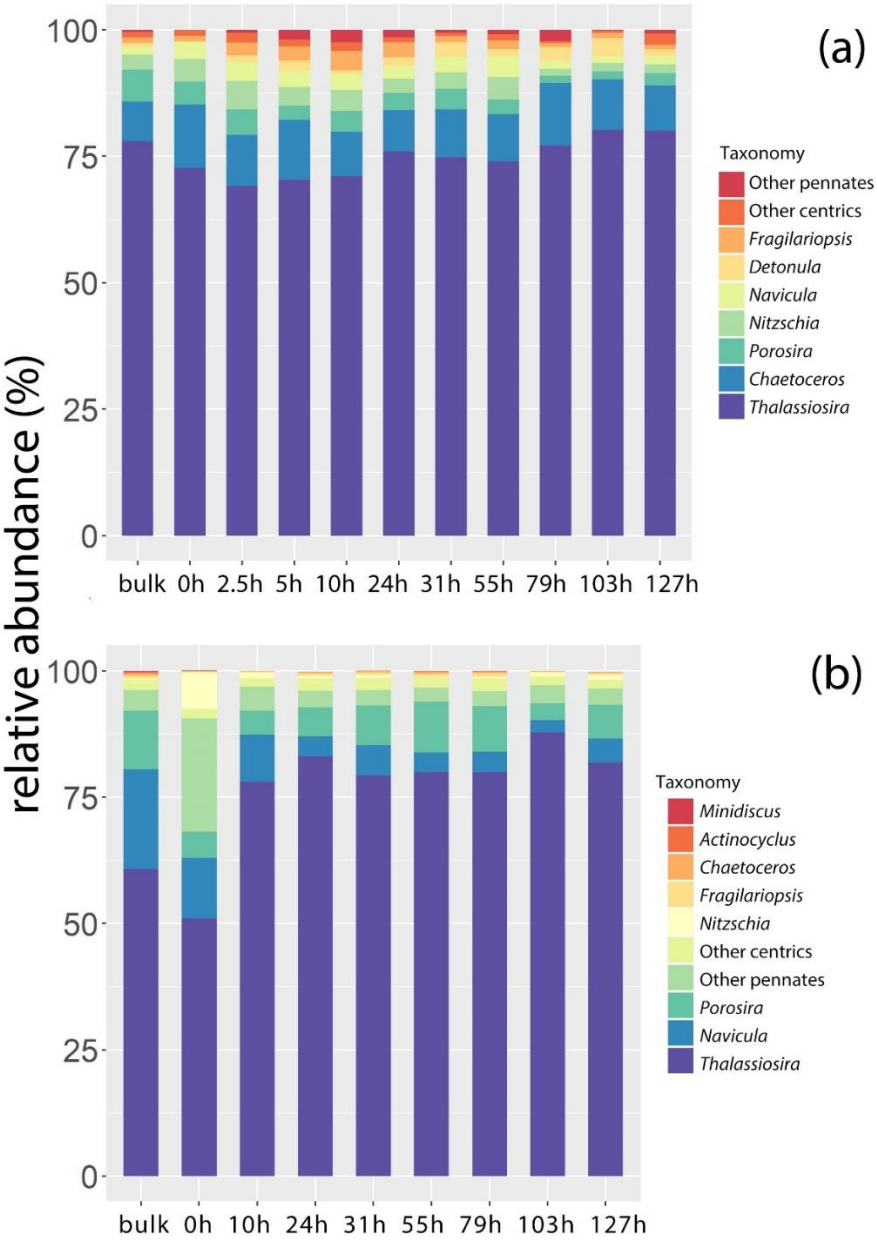

Fig. 2.4 Relative abundance of diatom genus or groups (%) in the bulk ice and during the incubation. (a) light microscopy (LM); (b) 18Sr DNA metabarcoding.

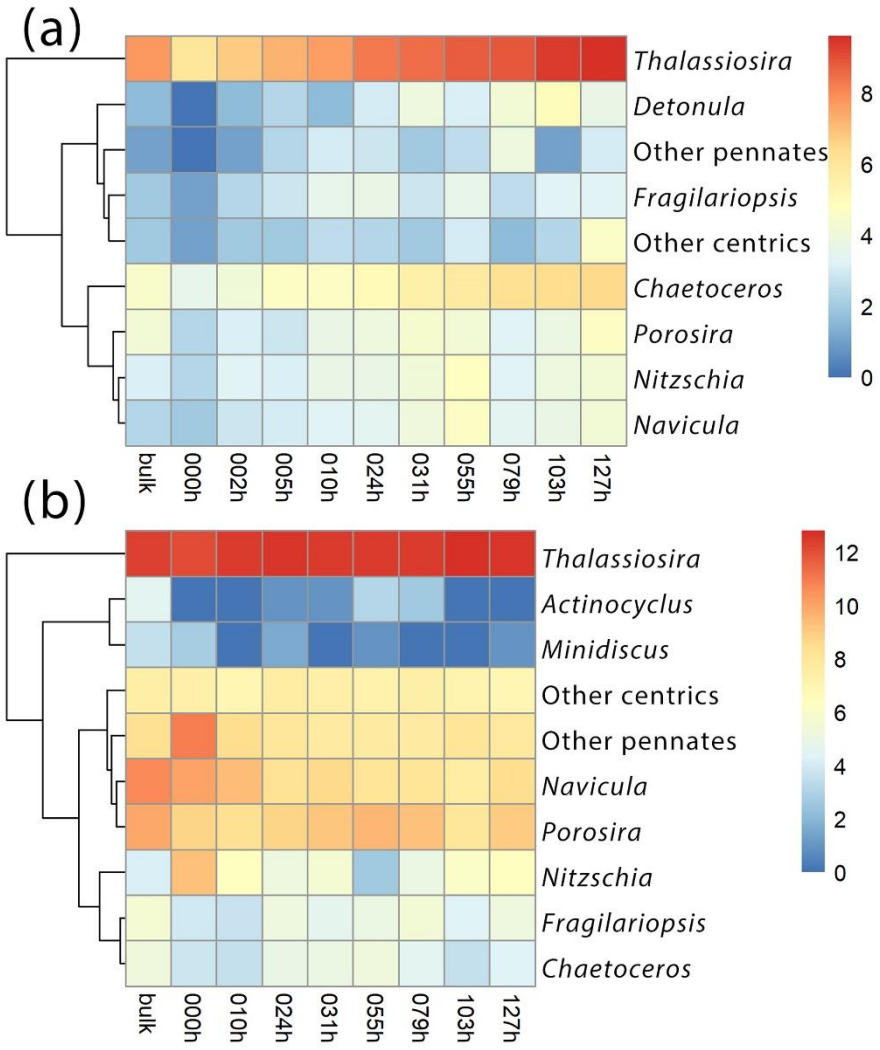

Fig. 2.5 Heatmap showing the abundance of different diatom groups in the community at different sampling time and the results of cluster analysis. The Unweighted arithmetic average clustering (UPGMA) was used to investigate the possible associations of the identified diatom groups. The abundance data were normalized by logarithmic transformation before analysis. (a) light microscopy (LM); (b) 18S rDNA metabarcoding.

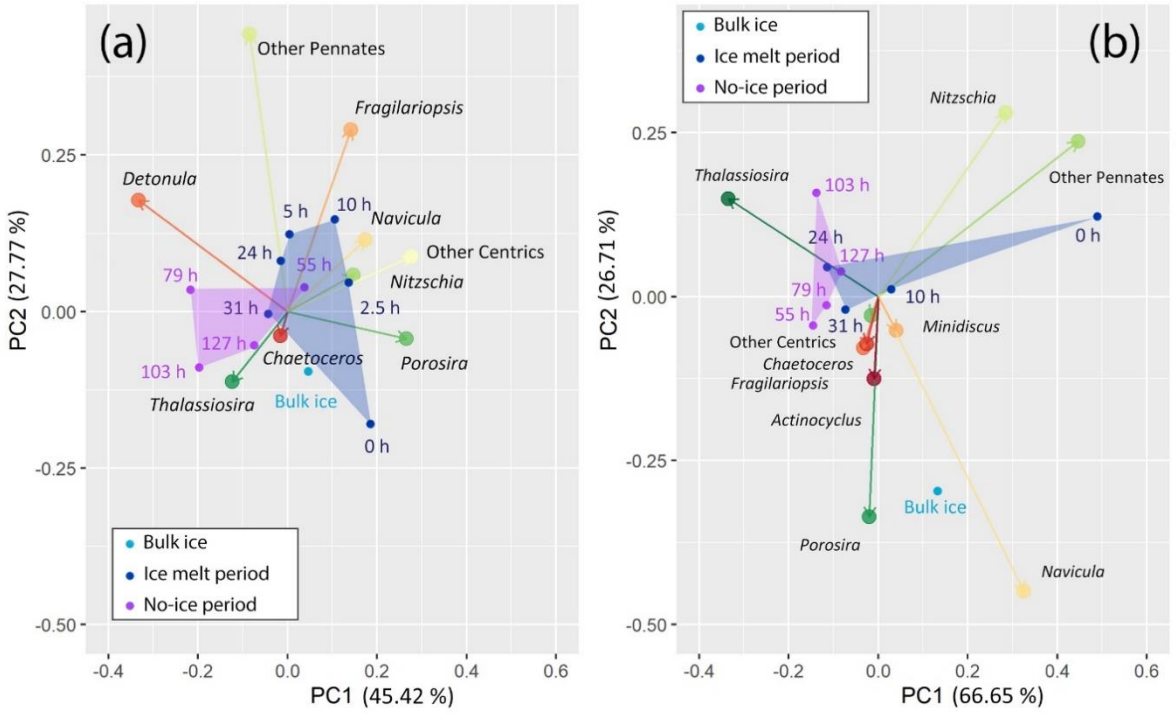

Fig. 2.6 Biplot of Principle component analysis (PCA) on the community composition at different sampling times. Light blue, the bulk ice; navy, during ice melt; purple, during the no-ice period. (a) light microscopy (LM); (b) 18S rDNA metabarcoding.

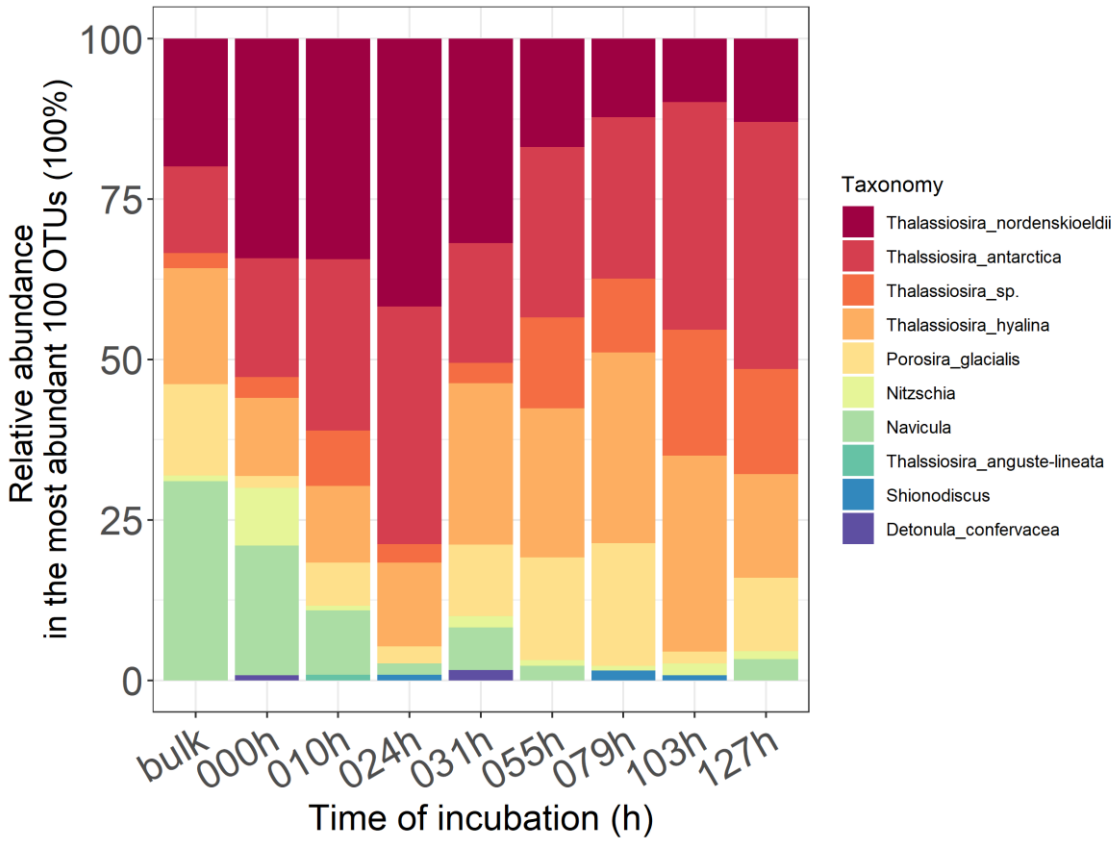

Fig. 2.7 The diatom composition in the top 100 most abundant OTUs after a local BLAST using the 18S rDNA library of the Okhotsk ice diatom isolates and the abundant diatom 18S sequences downloaded from the NCBI database.

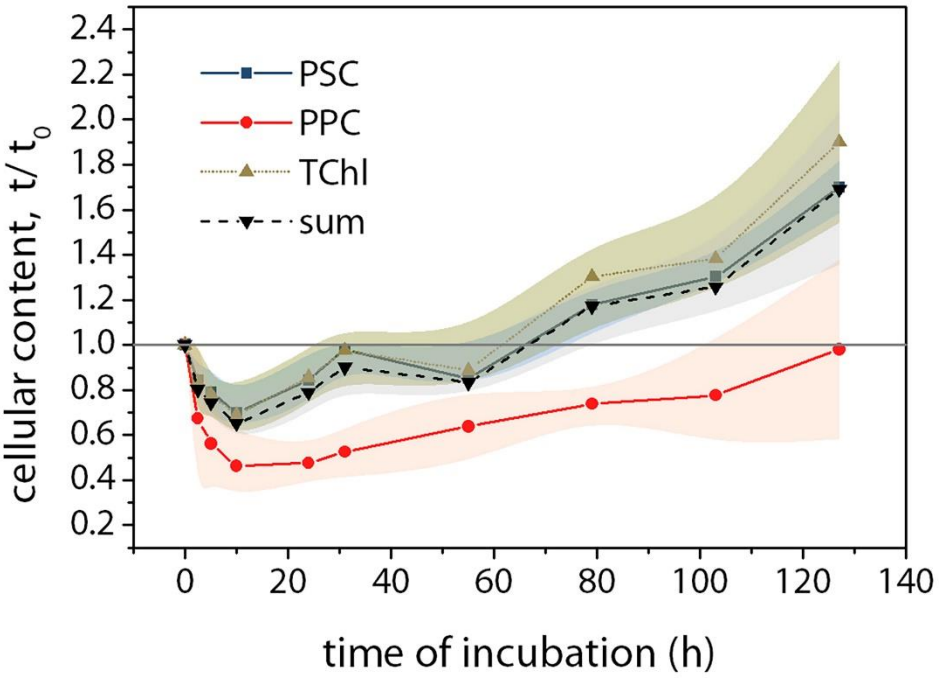

Fig. 2.8 Variatons of pigment contents during the incubation compared to that at t_0. Squares, photosynthetic carotenoids (PSC = fucoxanthin); Circles, photoprotective carotenoids (PPC = diadinoxanthin + diatoxanthin + β-carotene); upward triangles, total chlorophyll (TChl = Chl *c* + Chl *a*); downward triangles, the sum of all pigments. Mean values (± SD) are the average of four independent measurements.

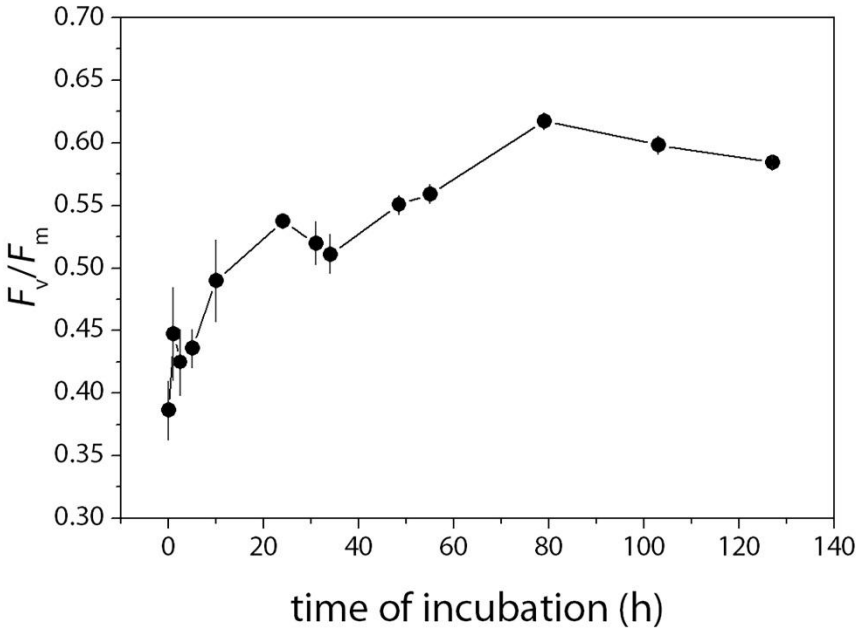

Fig. 2.9 Changes in the maximum photochemical efficiency (F_v/F_m) during the incubation. Mean values (± SD) are the average of four independent measurements.

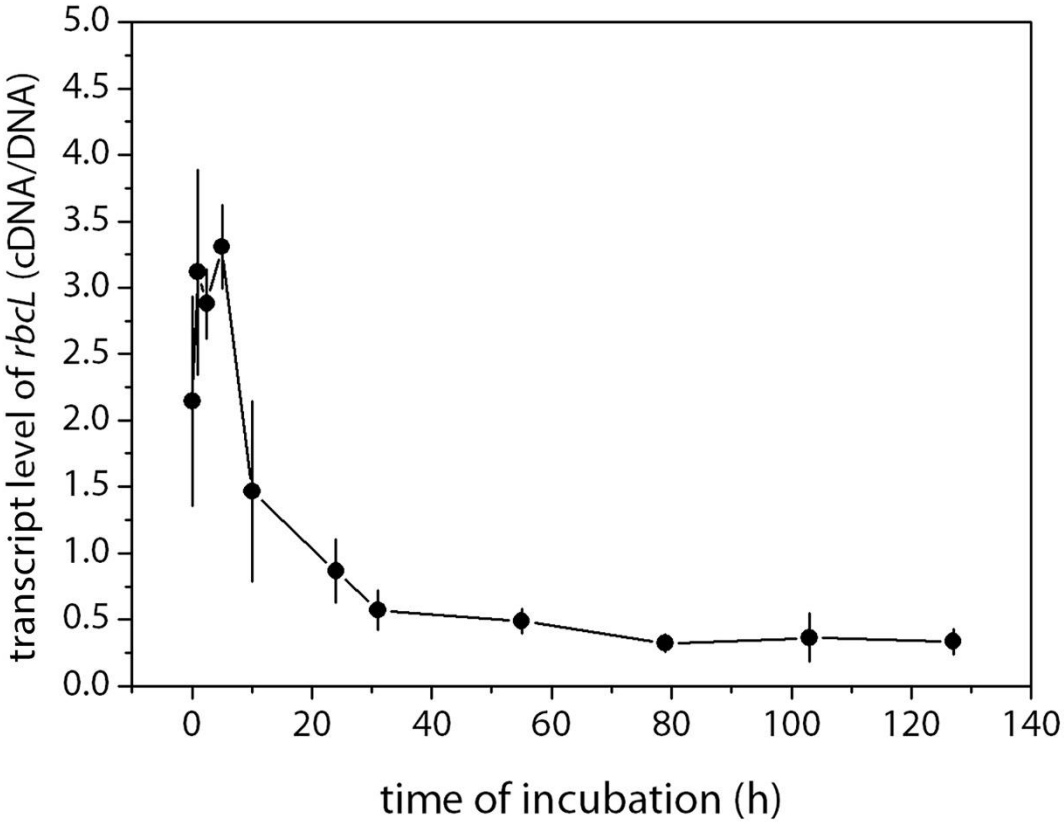

Fig. 2.10 Abundances of *rbcL* (cDNA) normalized to the gene copy number (cDNA/DNA) during the incubation. Mean values (± SD) are the average of four independent measurements.

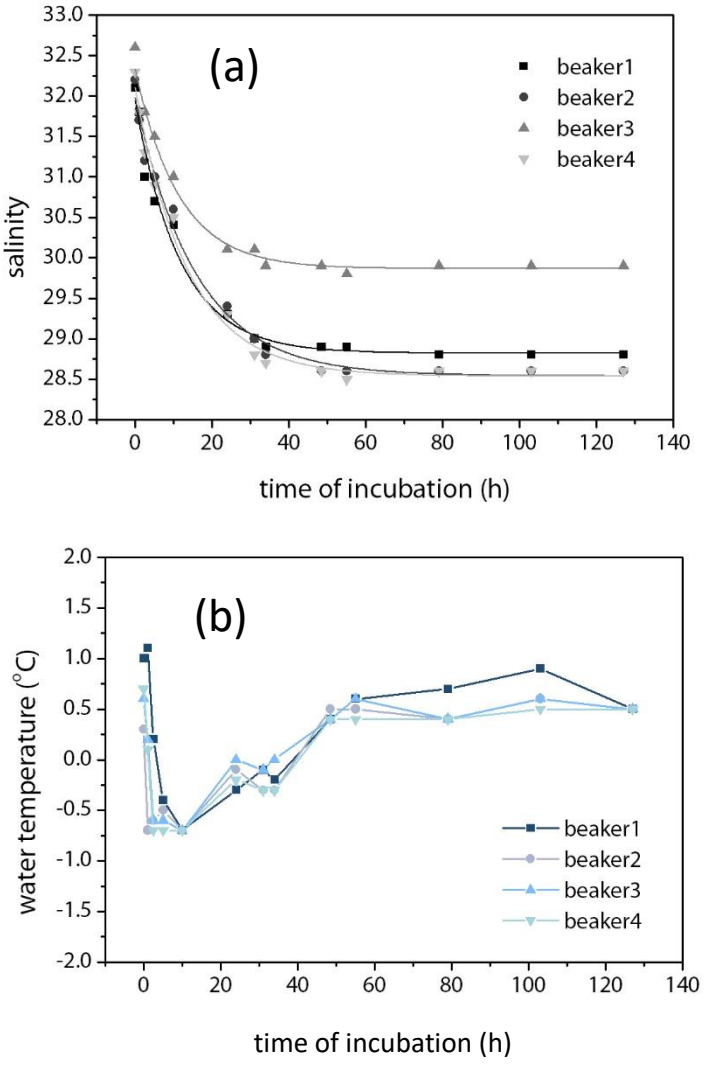

Fig. S2.1 Changes of salinity (a) and water temperature (b) in each beaker.

Chapter 3

Photophysiological response of the sea ice diatom Nitzschia *cf.* neglecta *to increased temperature and high light exposure*

1. Abstract

During ice melt in spring, ice algae are released from the ice and could be exposed to changeable temperature and irradiance in surface water. Saroma Lagoon is an embayment with two inlets leading to the Sea of Okhotsk. With seasonal development of sea ice, its water temperature changes dramatically throughout the year. To investigate the living and photoprotective strategies of ice algae in such a coastal water system, we grew *Nitzschia* cf. *neglecta*, an ice diatom isolated from the sea ice of this lagoon, under irradiance levels of 30 and 100 μmol photons m^{-2} s^{-1}, and temperatures of 2 and 10 °C. Then the acclimated cells were exposed to high light in order to investigate the plasticity of their photosynthetic apparatus. At 10 °C, cells grew faster and showed a weaker susceptibility to high light. At 2 °C, an immediate decrease in all pigment content upon exposure, as well as a higher cellular content of diatoxanthin was used to compensate for the more severe excitation stress. Highly efficient photoprotection was achieved through the diadinoxanthin-diatoxanthin cycle-dependent non-photochemical quenching. While regulation through *psbA* and *rbcL* at the transcription level played a minor role in the response to high light stress at both temperatures. The wide tolerance to both temperature and light changes suggest that the thinning of sea ice and higher temperatures in a warmer world will lead to more intense blooms in Saroma Lagoon.

2. Introduction

Microalgal populations, including sea ice algae, play an important role in primary production at high latitudes (Poulin, 1990; Arrigo, 2014). Growth of microalgae in ice-covered areas is primarily controlled by seasonal light climate (Smetacek and Nicol, 2005; Peck *et al.*, 2006). Low levels of photosynthetically active radiation (PAR) prevail under sea ice, since the incoming light is reduced by high albedo and attenuation by ice and snow (Ehn and Mundy 2013). In arctic and subarctic seas, increasing day length and solar angle, in conjunction with melting snow, gradually allow more light to penetrate through sea ice at the end of winter (Nicolaus *et al.*, 2012). This increase in light availability is a key driver of blooms in ice-covered seawaters (Legendre *et al.*, 1981; McMinn *et al.*, 2010; Ji *et al.*, 2013; Leu *et al.*, 2015). Although ice algae are unlikely to experience temperatures significantly above the melting point of the sea ice matrix, they may be exposed to temperatures that are several degrees higher in surface seawater. At the same time, irradiance levels can be orders of magnitude higher at the surface than under the ice (Fiala and Oriol 1990, Różańska et al. 2009, Rajanahally et al. 2014). Such large variations of light and temperature are likely to influence photophysiological performance of ice algae, where species with greater flexibility in photoacclimation are afforded a higher chance of survival.

Sea ice microalgal communities are dominated by diatoms (Cota, 1985). Emerging evidence indicates that ice diatoms may be plastic organisms that possess effective photoacclimative strategies (McMinn *et al.*, 2010; Petrou *et al.*, 2011; Reeves *et al.*, 2011; Young *et al.*, 2015). The capacity to dissipate short-term excess excitation pressure through the diadinoxanthin (Ddx)-diatoxanthin (Dtx) cycle provides a selective advantage for ice diatoms over other ice algal taxa in high light conditions (Mock and Valentin, 2004; Kropuenske *et al.*, 2009; Park *et al.*, 2010; Petrou *et al.*, 2010, 2011; Katayama and Taguchi, 2013). It is the de-epoxidation of the xanthophyll Ddx to Dtx during illumination and the reverse reaction in darkness, regulated by the proton gradient across thylakoid membranes (Goss and Lepetit, 2015). The increase in thermal dissipation, which can be quantified as non-photochemical quenching (NPQ) using the chlorophyll fluorescence technique, is related to the accumulation of cellular Dtx in both temperate and psychrophilic diatoms under high light conditions (Lavaud, 2002; Mock and Hoch, 2005; Goss and Jakob, 2010; Wilhelm *et al.*, 2014). In addition, the light-dependent fast regulation

of the Photosystem II (PSII) repair cycle, as well as a relatively stable pool of the reaction center-binding D1 protein, which is encoded by *psbA* gene, also contributes to the high tolerance of diatoms to changing light conditions (Key et al. 2010).

Global warming poses a serious challenge to marine ecosystems (Petrou *et al.*, 2010). However, there exist conflicting views of how increased temperature affects microalgal productivity in sea ice-covered waters. Martin et al. (2012) proposed that increasing temperature will not limit the ability of phytoplankton to survive polar winters and provide inocula for bloom events. After all, warmer seawater results in thinner sea ice with higher light transmission, favoring ice algal growth, as suggested by increasing under-ice blooms (Mundy *et al.*, 2009; Boetius *et al.*, 2013; Arrigo, 2014; Leu *et al.*, 2015; Horvat *et al.*, 2017). Besides, elevated temperature increases membrane fluidity and enzyme activity, and hence plays a positive role in optimizing photosynthetic performance of algal cells under stress (Kanervo *et al.*, 1997; Morgan-Kiss *et al.*, 2006). Nevertheless, earlier ice retreat caused by warming can change the timing of primary production (Ji *et al.*, 2013). Shorter bloom periods for ice algae, and increasing pelagic primary production, both underneath the sea ice and in open water, have been predicted (Arrigo *et al.*, 2008; Nicolaus *et al.*, 2012; Mundy *et al.*, 2014).

Seasonally covered by sea ice, Saroma Lagoon is a semi-closed embayment and is connected with the Sea of Okhotsk through two channels. The primary productivity of this region is largely affected by the abrupt seasonal environmental changes during the retreat of sea ice in spring (Hiwatari *et al.*, 2008; Suzuki *et al.*, 2014; Kasai and Hirakawa, 2015). The Sea of Okhotsk is currently undergoing a period of sustained seasonal sea ice loss, putatively due to global warming (Kashiwase *et al.*, 2014; Ohshima *et al.*, 2014). Elucidation of the photoacclimative strategies employed by ice algae in Saroma Lagoon will provide a better understanding of how warming affects the linkage of biogeochemical processes between Saroma Lagoon and the Sea of Okhotsk during ice melt. Here, we cultured the pennate diatom *Nitzschia* cf. *neglecta*, an ice alga of Saroma Lagoon, under different light and temperature conditions, and provided acclimated cells a short-term high light exposure to simulate light conditions during ice melt. Since Saroma Lagoon is only seasonally covered by sea ice, variation in water temperatures can be very large throughout the year. Therefore, the first aim of this study was to test their tolerance to a higher

temperature. We also focused on the flexibility of the photosynthetic performance in the exposure treatments, including photochemical efficiencies of PSII, cellular pigment composition, and the transcription of two key genes involved in photosynthesis, *rbcL* and *psbA*. The results provide us a better understanding of algal survival in highly changeable coastal water environments subject to seasonal sea ice.

3. Materials and methods

3.1. Identification of the species

A single cell of *Nitzschia* cf. *neglecta* was isolated from Saroma Lagoon (44.12 °N, 143.96 °E) in March, 2012. Following Sugie and Suzuki (2015), organic substances were removed for identification. Part of the 10 °C culture was cleaned using 37 % H_2O_2 and heated to 80 °C for one hour. Then, cells were collected onto polycarbonate filters (pore size 10 µm, Whatman) with gentle vacuum pressure (0.013 MPa) and illuminated with UV radiation for one hour. Cleaned frustules were rinsed with Milli-Q water at least three times and observed with a BZ-9000 epifluorescence microscope (KEYENCE) under a light field. For SEM, the filters with cleaned frustules were sputter coated with gold before analysis (VE-8800, KEYENCE).

A phylogenetic tree of *Nitzschia* spp. including the strain used in this study, together with the related outgroups of *Fragilariopsis* and *Pseudo-nitzschia*, was generated from 18S rRNA using the Neighbor-Joining method in MEGA7 (Kumar et al. 2016). The bootstrap consensus tree inferred from 1000 replicates is taken to represent the evolutionary history of the taxa analyzed. Branches corresponding to partitions reproduced in fewer than 50 % of the bootstrap replicates are collapsed. The evolutionary distances were computed using the Maximum Composite Likelihood method, and are presented as the number of base substitutions per site. 18S rDNA sequences of *Nitzschia* and outgroups downloaded from the NCBI database (National Center for Biotechnology Information, Maryland, USA) were trimmed at the ends and identical sequences were excluded before alignment. A final alignment included 98 unique sequences spanning 516 bp. The reverse transcription was conducted following the methods in section 2.4. The following primers were set using Primer Premier 6 (PREMIER Biosoft International) for *Nitzschia* 18S rDNA amplification: forward 5' AATTCCAGCTCCAATAGCGT 3', reverse 5'

TAAGTTTCAGCCTTGCGACC 3'. The partial 18S region that was amplified includes the V4 region, which represents the largest and most complex of the highly variable regions within the 18S locus (Kermarrec et al. 2013). The sequencing work was conducted in the same way as described for *psbA* in Section 2.4.

3.2. Experimental setup

The strain was maintained in f/2 medium (Guillard, 1975) at 2 °C at an irradiance of 20 µmol photons m^{-2} s^{-1}, which was provided by cool white fluorescent light (Panasonic FL20SS・W/18, Osaka, Japan). Before the experiment, penicillin and streptomycin (final concentrations of 25 U mL^{-1} and 25 µg mL^{-1}, respectively, 17-603E, Lonza Group Ltd., Basel, Swiss) were added to the culture medium to inhibit bacterial growth following the methods of Sugimoto et al. (2007). After antibiotic treatment, culture samples were stained with DAPI (4, 6-diamidino-2-phenylindole, final concentration of 2 µg mL^{-1}) and were checked for bacteria with BZ-9000 epifluorescence microscope (KEYENCE, Osaka, Japan; Cottrell and David 2003).

Natural seawater was filtered through Whatman GF/F glass fiber filter (47 mm in diameter, nominal pore size 0.7 µm) and was adjusted to the *in situ* salinity of 30 (Kudoh, 1993; Kudoh *et al.*, 1997; McMinn and Hattori, 2006) with Millipore Milli-Q water. The addition of f/2 nutrients and vitamins were conducted before autoclaving. The cultures were maintained in 2 L polycarbonate bottles (Thermo Scientific Nalgene, Rochester, USA) to reach a final cell concentration of around 25,000 cells mL^{-1} on day 5 or 6 in a batch culture. Temperature and light conditions were controlled in an incubator (MIR-554, Sanyo Electric Co., Ltd., Osaka, Japan). The light was provided by fluorescent lamps for plants (20W FL20SS・BRN/18, TOSHIBA, Tokyo, Japan) and different light intensities were achieved by adjusting the distances between the bottles and the light source. The light/dark cycle was 12 h/12 h. The irradiance levels of the upper and lower ice algal layers were 11 to 52 µmol photons m^{-2} s^{-1} at the sampling site (Katayama and Taguchi, 2013), so a mean value of around 30 µmol photons m^{-2} s^{-1} was chosen as the low irradiance level (LL) in this work. The high level (HL) was set at 100 µmol photons m^{-2} s^{-1}. Although the measured water temperature was around –1.5 °C in March at the sampling site (Kudoh, 1993; Kudoh *et al.*, 1997; McMinn and Hattori, 2006), the temperature

levels were set at 2 and 10 °C. An experimental temperature below zero was not feasible due to frost formation in the incubator used in this study. PAR in culture bottles was measured with a 4 π irradiance sensor (QSL-2100, Biospherical Instruments Inc., San Diego, USA).

After a 6-day incubation period, the cells acclimated to different light and temperature conditions were transferred to new f/2 medium, so they could reach a concentration of around 10,000 cells mL^{-1}. The newly transferred cells were used in the high light exposure experiment the next day. The high light condition was established at 450 μmol photons m^{-2} s^{-1} using the same fluorescent lamp systems mentioned above. The exposure (hereafter E) lasted for 120 min. After being exposed for 60 min, some cells were transferred to incubators to recover (hereafter R) in the dark for 60 min, and the remaining cells were exposed for another 60 min. During the E and R experiments, we collected samples to measure cellular pigment composition, photochemical efficiency of PSII (YII), nonphotochemical quenching (NPQ), and the transcription of *rcbL* and *psbA* genes, which encode the large subunits of RuBisCO and the D1 protein of PSII, respectively. For cells grown at 2 °C, sample treatments for the E and R experiments were conducted in a low temperature laboratory, which was maintained at 2 °C. Similarly, for the cells grown at 10 °C, the experiment was conducted in a room maintained at ca. 10 °C. All exposure experiments were conducted at the same time in the middle of the light phase to avoid physiological patterns that are related to circadian rhythm rather than to temperature and light effects.

3.3. Growth rates

Cell abundance was counted daily using an inverted light microscope (CKX41-FI, Olympus, Tokyo, Japan). The specific growth rate (μ, d^{-1}) was calculated using the following equation (Stein, 1979): $\mu = \ln (N_t - N_0)/ (t - t_0)$, where N_t and N_0 are the cell abundance at day t and day 0, respectively, and t and t_0 are days t and 0 of incubation.

3.4. Pigments

Samples were taken at E0, E2, E5, E15, E30, E60, and E120, and at R5, R15, R30, and R60, with the letter corresponding to the exposure or recovery period, respectively, and the number corresponding to the time in minutes. Samples of 15 mL was filtered onto GF/F glass fiber

filters (25 mm in diameter, nominal pore size 0.7 μm, Whatman, Buckinghamshire, UK) under gentle vacuum pressure (< 0.013 MPa) and dithiothreitol (DTT) solution (Sigma-Aldrich, St. Louis, USA) were immediately added to each filter (final concentration of 300 μmol L^{-1}; Olaizola et al. 1994) to inhibit the operation of the Ddx-Dtx cycle. The filter samples obtained were frozen quickly in a deep freezer at –80 °C for later analysis. Following Suzuki et al. (2015), pigments were extracted from each filter into *N,N*-dimethylformamide (DMF) using a bead-beating technique, and then chlorophylls and carotenoids were analyzed using Ultra-High Performance Liquid Chromatography (UHPLC). The identified pigments were grouped as photosynthetic carotenoids (PSC = fucoxanthin (Fxn)), photoprotective carotenoids (PPC = diadinoxanthin + diatoxanthin + β-carotene (Car)), or total chlorophyll (TChl = Chl *c*1 + Chl *c*2 + Chl *a*), to assess the extent of light stress and photoacclimation in algal cells (Roy *et al.*, 2011; Schuback *et al.*, 2017). The de-epoxidation state index (DES) of the Ddx-Dtx cycle was calculated as DES = Dtx/(Ddx + Dtx) (Ruban *et al.*, 2004). Ddx and Dtx represent the cellular content of diadinoxanthin and diatoxanthin, respectively. To investigate the contribution of Dtx from different sources to NPQ increase, some assumptions were made based on previous studies (Olaizola *et al.*, 1994; Lavaud *et al.*, 2004; Lavaud and Lepetit, 2013). Specifically, we assumed that the only cause for a decrease in Ddx during exposure was its transformation to Dtx. Changes in the contents of each pigment and NPQ, compared to those at E0, are represented by ΔDdx (-), ΔDtx (+), and ΔNPQ (+). Then, ΔDtx (+) could be divided into two parts: Dtx that resulted from the transformation of Ddx (absolute ΔDdx (-)), and Dtx that was synthesized *de novo* (the difference between the two absolute delta values at a given time point). We assume that all increases of Ddx were a result of transformation from Dtx in the darkness. Changes in the contents of each pigment and NPQ, compared to those at E60, are represented by ΔDdx (+), ΔDtx (-) and ΔNPQ (-).

3.5. qPCR and RT-qPCR of rbcL and psbA genes

DNA and RNA samples were taken at E0, E15, E60, and at R15 and R60. The DNA and RNA sampling, extraction and purification were conducted following Endo et al. (2013, 2015). The quantitative PCR (qPCR) of *rbcL* was also conducted following Endo et al. (2015). The transcription level of each gene was determined as the number of cDNA gene copies

standardized by the DNA gene copies in samples taken at the same time point. For the *psbA* gene, standards were generated from plasmid DNA (T-Vector pMD20, TaKaRa) with *psbA* gene fragments (105 bp in size) from the culture strain. The plasmid DNA standard was then linearized with *Hind*III (TaKaRa) and quantified using a NanoDrop spectrophotometer (ND-1000, ThermoFisher Scientific Inc.). The *psbA* gene sequence was obtained using the BigDye v.3.1 Terminator Cycle Sequencing technology (ThermoFisher Scientific Inc.). PCR products were analyzed on an Automated Capillary Electrophoresis Sequencer ABI 3130*xl* (ThermoFisher Scientific Inc.). The following primers were set using Primer Premier 6 (PREMIER Biosoft International, Palo Alto, CA, USA) for the amplification of the *psbA* gene: forward 5' GGTTACAAATTCGGTCAAG 3', reverse 5' AGCACGAGAGTTGTTGAATGA 3'. The thermal cycler conditions for the *psbA* gene were the same as for *rbcL* in Endo et al. (2015), except that the annealing temperature was 59 °C for the *psbA* gene.

3.6. Chlorophyll fluorescence parameters

A pulse-amplitude modulated fluorometer (Water-PAM, Walz, Effeltrich, Germany) was used to determine the chlorophyll fluorescence parameters of cells. Samples for fluorescence analysis were placed in a quartz cuvette and illuminated by red-LED with a peak illumination at 655 nm. The maximum photochemical efficiency (F_v/F_m), effective photochemical efficiency under growth light (YII), NPQ, and rapid light curve (RLC) were measured for the acclimated cells. F_v/F_m and YII values were provided directly by the software. YII was calculated as YII = $(F_m' - F_t)/F_m'$. F_t is the steady-state fluorescence under actinic light and F_m' is the maximum fluorescence with actinic light. NPQ was calculated as NPQ = $(F_m - F_m')/F_m'$, where F_m is the maximum fluorescence after a 15-min period of darkness and F_m' is the maximum fluorescence with actinic light. Eight irradiance levels, the maximum of which was approximately 2,000 μmol photons m^{-2} s^{-1}, were used for RLC determination. At the end of the 20 s illumination, a saturating pulse was applied to get F_m'. The saturating pulse was 7,000 μmol photons m^{-2} s^{-1} and lasted for 400 ms for all measurements. Relative Electron Transport Rate (rETR, relative unit) was calculated as rETR = YII × PAR × 0.5, assuming that light was equally distributed between the two photosystems. The α-slope (α), minimum saturation irradiance for rETR (I_k), and maximal relative electron transport rate ($rETR_{max}$) were obtained by fitting the curves with a

quadratic equation model following Eilers and Peeters (1988). The α and I_k are proxies for the photosynthetic efficiency of low light capture and the minimum saturating irradiance in photosynthesis (i.e., an indicator of the photoacclimation or photoadaptation to the light environment), respectively. The rETRmax is a proxy for the maximum electron transport capacity through PS II.

During the exposure experiment, YII was determined with actinic light of around 450 µmol photons m^{-2} s^{-1}. To quantify the changes in YII and NPQ during exposure and recovery, YII or NPQ were plotted against exposure or recovery time and the curves were fitted with first-order exponential decay functions in the form of $y = y_0 + Ae^{-kx}$. The decay constants (k) were used to estimate the rates of change in YII and NPQ.

3.7. Statistics

Factorial Analysis of Variance was carried out to test the combined and individual effects of temperature and irradiance. All analyses of variance were conducted after performing a test for homogeneity of variance. For data that did not satisfy the requirement for homogeneity of variance, the treatment effects were examined using Mann-Whitney tests. The significance level was set at 0.05. The statistical analysis was conducted with SPSS Statistics software version 19.0 (SPSS Inc., Chicago, USA).

4. Results

4.1. Identification of the species

Light Microscopy: The cells are solitary with nitzschioid symmetry (Fig. 3.1, b, e, and f). Valves are linear to narrowly lanceolate in valve view, with rounded apices. The cell contains two large chloroplasts, one towards each pole (Fig. 3.1, a-b). Valve dimensions (n =20) are as follows: length 22.3–75 µm, width 7.2–8.4 µm. Striae are not discernible in LM. There are six to nine fibulae per 10 µm, and these are evenly spaced, except for a distinct central nodule, (Fig. 3.1, d–i). The raphe is eccentric, raised on a keel above the valve surface (Fig. 3.1, a–i).

Scanning Electron Microscopy: The valve face curves up from the mantle towards a raphe lying atop a prominent keel. The external distal raphe endings terminate into fissures, which are

slightly curved around each valve apex (Fig. 3.2, i and m). The internal proximal raphe endings are straight (Fig. 3.2, h, j, and l). Striae are mostly composed of evenly spaced elliptical to round areolae, with about 35–37 per 10 µm, continuing from the valve face onto the keel (Fig. 3.2, i). Fibulae are evenly spaced throughout the valve, located every two to three striae, with the central two fibulae widely separated (up to 3 µm).

The phylogenetic tree of *Nitzschia* spp. generated from the 18S rRNA gene is shown in Fig. 3.3. The morphology resembles that of *N. neglecta* (Medlin and Hasle, 1990), which so far has only been reported from the Antarctic, and for which no 18S rDNA sequence is available. The sequence of our culture has been deposited to the nucleotide database in NCBI GenBank (accession number LC387780). In the following we refer to the species as *N.* cf. *neglecta*.

4.2. Growth rate

The specific growth rates in batch culture showed some variations (Fig. 3.4, a and b). The maximum growth rate was found under 100 µmol photons m^{-2} s^{-1} (HL) at 10 °C on day 3, reaching 0.65 ± 0.04 d^{-1}, while the minimum was 0.35 ± 0.02 d^{-1} under 30 µmol photons m^{-2} s^{-1} (LL) at 2 °C on day 6. There was a decreasing trend towards the end of incubation. Higher light enhanced growth from day 3 to 6 at 10 °C but only on Day 3 and 4 at 2 °C ($p < 0.05$). On average, there was no significant difference between growth rates at different irradiance levels at 2 °C, while higher light enhanced growth by around 30 % at 10 °C (Fig. 3.4c, $p < 0.05$). Higher temperatures increased growth rate by around 40 and 30 % under the low and high irradiance levels, respectively (Fig. 3.4c, $p < 0.05$).

4.3. Photoacclimation

With PAM fluorometry, alpha (α) was stable under the four growth conditions and only affected by irradiance levels at 2 °C (Table 3.1), with higher light capture efficiency occurring in LL ($p < 0.01$). $rETR_{max}$ showed large variation only at 10 °C ($p < 0.05$). The highest and lowest $rETR_{max}$ values were around 135 and 80 (relative units) at HL and LL at 10 °C, while similar values of around 100 were found at 2 °C. I_k was higher under HL at both temperatures ($p < 0.01$). Similar to $rETR_{max}$, a larger variation of I_k was also observed at 10 °C. I_k under HL was nearly two times higher than that at LL at 10 °C, reaching over 430 µmol photons m^{-2} s^{-1}, while at 2 °C the HL to

LL ratio was less than 1.2. LL-acclimated cells had higher F_v/F_m ($p < 0.01$, Table 3.1).

4.4. Changes in YII and NPQ during exposure and recovery

Changes in YII and NPQ over time showed opposite trends during the E (exposure) and R (recovery) experiments (Fig. 3.5). The decay constant (k) implies that changes of YII during exposure were affected by both growth temperature and light history. The cells grown in LL at 2 °C had the largest k ($p < 0.01$), implying the fastest decrease among treatments. The lowest decrease was found in cells grown in HL at 10 °C, and under such conditions k only reached 14 % of the maximum in LL at 2 °C. The effect of light history on NPQ after exposure was temperature-dependent. The fastest onset of NPQ was found in cells grown in HL at 2 °C and in LL at 10 °C ($p < 0.05$). The recovery of YII and NPQ in the dark was faster at 2 °C ($p < 0.01$). YII at E120 was only affected by temperature. Larger values (>0.2) of YII were found at 10 °C ($p < 0.01$), while YII were less than 0.1 at 2 °C. Similarly, YII at R60 was also higher at 10 °C ($p < 0.01$). After a 60-min period of darkness, full recovery of YII (reaching F_v/F_m value at E0) was only found in the cells grown in HL at 10 °C, while under other conditions the recovery was around 90 %. NPQ at E120 was highest in HL at 2 °C, and lowest in HL at 10 °C ($p < 0.05$). At 10 °C, NPQ reached 0 only 20 min from the onset of the R treatment.

4.5. Pigments

After an incubation period of six days, cellular Ddx content was not affected by either growth light or temperature (Table 3.2). Only TChl and total pigments were affected by the interaction of the two factors. In the HL condition, the extent of difference between the two temperatures was small for most pigments. However, in the LL condition, the cellular content of the PSC pigment Fxn and the two chlorophylls were higher at 10 °C ($p < 0.05$), and the values were nearly 1.6-fold higher than those at 2 °C. Cellular β-Carotene (Car) levels only showed a difference under different light conditions, and were more abundant in LL ($p < 0.05$). Generally, the LL to HL ratios of each cellular pigment content at 10 °C were higher than those at 2 °C, except for Ddx and Dtx. The highest ratios were found in Fxn and the two chlorophylls at 10 °C, reaching around 2.2. Yet, this ratio for PPC was only 1.53. The ratios for 2 °C were similar for all pigments, and were around 1.1, except for the PPC pigments. Due to a larger Ddx-Dtx pool, this ratio for

PPC was larger and reached 1.42. It should be noted that Dtx was more abundant at the lower temperature in both light conditions ($p < 0.05$).

Temperature was likely to be the main cause of variations in cellular pigment content with changing light conditions. At 2 °C, there was a joint decreasing trend for all four pigment groups as soon as the cells were exposed to high light (Fig. 3.6, a and b, $p < 0.001$). The minimum values were found at E30. For the cells grown in LL, cellular contents of all pigments were reduced by around 18 % at E30, fully recovered by E60, and then remain little changed until E120 (Fig. 3.6b). However, for HL-grown cells, recovery in light was only found for PPC. Absolute cellular PSC levels continued to decrease and reached a minimum at E120 (Fig. 3.6a, $p < 0.001$). Contrary to the decreases at 2 °C, increasing trends of relative cellular PPC and TChl content were found after the onset of the exposure at 10 °C (Fig. 3.6, c and d), although those of PSC were little changed. For HL-grown cells, PPC continued to increase and was 28 % higher at E120 than that at E0 ($p < 0.001$). At 10 °C, absolute cellular TChl contents increased by 10 % during the first minute of exposure ($p < 0.01$) then stayed stable until E60, but then decreased to the original level at E120. For LL-grown cells at 10 °C, relative cellular PPC levels also increased when transferred to the exposure; however, the maximum PPC levels were reached at an earlier time point, E60, and remained almost constant until E120 (Fig. 3.6d, $p < 0.001$). During the first 5 min of the dark recovery, a 10 % decrease of all pigment groups was found in cells grown in LL at 2 °C (Fig. 3.6b, $p < 0.001$). They then returned to the E0 level at R15 and remained stable until the end ($p < 0.001$). Recovery was also found in HL-grown cells at 2 °C (Fig. 3.6a, $p < 0.001$), despite a lack of a decrease at the beginning of darkness. This decrease was found in cells grown at 10 °C in HL (Fig. 3.6c, $p < 0.05$). Regardless of this decrease, absolute cellular PPC levels in these cells was still over 13 % greater than those at E0 and remained at higher levels until the end of the darkness period ($p < 0.001$). For cells grown in LL at 10 °C, absolute cellular PPC contents continued to increase and, compared to those observed at E0, were around 14 % higher after 60 min in the dark.

The two pigments in the Ddx-Dtx cycle showed reverse patterns during the E and R treatments (Fig. 3.7). At E0, the Ddx-Dtx cycle pool was mostly consisted of Ddx, and Dtx accounted for less than 10 % in all cells. A large part of the Ddx to Dtx transformation was finished during

the first 15 min of exposure, which reduced cellular Ddx content to half of its original value (Fig. 3.7, a and b). At E120, cellular Ddx contents of all cells reached the minimum and became less than one third of initial values. Changes in the De-epoxidation State Index (DES) during the E and R treatments showed similar trends under all conditions (Fig. 3.7, c and f). DES curves were fitted with exponential decay functions used for NPQ fitting and the decay constant (k) values were mainly controlled by growth temperatures. The increasing rate in the light was nearly 1.8 times higher, and the decreasing rate in the dark was 1.4 times higher, at 10 °C compared to that at 2 °C ($p < 0.05$). Changes in the dark were much slower than those in the light at both temperatures. The k values for the E treatment were nearly 3 and 3.7 times greater than that for the R treatment at 2 and 10 °C, respectively ($p < 0.05$ for 2 °C; $p < 0.01$ for 10 °C). After R60, cellular Dtx levels at both temperatures had declined by more than 50 %.

Significant correlations between Ddx-transformed Dtx and ΔNPQ were found ($r > 0.8$) at both temperatures (Fig. 3.8), whereas the *de novo* synthesized Dtx and ΔNPQ were moderately correlated ($r \sim 0.5$) at 10 °C. Total cellular Dtx and NPQ were also positively correlated with each other at both temperatures.

4.6. Changes in rbcL and psbA gene transcription

No clear trends were found in the transcription levels of the *rbcL* gene (Fig. 3.9). For the HL-grown cells, the transcription levels of *rbcL* gene at E15 were higher at 2 °C ($p < 0.05$). *psbA* transcription levels showed a similar decreasing trend during the E and R treatments at the lower temperature. Transcription levels of the *psbA* gene in HL-grown cells at 2 °C were nearly three times higher, when compared with those of LL-grown cells (all $p < 0.01$) .

5. Discussion

Some ice algal species may not be able to survive at high temperatures due to a limited thermal tolerance range. Previous studies have shown that most ice diatoms are only able to tolerate temperatures as high as 8 °C (Fiala and Oriol, 1990; Mock and Valentin, 2004; Coello-Camba *et al.*, 2015). However, Sakshaug (2004) proposed that arctic species do not grow better at low temperatures than their temperate counterparts. Furthermore, species from both polar and temperate waters have often been found to have optimal growth temperatures considerably

higher than the mean annual temperatures in their habitats (Thomas et al. 2012, Karentz and Smayda, 1984). The strain used in this study not only exhibited a high temperature tolerance of up to 10 °C, which is much higher than that of the environment in the sea below the ice, but also grew faster at that temperature under both irradiance levels. Interestingly, this species can grow at 20 °C under dim light in an incubator (data not shown). Indeed, the fastest specific growth rate of around 0.65 was found in cells grown in HL at 10 °C, and was higher than that previously reported for sea ice diatom communities *in situ*, as well as the reported maximum growth rates under optimal temperatures (Lacour et al. 2017). However, although growth rates were comparable to those of temperate diatom species grown at similar temperatures, they were still much lower than the maximum growth rates of those temperate species (McMinn A. *et al.*, 2005; McMinn *et al.*, 2014; Coello-Camba *et al.*, 2015; Lacour *et al.*, 2017). Considering that the water temperature of Saroma Lagoon may rise up to around 20 °C in summer, this result suggests that despite being isolated from an ice core, the species we used here can tolerate a wide range of temperatures and can continue its growth throughout the year.

The high F_v/F_m and I_k values in high light, as well as the fast recovery of YII in the dark indicates a weak susceptibility to high light stress of this species. F_v/F_m values were above 0.65, indicating that the photosynthetic apparatus was functional under the culture conditions. Variations of $rETR_{max}$ and I_k between HL and LL were higher at 10 °C compared with 2 °C (see Table 3.1). These results suggest a larger flexibility of photoacclimation at the higher temperature. Similarly, Torstensson et al. (2013) found significant increases of F_v/F_m and primary productivity at 2.5 °C compared to −1.8 °C in the ice diatom *N. lecointei*, isolated from sea ice of the Amundsen Sea. Considering the seeding role of ice algae due to their release from the bottom layer of sea ice into the surrounding seawater after ice melt (Mundy *et al.*, 2011), we propose that the observed ice algal bloom in early spring can be partly ascribed to liberation of cells into the surrounding sea water from the restrictive freezing temperature in sea ice.

Contents of the PSC Fxn (fucoxanthin) and the two chlorophylls were higher in LL than in HL, and the extent of the difference was similar for each temperature. A study on the pigment composition of early spring microalgal communities in Saroma Lagoon revealed that Chl *c* and Fxn, normalized to Chl *a* values, were higher in microalgae living in the upper ice layer, indicating

that these two pigments might contribute to high light acclimation (Kashino *et al.*, 1998). Another study reported that contents of cellular Chl *c* and Fxn in the psychrophilic diatom *Fragilariopsis cylindrus* increased when shifting cells grown at 35 µmol photons m^{-2} s^{-1} from 5 to –1.8 °C (Mock and Valentin 2004). However, the ratios in this study were almost identical under the four culturing conditions, with Chl *c* to Chl *a* ratio around 0.16, and Fxn to Chl *a* ratio around 0.56 (see Table 3.2). Furthermore, the pigment ratios remained almost steady during the exposure and dark recovery periods. We suggest that these ratios could be rather conservative even under changing light conditions in the present species.

The PPC pigment Dtx content at lower temperature was higher and showed a larger variation. Because Dtx is known as an energy quencher in photoprotection (Goss and Jakob, 2010), we expected less accumulation of this pigment under lower irradiance levels. Instead, our results suggest that cells grown at 2 °C used more Dtx for acclimation to the colder environment. Such an increase in Dtx content in response to cold exposure was also reported in *F. cylindrus*, even in cells grown at 3 µmol photons m^{-2} s^{-1} (Mock and Valentin 2004, Mock and Hoch 2005). Acclimation of photosynthesis to low temperatures is probably regulated similarly to acclimation to high irradiance (Öquist, 1983; Maxwell *et al.*, 1994; Ensminger *et al.*, 2006; Hüner *et al.*, 2012). Under both circumstances, algae generally absorb more light, while less energy flows to the Electron Transport Chains (ETCs) due to lowered membrane fluidity and enzyme activity (Kanervo *et al.*, 1997; Morgan-Kiss *et al.*, 2006). This may also explain a phenomenon that only occurred at 2 °C, irrespective of light history: the immediate decrease of cellular pigment content when cells were transferred to the exposure condition (see Fig. 3.6). The sudden exposure to high light can induce high excitation pressure on photosynthetic ETCs, causing photoinhibition. This situation is exacerbated by the low temperature (Ensminger et al. 2006). Therefore, it was not unexpected that cells grown in LL at 2 °C exhibited the fastest decreasing rate of YII when exposed to 450 µmol photons m^{-2} s^{-1} (see Fig. 3.5). A reduction in cellular pigment content was likely one of their emergency responses, since the absorption properties of densely packed pigments would be disadvantageous under such conditions (Wilhelm et al. 2014).

Compared to the simple pattern of a faster YII decrease at the lower temperature, the NPQ pattern of increase during the E treatment appeared to be complex and was probably affected

by multiple factors. Here, we show that NPQ and cellular Dtx content during the E and R treatments were linearly correlated (see Fig. 3.8g and h). Consequently, given a group of cells cultured in a certain condition, higher values of NPQ could be explained by higher content of Dtx. The slopes of the fitted lines in Fig. 3.8g and 5h reflect different quenching efficiencies of cells under each growth condition. Overall the quenching efficiency was greater at the lower temperature. At 10 °C, the final Dtx increased by 15–22 folds, which was much higher than that at 2 °C. While the final NPQ values at the two temperatures were similar to each other. Some studies proposed that Dtx synthesized *de novo* in high light illumination did not participate in the NPQ mechanism (Schumann *et al.*, 2007; Lepetit *et al.*, 2010). In the present study, both components of ΔDtx were found to be correlated to the changed NPQ at 10 °C (see Fig. 3.8), while the Dtx synthesized *de novo* was not linearly correlated to ΔNPQ at 2 °C. One problem was that the difference between ΔDtx (+) and the absolute value of ΔDdx (-) was negative at most time points at 2 °C. Consequently, even if there was some newly synthesized Dtx, it is impossible to separate it from the total ΔDtx (+). Further studies are needed to investigate whether this part of Dtx can contribute to NPQ at a temperature as low as 2 °C. It was surprising that both YII recovery and NPQ relaxation in the dark were faster at 2 °C. This is also reflected by the difference in the intercept between the two temperatures in Fig. 3.8c and 5d. At 2 °C, the intercept was higher, mainly resulting from the mismatch between the decreasing rates of Dtx and NPQ. This suggests that NPQ relaxation in the dark may include mechanisms other than the Ddx-Dtx cycle in this species. Mock et al. (2017) found 11 light-harvesting complex stress-related (*Lhcx*) sequences in the psycrophilic pennate diatom *Fragilariopsis cylindrus*. This indicates that *Lhcx* proteins possibly play an important role in response to stressful conditions at low temperatures. Additionally, Bailleul et al. (2010) demonstrated that the *Lhcx* proteins act as molecular controllers of NPQ in the pennate diatom *Phaeodactylum tricornutum*. *Lhcx* proteins belong to the light harvesting protein family and can bind Dtx to the Fucoxanthin Chl *a*/*c*-binding Protein (FCP) antenna in diatoms. Based on the model for NPQ proposed by Goss and Lepitit (2015), higher concentrations of the *Lhcx* protein bound Dtx induce higher NPQ in diatom cells. During the light exposure, *Lhcx* proteins were synthesised and bound to Dtx. In the darkness, the decrease in NPQ is resulted from the detachment of Dtx as well as its

subsequent conversion to Ddx. It is likely that more *Lhcx* proteins were synthesised at 10 °C in this study, which means more time would be needed for the full Dtx detachment. This may explain the remaining NPQ during the first 15 min of darkness at the higher temperature.

It is difficult to determine whether a fast regulation of PSII repair cycle was involved in the photoprotective strategies from the *psbA* transcription data. Petrou et al. (2010) found that ice algae are possibly intrinsically unsusceptible to high irradiance levels and a modest PSII repair rate could keep in pace with the photoinactivation. Besides, psychrophilic algae are likely to maintain a large reserve of PSII subunits to compensate for restricted D1 clearance even under moderate light conditions (Ni *et al.*, 2017). This is in accordance with our results that the transcription levels of *psbA* were highest in HL-grown cells at 2 °C. The above studies also found that it was the NPQ-induced downregulation of PSII that mainly contributed to the strong capacity to withstand high light at low temperatures in the studied psychrophilic algae. In the present study, no clear upregulated transcription was found during the exposure. Considering the full or nearly full recovery of YII in the dark in the present work, it is likely that the main photoprotection was dependent on the Ddx-Dtx cycle while PSII repair played a minor role in *Nitzschia* cf. *neglecta*. The transcription level of the *rbcL* gene can be used as a proxy for the carbon fixation activity of marine phytoplankton (Corredor *et al.*, 2004; John *et al.*, 2007), as it catalyzes the first step in inorganic carbon fixation for eukaryotic phytoplankton. With a turnover rate that decreases dramatically with temperature, its high production has been suggested to be one adaptive mechanism in response to cold environments, in order to counterbalance its poor catalytic efficiency at low temperatures (Devos *et al.*, 1998; Morgan-Kiss *et al.*, 2006; Young *et al.*, 2015). In the present study, no clear pattern has been found in *rbcL* transcription. Although a post-transcriptional regulation cannot be ruled out, we suggest that this species has a high temperature flexibility in their carbon fixation. Further studies are needed for better interpretation of our results and for understanding the function of photosynthetic genes in ice algae in response to changing environments.

6. Conclusions

Our investigation of photosynthetic responses of *N.* cf. *neglecta* to high light revealed that the

photoacclimative plasticity of this species was largely shaped by temperature. Its survival and prevalence benefit from higher temperature due to more effective photoprotection. The weak shade adaptation may contribute to a rapid response to changing light when released into shallow coastal waters during ice melt. The rapid decrease of cellular pigment content in high light only occurred at 2 °C, indicating an intimate coupling of acclimation of photosynthesis to low temperatures and high light. The operation of the Ddx-Dtx cycle served as the main photoprotective strategy against high light while regulation of *psbA* and *rbcL* at transcription levels played a minor role. Despite its occurrence in sea ice, this species is not strictly psychrophilic, but has a wide temperature tolerance that can contribute to its ecological success in Saroma Lagoon ice algal and phytoplankton communities. We believe that these findings can apply to some other species in Saroma Lagoon. The wide tolerance to both temperature and light changes suggest that the thinning of sea ice and higher temperatures in a warmer world may cause more intense blooms in Saroma Lagoon, and potentially other coastal waters with seasonal ice cover.

7. Figures and tables

Table 3.1 Photoacclimation parameters of rapid light curves fitted with the quadratic equation model in Eilers and Peeters (1988) and photochemical efficiencies of PSII. Mean values (± SD) are the average of three independent measurements.

Temperature	Light	α-slope	$rETR_{max}$ (relative unit)	I_k (µmol photons m^{-2} s^{-1})	F_v/F_m	YII
2 °C	HL	0.29 ± 0.01	98.21 ± 1.07	334.15 ± 9.89	0.65 ± 0.00	0.54 ± 0.01
	LL	0.34 ± 0.01	97.35 ± 2.18	284.60 ± 11.34	0.70 ± 0.00	0.63 ± 0.01
10 °C	HL	0.31 ± 0.04	135.44 ± 26.08	433.17 ± 27.77	0.68 ± 0.00	0.50 ± 0.01
	LL	0.34 ± 0.06	79.94 ± 5.75	239.41 ± 34.26	0.70 ± 0.00	0.57 ± 0.01

Table 3.2 Cellular pigment content (pg cell^{-1}) under different conditions. Mean values (± SD) are the average of three independent measurements.

	2°C		**10°C**	
	HL	**LL**	**HL**	**LL**
Fxn	3.70 ± 0.16	3.90 ± 0.15	3.41 ± 0.32	7.43 ± 1.61
Ddx	0.75 ± 0.04	0.80 ± 0.04	0.79 ± 0.05	1.08 ± 0.22
Dtx	0.05 ± 0.01	0.07 ± 0.00	0.02 ± 0.01	0.03 ± 0.01
Car	0.14 ± 0.01	0.15 ± 0.00	0.15 ± 0.02	0.25 ± 0.05
Chl *a*	6.62 ± 0.30	6.92 ± 0.22	5.89 ± 0.48	12.96 ± 2.79
Chl *c*	1.06 ± 0.05	1.10 ± 0.03	0.98 ± 0.10	2.17 ± 0.47
PSC	3.70 ± 0.16	3.90 ± 0.15	3.41 ± 0.32	7.43 ± 1.61
PPC	0.94 ± 0.05	1.02 ± 0.04	0.90 ± 0.05	1.38 ± 0.09
TChl	7.68 ± 0.34	8.03 ± 0.25	6.48 ± 0.25	14.67 ± 0.85
sum	12.32 ± 0.55	12.94 ± 0.43	11.25 ± 0.97	23.91 ± 5.15

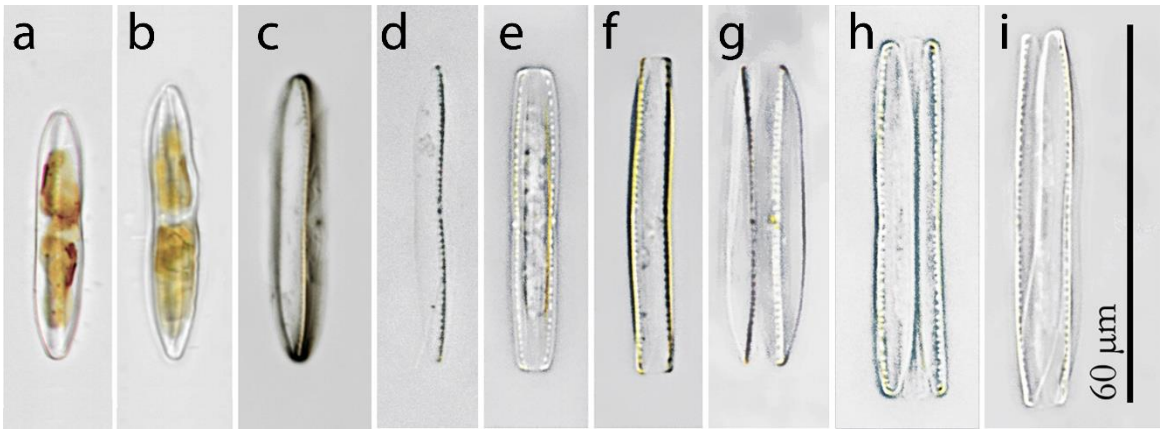

Fig. 3.1 LM photos of *Nitzschia* cf. *neglecta*. (a) and (b), living cells in the culture; (c) empty frustule in the culture; (d–i), valves treated with 30 % H_2O_2 plus UV radiation.

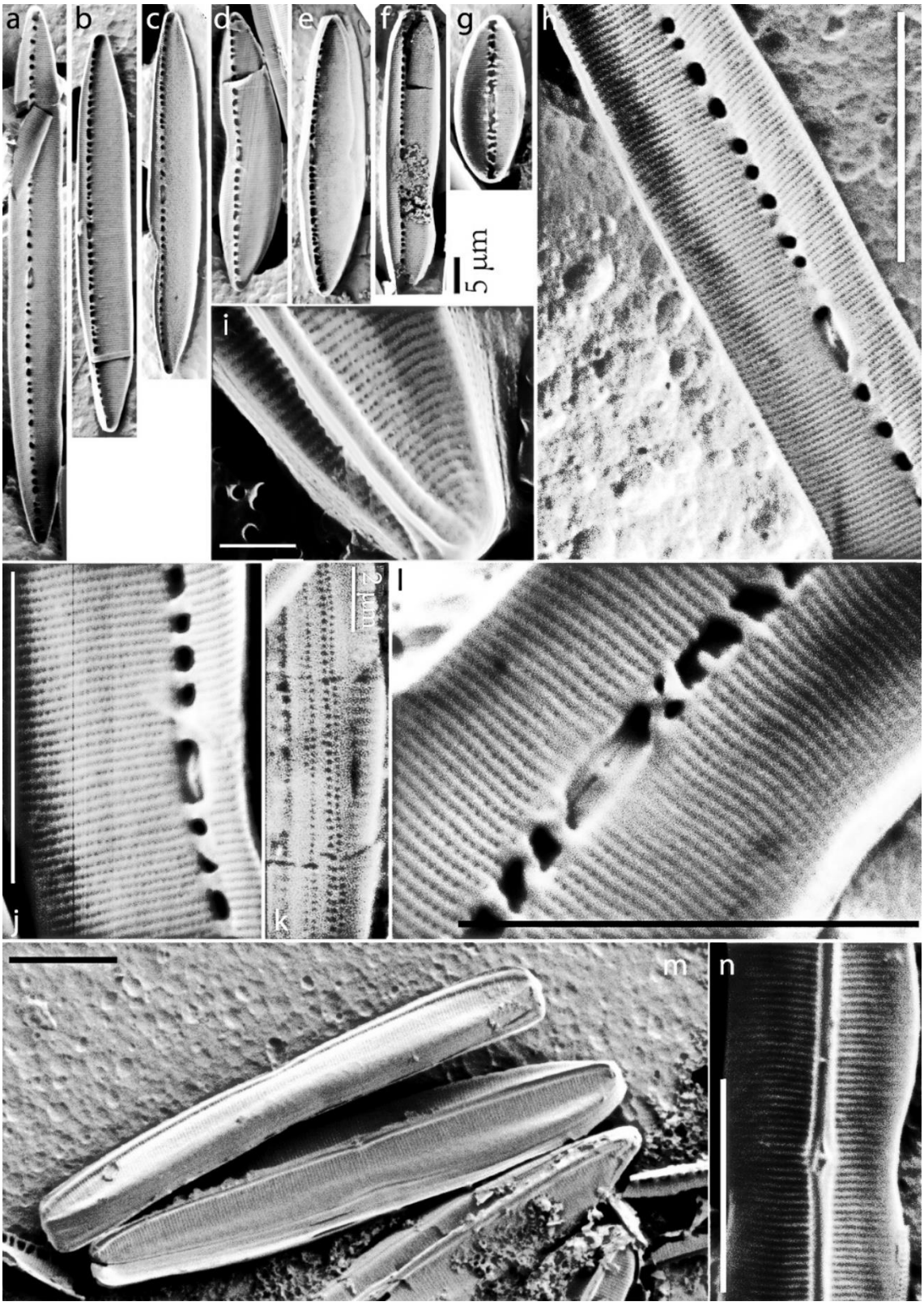
a
b
c
d
e
f
g
5 µm
h
i
j
k
2 µm
l
m
n

Fig. 3.2 SEM photos of *Nitzschia* cf. *neglecta*. (a–g), interior whole single valves showing observed size range; (i), external valve showing raphe end; (h), (j) and (l), internal valve showing detail of fibulae with central raphe endings; (k), external valve showing girdle band; (m), girdle and girdle-valve view of two cells; (n), external valve showing central nodule. Bar in (a–g), 5 μm; In (h), (j), (l), (m) and (n), 10 μm; In (i) and (k), 2 μm.

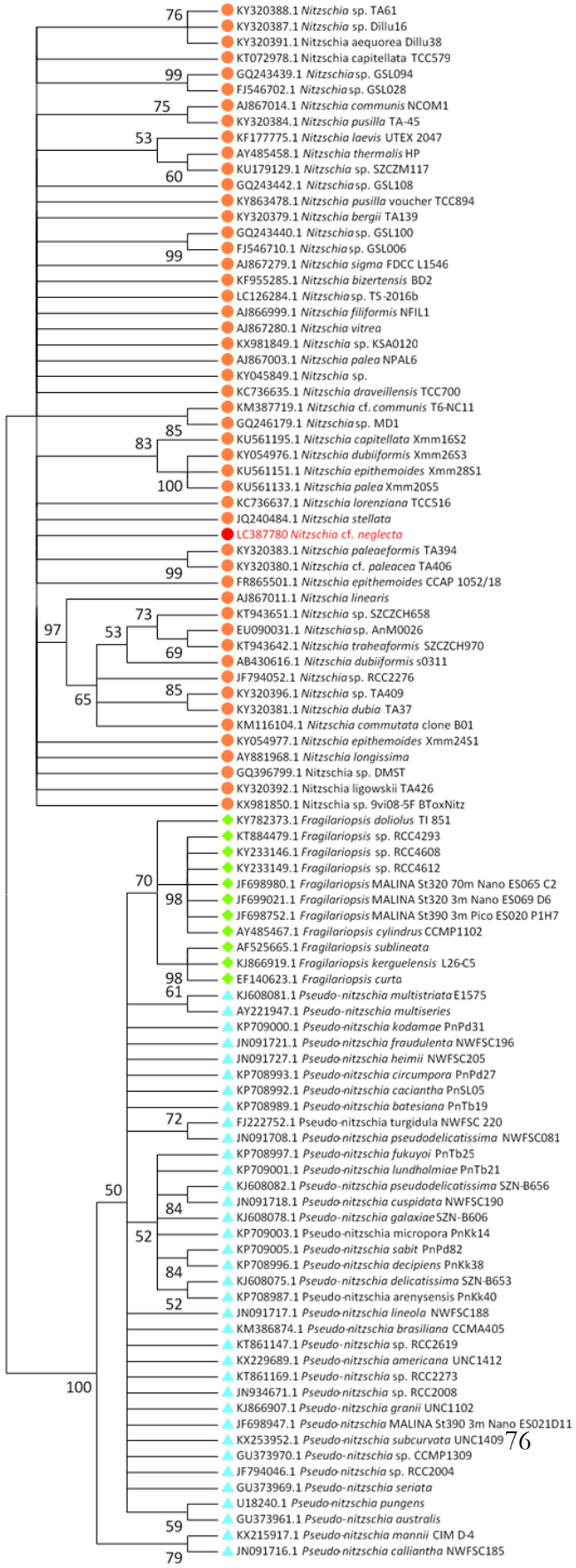
KY320388.1 Nitzschia sp. TA61
KY320387.1 Nitzschia sp. Dillu16
KY320391.1 Nitzschia aequorea Dillu38
KT072978.1 Nitzschia capitellata TCC579
GQ243439.1 Nitzschia sp. GSL094
FJ546702.1 Nitzschia sp. GSL028
AJ867014.1 Nitzschia communis NCOM1
KY320384.1 Nitzschia pusilla TA-45
KF177775.1 Nitzschia laevis UTEX 2047
AY485458.1 Nitzschia thermalis HP
KU179129.1 Nitzschia sp. SZCZM117
GQ243442.1 Nitzschia sp. GSL108
KY863478.1 Nitzschia pusilla voucher TCC894
KY320379.1 Nitzschia bergii TA139
GQ243440.1 Nitzschia sp. GSL100
FJ546710.1 Nitzschia sp. GSL006
AJ867279.1 Nitzschia sigma FDCC L1546
KF955285.1 Nitzschia bizertensis BD2
LC126284.1 Nitzschia sp. TS-2016b
AJ866999.1 Nitzschia filiformis NFIL1
AJ867280.1 Nitzschia vitrea
KX981849.1 Nitzschia sp. KSA0120
AJ867003.1 Nitzschia palea NPAL6
KY045849.1 Nitzschia sp.
KC736635.1 Nitzschia draveillensis TCC700
KM387719.1 Nitzschia cf. communis T6-NC11
GQ246179.1 Nitzschia sp. MD1
KU561195.1 Nitzschia capitellata Xmm16S2
KY054976.1 Nitzschia dubiiformis Xmm26S3
KU561151.1 Nitzschia epithemoides Xmm28S1
KU561133.1 Nitzschia palea Xmm20S5
KC736637.1 Nitzschia lorenziana TCC516
JQ240484.1 Nitzschia stellata
LC387780 Nitzschia cf. neglecta
KY320383.1 Nitzschia paleaeformis TA394
KY320380.1 Nitzschia cf. paleacea TA406
FR865501.1 Nitzschia epithemoides CCAP 1052/18
AJ867011.1 Nitzschia linearis
KT943651.1 Nitzschia sp. SZCZCH658
EU090031.1 Nitzschia sp. AnM0026
KT943642.1 Nitzschia traheaformis SZCZCH970
AB430616.1 Nitzschia dubiiformis s0311
JF794052.1 Nitzschia sp. RCC2276
KY320396.1 Nitzschia sp. TA409
KY320381.1 Nitzschia dubia TA37
KM116104.1 Nitzschia commutata clone B01
KY054977.1 Nitzschia epithemoides Xmm24S1
AY881968.1 Nitzschia longissima
GQ396799.1 Nitzschia sp. DMST
KY320392.1 Nitzschia ligowskii TA426
KX981850.1 Nitzschia sp. 9vi08-5F BToxNitz
KY782373.1 Fragilariopsis doliolus TI 851
KT884479.1 Fragilariopsis sp. RCC4293
KY233146.1 Fragilariopsis sp. RCC4608
KY233149.1 Fragilariopsis sp. RCC4612
JF698980.1 Fragilariopsis MALINA St320 70m Nano ES065 C2
JF699021.1 Fragilariopsis MALINA St320 3m Nano ES069 D6
JF698752.1 Fragilariopsis MALINA St390 3m Pico ES020 P1H7
AY485467.1 Fragilariopsis cylindrus CCMP1102
AF525665.1 Fragilariopsis sublineata
KJ866919.1 Fragilariopsis kerguelensis L26-C5
EF140623.1 Fragilariopsis curta
KJ608081.1 Pseudo-nitzschia multistriata E1575
AY221947.1 Pseudo-nitzschia multiseries
KP709000.1 Pseudo-nitzschia kodamae PnPd31
JN091721.1 Pseudo-nitzschia fraudulenta NWFSC196
JN091727.1 Pseudo-nitzschia heimii NWFSC205
KP708993.1 Pseudo-nitzschia circumpora PnPd27
KP708992.1 Pseudo-nitzschia caciantha PnSL05
KP708989.1 Pseudo-nitzschia batesiana PnTb19
FJ222752.1 Pseudo-nitzschia turgidula NWFSC 220
JN091708.1 Pseudo-nitzschia pseudodelicatissima NWFSC081
KP708997.1 Pseudo-nitzschia fukuyoi PnTb25
KP709001.1 Pseudo-nitzschia lundholmiae PnTb21
KJ608082.1 Pseudo-nitzschia pseudodelicatissima SZN-B656
JN091718.1 Pseudo-nitzschia cuspidata NWFSC190
KJ608078.1 Pseudo-nitzschia galaxiae SZN-B606
KP709003.1 Pseudo-nitzschia micropora PnKk14
KP709005.1 Pseudo-nitzschia sabit PnPd82
KP708996.1 Pseudo-nitzschia decipiens PnKk38
KJ608075.1 Pseudo-nitzschia delicatissima SZN-B653
KP708987.1 Pseudo-nitzschia arenysensis PnKk40
JN091717.1 Pseudo-nitzschia lineola NWFSC188
KM386874.1 Pseudo-nitzschia brasiliana CCMA405
KT861147.1 Pseudo-nitzschia sp. RCC2619
KX229689.1 Pseudo-nitzschia americana UNC1412
KT861169.1 Pseudo-nitzschia sp. RCC2273
JN934671.1 Pseudo-nitzschia sp. RCC2008
KJ866907.1 Pseudo-nitzschia granii UNC1102
JF698947.1 Pseudo-nitzschia MALINA St390 3m Nano ES021D11
KX253952.1 Pseudo-nitzschia subcurvata UNC1409
GU373970.1 Pseudo-nitzschia sp. CCMP1309
JF794046.1 Pseudo-nitzschia sp. RCC2004
GU373969.1 Pseudo-nitzschia seriata
U18240.1 Pseudo-nitzschia pungens
GU373961.1 Pseudo-nitzschia australis
KX215917.1 Pseudo-nitzschia mannii CIM D-4
JN091716.1 Pseudo-nitzschia calliantha NWFSC185
76
99
75
53
60
99
85
83
100
99
73
97
53
69
85
65
70
98
98
61
72
50
84
52
84
52
100
59
79

Fig. 3.3 Evolutionary relationships of *Nitzschia* spp. on Neighbor-Joining phylogenetic tree generated from 18S rRNA gene sequences of *Nitzschia* and outgroup species downloaded from NCBI GenBank. Branches corresponding to partitions reproduced in less than 50 % bootstrap replicates are collapsed. The percentage of replicate trees in which the associated taxa clustered together in the bootstrap test (1000 replicates) are shown next to the branches.

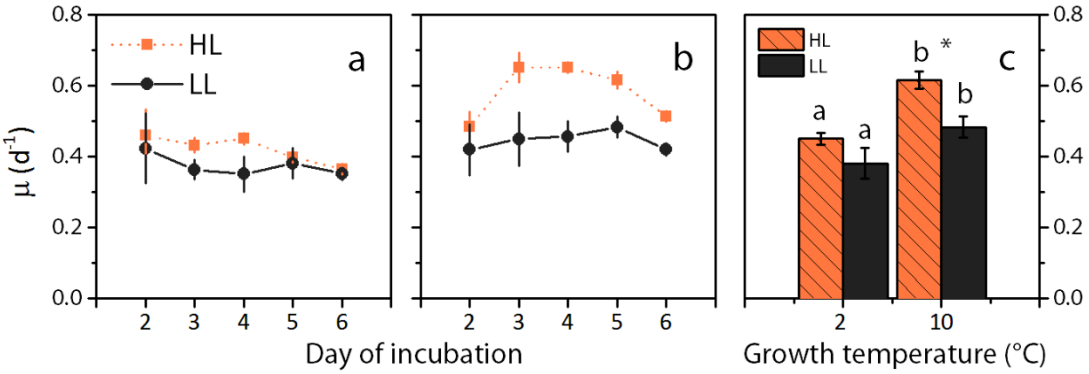

Fig. 3.4 Specific growth rate (μ, day^{-1}) of different incubation days. (a) 2°C; (b) 10°C; (c) Average during the whole incubation period. Squares, growth light of 100 μmol photons m^{-2} s^{-1}; Circles, growth lignt 30 μmol photons m^{-2} s^{-1}. Mean values (± SD) are the average of three independent measurements. Letters and asterisks represent significant differences between growth temperatures and growth lights, respectively. ANOVA was performed to check the effect of each individual factor. The significance level was 0.05.

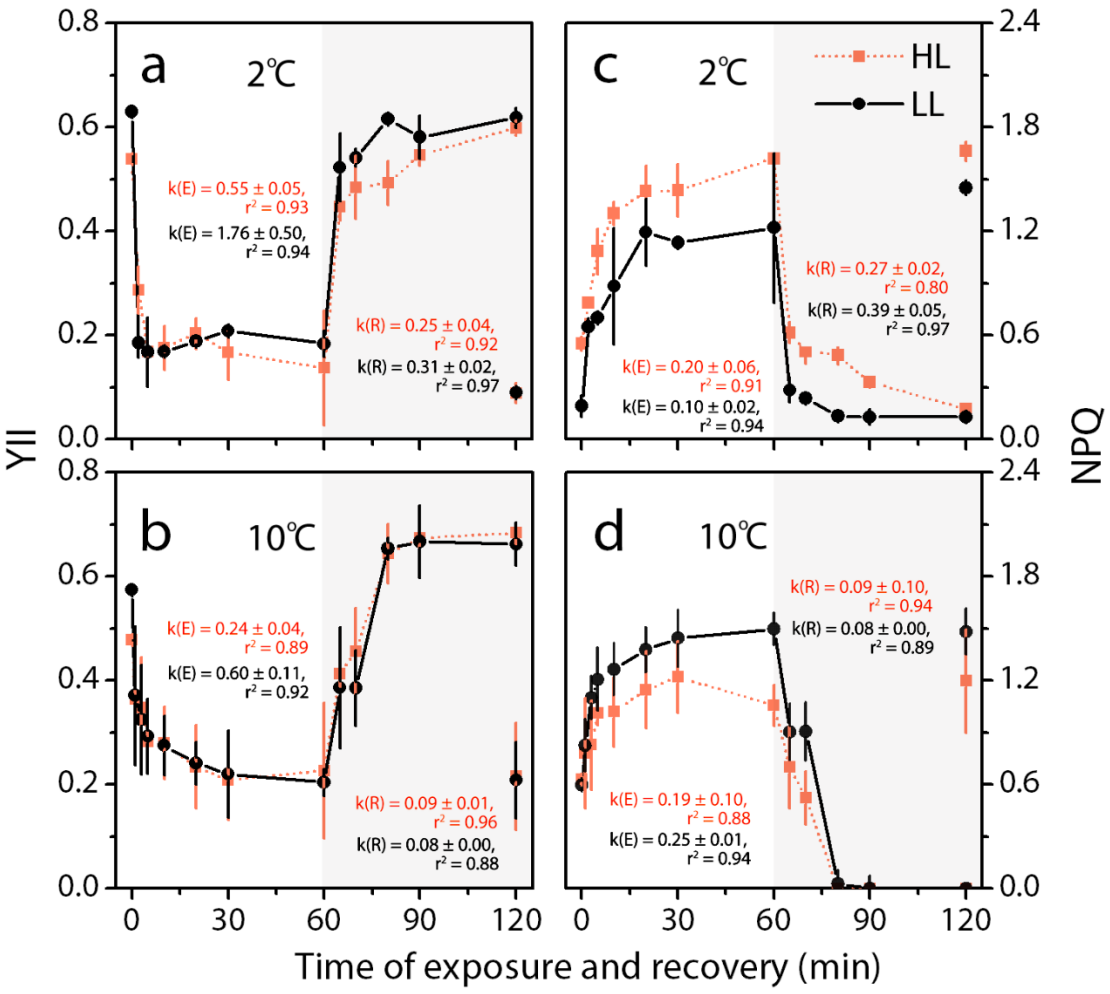

Fig. 3.5 Changes of YII (a and b), and NPQ (c and d), during the E and R treatment. Mean values (± SD) are the average of three independent measurements. To quantify the changes of YII and NPQ during exposure and recovery, YII or NPQ were plotted against exposure or recovery time and the curves were fitted with first-order exponential decay functions in the form of $y = y0 + Ae^{-kx}$. The decay constants (k) are shown in the figures. The data of an exposure of 120 min are shown as dots.

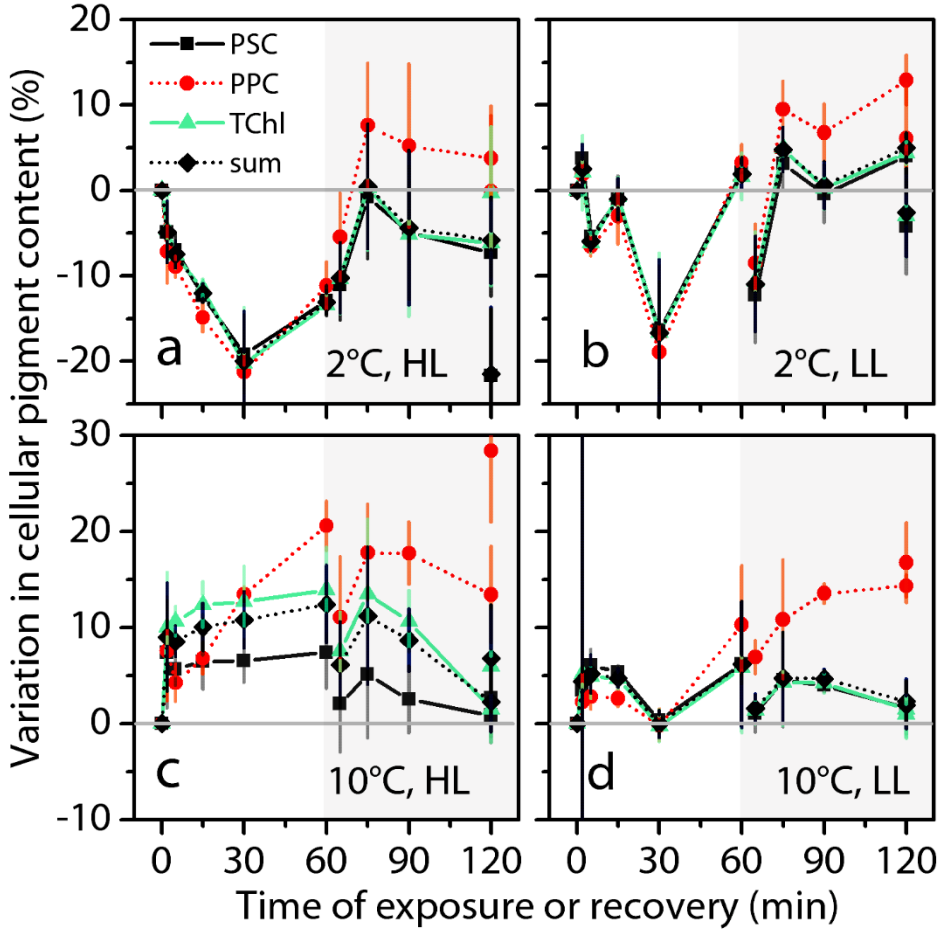

Fig. 3.6 Variations of pigment content during E and R treatment compared to that at E0. (a) and (c), 100 µmol photons m^{-2} s^{-1}, (b) and (d) 30 µmol photons m^{-2} s^{-1}. Squares, photosynthetic carotenoids (PSC = fucoxanthin); Circles, photoprotective carotenoids (PPC = diadinoxanthin + diatoxanthin + β-carotene); Triangles, total chlorophyll (TChl = Chl *c* + Chl *a*); Diamonds, the sum of all pigments. Mean values (± SD) are the average of three independent measurements. The data of an exposure of 120 min are shown as dots. The grey horizontal line represents that the cellular pigment content equals to that at E0.

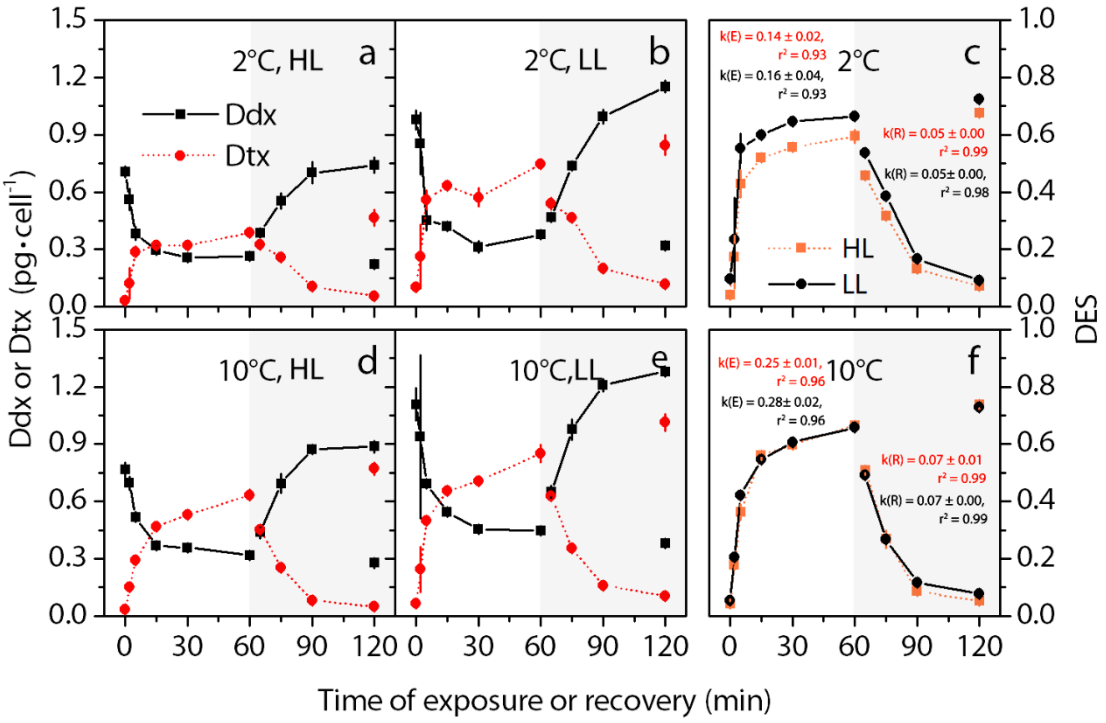

Fig. 3.7 Changes of Ddx and Dtx content during E and R treatment. (a), (b), (d), and (e) are the absolute cellular contents of the two pigments in cells. (c) and (f) show the de-epoxidation state index (DES). Squares and circles represent Ddx and Dtx, in (a), (b), (d) and (e), respectively. Squares and circles represent 100 µmol photons m^{-2} s^{-1}, and 30 µmol photons m^{-2} s^{-1}, in (c) and (f), respectively. Mean values (± SD) are the average of three independent measurements. The curves in (c) and (f) were fitted with exponential decay model (same as NPQ) and the decay constants of the fitted curves are shown in the figures. The data of an exposure of 120 min are shown as dots.

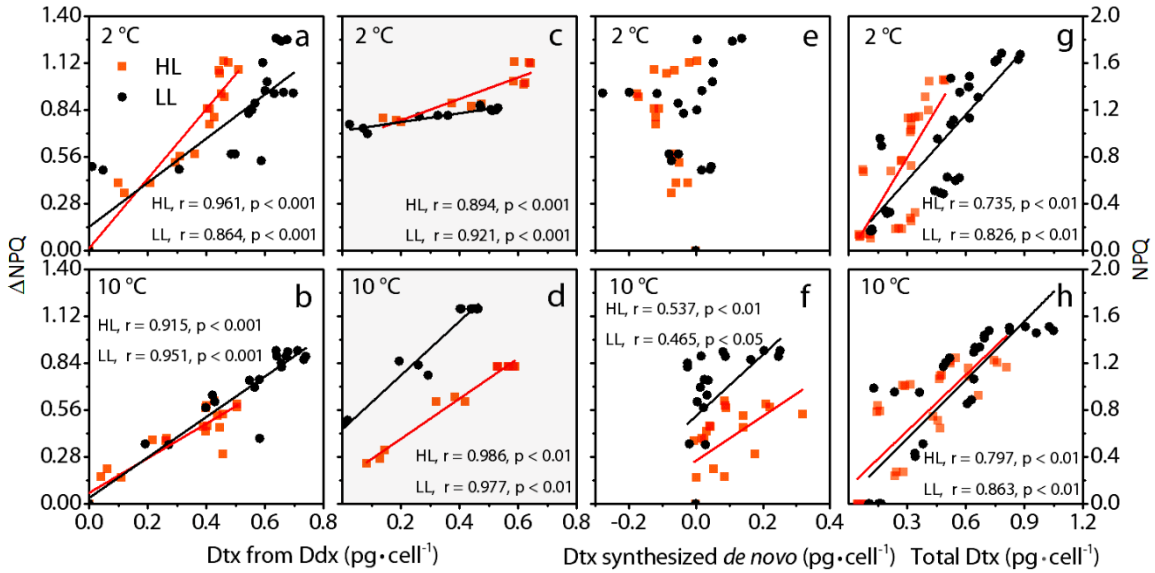

Fig. 3.8 The relationship between ΔNPQ and Ddx-transformed Dtx content (pg cell^{-1}) in E treatment, (a) and (b), and R treatment, (c) and (d). (e) and (f) are the relationship between ΔNPQ and Dtx synthesized *de novo* (pg cell^{-1}) during E. (g) and (h) are the relationship between total NPQ and total cellular Dtx content (pg cell^{-1}) during E and R. Fitted values are shown as solid lines. Squares, 100 μmol photons m^{-2} s^{-1}. Circles, 30 μmol photons m^{-2} s^{-1}. The formula of the linear regressions in g and h are as follows: 2HL, NPQ = Dtx(total) × 2.77 -0.03; 2LL, NPQ = Dtx(total) × 1.87 + 0.04; 10HL, NPQ = Dtx(total) × 1.60 - 0.15; 10LL, NPQ = Dtx(total) × 1.67 - 0.06.

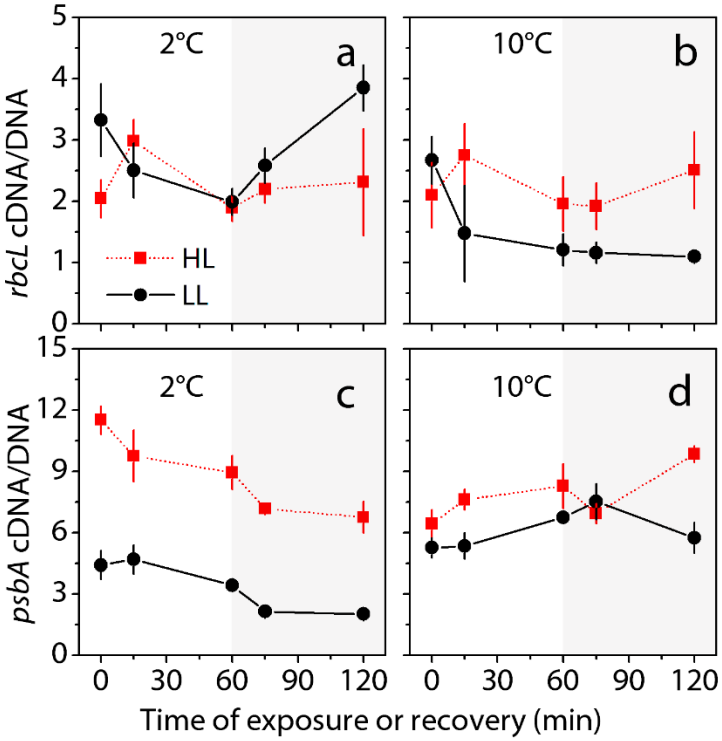

Fig. 3.9 Abundances of *rbcL* (a and b) and *psbA* (c and d) mRNA (cDNA) normalized to their gene copy number (cDNA/DNA) during the E and R treatment. Squares, 100 µmol photons m^{-2} s^{-1}; Circles, 30 µmol photons m^{-2} s^{-1}. Mean values (± SD) are the average of three independent measurements.

Chapter 4

General conclusions and perspectives

The centric diatom *Thalassiosira* was quite abundant in the ice algal community of the Sea of Okhotsk. This is in contrast with previous observations that pennate diatoms with large cell sizes usually dominate ice algal communities. Though pennate diatoms such as *Navicula* and *Nitzschia* were relatively abundant in the bulk ice in this work, they did not dominate the community in terms of cell number. The results showed that *Thalassiosira* had a large seeding effect on the bloom during and after ice melt. The first reason for their ecological success was the large abundance of *Thalassiosira* cells in the community in sea ice at the beginning. Another reason is they can quickly acclimate to changes in salinity under the ice melt condition, which is supported by physiological data and mortality of the community during and after ice melt. The declining contribution of pennate diatoms during the incubation suggest that they have a lower potential to seed the phytoplankton bloom after ice disappears. This is possibly due to their low tolerance to changes in salinity during ice melt, which resulted in lower growth rate and faster sinking rate.

Similar to temperate diatom species, the physiological performance of the ice diatoms can also be largely affected by temperature. The ice diatom *Nitzschia* cf. *neglecta* showed better growth and more effective photoprotection at 10 °C, a temperature much higher than that in sea ice. Though the light for culture was maintained at a low irradiance level, the cells showed large plasticity in photoprotection under the high-light exposure. The Ddx-Dtx cycle was the main photoprotective strategy against high light while regulation of *psbA* and *rbcL* at transcription levels played a minor role.

Some ice diatoms cannot survive at temperatures significantly higher than sea ice (e.g. *Nitzschia frigida*). Only the species that can tolerate higher temperatures can seed the phytoplankton bloom. Meanwhile, they cannot sink too fast. This means they have to maintain phytoplanktonic populations. Benthic diatoms such as most species of *Nitzschia* and *Navicula* are thus not likely to form bloom after ice melt, though they usually occur in large abundance in sea ice. My study

on the ice diatom *Nitzschia* cf. *neglecta* demonstrates that pennate diatoms can tolerate high temperature and has effective photoprotective strategies against high light exposure. The growth of pennate diatoms was thus most likely hindered by salinity changes during ice melt. The osmotic stress to the cells resulted in cell damage and cell death, which possibly contributed to the faster sedimentation of the cells. In this study planktonic species such as *Thalassiosira* showed a larger seeding potential to phytoplankton blooms. Whether the result of this study can be extended to other parts of the Sea of Okhotsk would be interesting to see and more field studies would be needed. Incubation experiments using isolates from the Okhotsk sea ice is also needed because there is little information on the species properties which may be more important factors determining the dynamics of the community than environmental factors.

Acknowledgements

I would like to express my sincere gratitude to my supervisor Prof. Koji Suzuki for the continuous support of my PhD study, for his patience, motivation, and immense knowledge.

My sincere thanks also goes to Prof. Jun Nishioka for supporting my PhD study.

I would like to thank Prof. Takenobu Toyota, Dr. Masato Ito for taking sea ice samples and providing sea ice data during the P/V *Soya* SIRAS-19 expedition. I thank the captain, crew, and colleagues for supporting the sampling of sea ice.

I would like to thank Ms. Akiko Kamimura for analyzing my pigment samples and helping with some of the molecular work. I also want to thank Dr. Hisashi Endo and C. Tsurumoto for their instructions on the molecular work. I thank the Graduate School of Environmental Science and the Institute of Low Temperature Science, Hokkaido University, for the experimental facilities and technical support.

I appreciate the valuable comments provided by Prof. Gustaaf Hallegraeff for identifying the *Nitzschia* species and improving English writing. I thank Prof. Douglas Campbell and the two anonymous reviewers for giving comments on the work in Chapter 3.

I would like to thank Prof. Y. W. Watanabe for lending me his cooler box for my ice algal strains and the assistance during the 2018 earthquake. I would like to thank Prof. Sohiko Kameyama for translating the sentences in the reading circle.

I would like to thank Dr. B. Li, Kaori Ito, Z. Chen, X. Yu, and X. Pan for helping my life in Japan. I also thank any other MAG members who once helped me.

I would like to thank Prof. Takafumi Hirata for his teachings and suggestions.

I would like to thank Prof. K. Gao and Xiamen University. They introduced me to the world of photosynthesis and phytoplankton and they provided me the first chance to come here. I thank Profs. Changzi Ge, Junxue Mei, Yingmei Chai, Lifang Li and Jian Liu for their teachings.

I would like to thank Dr. Kazuhiro Yoshida for his instructions on experiments, guidance, inspiration, exchange of ideas, and friendship.

Last but not the least, I thank my parents.

The PhD study is partly supported by JSPS Grants-in-Aid for Scientific Research JP18H03352 and JP17H00775. And JSPS Research Fellowship for Young Scientists 20J10963.

References

Abdullahi, A.S., Underwood, G.J.C., and Gretz, M.R. (2006) Extracellular matrix assembly in diatoms (Bacillariophyceae). V. Environmental effects on polysaccharide synthesis in the model diatom, *Phaeodactylum tricornutum*. *J. Phycol.* **42**: 363–378.

Agusti, S., González-Gordillo, J.I., Vaqué, D., Estrada, M., Cerezo, M.I., Salazar, G., et al. (2015) Ubiquitous healthy diatoms in the deep sea confirm deep carbon injection by the biological pump. *Nat. Commun* **6**: 7608.

Aizdaicher, N.A. and Markina, Z.V. (2010) The effect of decrease in salinity on the dynamics of abundance and the cell size of *Corethron Hystrix* (Bacillariophyta) in laboratory culture. *Ocean Sci J* **45**: 1–5.

Aletsee, L. and Jahnke, J. (1992) Growth and productivity of the psychrophilic marine diatoms Thalassiosira antarctica and Nitzschia frigida Grunow in batch cultures at temperatures below the freezing point of sea water. *Polar Biol* **11**: 643–647.

Andersson, B. and Aro, E.-M. (2001) Photodamage and D1 Protein Turnover in Photosystem II. In *Regulation of Photosynthesis*. Advances in Photosynthesis and Respiration. Springer, Dordrecht, pp. 377–393.

Aota, M. (1979) Variability of hydrography in coastal area along Hokkaido, the Sea of Okhotsk. *Note Coast Oceanogr Study* **17**: 1–11.

Aota, M. (Hokkaido U. and Ishikawa, M. (1991) Fresh water supply to the sea of Okhotsk and volume transport of Soya warm current. *Bulletin of the Hokkaido National Fisheries Research Institute (Japan)*.

Arrigo, K.R. (2016) Sea ice as a habitat for primary producers. In *Sea Ice*. John Wiley & Sons, Ltd, pp. 352–369.

Arrigo, K.R. (2014) Sea Ice Ecosystems. *Annu Rev Mar Sci* **6**: 439–467.

Arrigo, K.R., van Dijken, G., and Pabi, S. (2008) Impact of a shrinking Arctic ice cover on marine primary production. *Geophys Res Lett* **35**: L19603.

Arrigo, K.R. and Sullivan, C.W. (1992) The influence of salinity and temperature covariation on the photophysiological characteristics of Antarctic sea ice microalgae. *J Phycol* **28**: 746–756.

Arrigo, K.R., Worthen, D.L., Lizotte, M.P., Dixon, P., and Dieckmann, G. (1997) Primary production in Antarctic sea ice. *Science* **276**: 394–397.

Aslam, S.N., Cresswell-Maynard, T., Thomas, D.N., and Underwood, G.J.C. (2012) Production and characterization of the intra- and extracellular carbohydrates and polymeric substances (EPS) of three sea-ice diatom species, and evidence for a cryoprotective role for EPS. *J Phycol* **48**: 1494–1509.

Aslam, S.N., Strauss, J., Thomas, D.N., Mock, T., and Underwood, G.J.C. (2018) Identifying metabolic pathways for production of extracellular polymeric substances by the diatom *Fragilariopsis cylindrus* inhabiting sea ice. *The ISME Journal* **12**: 1237.

Assur, A. (1960) Composition of Sea Ice and Its Tensile Strength, U.S. Army Snow, Ice and Permafrost Research Establishment.

Aumack, C.F. and Juhl, A.R. (2015) Light and nutrient effects on the settling characteristics of the sea ice diatom Nitzschia frigida. *Limnol Oceanogr* **60**: 765–776.

Baars, J.W.M. (1982) Autecological investigation on marine diatoms 3. *Thalassiosira nordenskioeldii* and *Chaetoceros diadema*. *Mar Biol* **68**: 343–350.

Bailleul, B., Rogato, A., de Martino, A., Coesel, S., Cardol, P., Bowler, C., et al. (2010) An atypical member of the light-harvesting complex stress-related protein family modulates diatom responses to light. *Proc. Natl. Acad. Sci. U.S.A* **107**: 18214–18219.

Beardall, J. (1989) Photosynthesis and photorespiration in marine phytoplankton. *Aquat. Bot.* **34**: 105–130.

Boetius, A., Albrecht, S., Bakker, K., Bienhold, C., Felden, J., Fernández-Méndez, M., et al. (2013) Export of Algal Biomass from the Melting Arctic Sea Ice. *Science* **339**: 1430–1432.

Boetius, A., Anesio, A.M., Deming, J.W., Mikucki, J.A., and Rapp, J.Z. (2015) Microbial ecology of the cryosphere: sea ice and glacial habitats. *Nat Rev Micro* **13**: 677–690.

Brand, L.E. (1984) The salinity tolerance of forty-six marine phytoplankton isolates. *Estuar, Coast Shelf S* **18**: 543–556.

Bussard, A., Corre, E., Hubas, C., Duvernois-Berthet, E., Corguillé, G.L., Jourdren, L., et al. (2017) Physiological adjustments and transcriptome reprogramming are involved in the acclimation to salinity gradients in diatoms. *Environ. Microbiol.* **19**: 909–925.

Chen, L., Weng, D., Du, C., Wang, J., and Cao, S. (2019) Contribution of frustules and mucilage trails to the mobility of diatom *Navicula* sp. *Sci Rep* **9**: 1–12.

Coello-Camba, A., Agustí, S., Vaqué, D., Holding, J., Arrieta, J.M., Wassmann, P., and Duarte, C.M. (2015) Experimental assessment of temperature thresholds for Arctic phytoplankton communities. *Estuaries and Coasts* **38**: 873–885.

Comeau, A.M., Philippe, B., Thaler, M., Gosselin, M., Poulin, M., and Lovejoy, C. (2013) Protists in Arctic drift and land-fast sea ice. *J Phycol* **49**: 229–240.

Cooper, T.G., Filmer, D., Wishnick, M., and Lane, M.D. (1969) The active species of "CO_2" utilized by ribulose diphosphate carboxylase. *J Biol.* **244**: 1081–1083.

Corredor, J.E., Wawrik, B., Paul, J.H., Tran, H., Kerkhof, L., López, J.M., et al. (2004) Geochemical rate-RNA integration study: ribulose-1, 5-bisphosphate carboxylase/oxygenase gene transcription and photosynthetic capacity of planktonic photoautotrophs. *Appl Environ Microbiol* **70**: 5459–5468.

Cota, G.F. (1985) Photoadaptation of high Arctic ice algae. *Nature* **315**: 219–222.

Cottrell, M.T. and David, K.L. (2003) Contribution of major bacterial groups to bacterial biomass production (thymidine and leucine incorporation) in the Delaware estuary. *Limnol Oceanogr* **48**: 168–178.

Cox, G.F.N. and Weeks, W.F. (1986) Changes in the salinity and porosity of sea-ice samples during shipping and storage. *J. Glaciol.* **32**: 371–375.

Curien, G., Flori, S., Villanova, V., Magneschi, L., Giustini, C., Forti, G., et al. (2016) The water to water cycles in microalgae. *Plant Cell Physiol* **57**: 1354–1363.

Demers, S., Roy, S., Gadnon, S., and Vignault, C. (1991) Rapid light-induced changes in cell

fluorescence and in xanthophyll-cycle pigments of *Alexandrium excavatum* (Dinophyceae) and *Thalassiosira pseudonana* (Bacillariophyceae): a photo-protection mechanism. *Mar. Ecol. Prog. Ser.* **76**: 185–193.

Devos, N., Ingouff, M., Loppes, R., and Matagne, R.F. (1998) Rubisco adaptation to low temperatures: A comparative study in psychrophilic and mesophilic unicellular algae. *J. Phycol* **34**: 655–660.

Dixon, P. (2003) VEGAN, a package of R functions for community ecology. *J Veg Sci* **14**: 927–930.

Dubinsky, Z. and Stambler, N. (2009) Photoacclimation processes in phytoplankton: mechanisms, consequences, and applications. *Aquat. Microb. Ecol* **56**: 163–176.

Durkin, C.A., Mooy, B.A.S.V., Dyhrman, S.T., and Buesseler, K.O. (2016) Sinking phytoplankton associated with carbon flux in the Atlantic Ocean. *Limnol. Oceanogr.* **61**: 1172–1187.

Ehn, J.K. and Mundy, C.J. (2013) Assessment of light absorption within highly scattering bottom sea ice from under-ice light measurements: Implications for Arctic ice algae primary production. *Limnol Oceanogr* **58**: 893–902.

Eilers, P. and Peeters, J. (1988) A model for the relationship between light intensity and the rate of photosynthesis in phytoplankton. *Ecol Model* **42**: 199–215.

Endo, H., Ogata, H., and Suzuki, K. (2018) Contrasting biogeography and diversity patterns between diatoms and haptophytes in the central Pacific Ocean. *Sci Rep* **8**: 1–13.

Endo, H., Sugie, K., Yoshimura, T., and Suzuki, K. (2015) Effects of CO_2 and iron availability on *rbc*L gene expression in Bering Sea diatoms. *Biogeosciences* **12**: 2247–2259.

Endo, H., Yoshimura, T., Kataoka, T., and Suzuki, K. (2013) Effects of CO_2 and iron availability on phytoplankton and eubacterial community compositions in the northwest subarctic Pacific. *J. Exp. Mar. Biol. Ecol.* **439**: 160–175.

Ensminger, I., Busch, F., and Huner, N.P.A. (2006) Photostasis and cold acclimation: sensing low temperature through photosynthesis. *Physiol Plant* **126**: 28–44.

Ewert, M. and Deming, J.W. (2013) Sea ice microorganisms: environmental constraints and extracellular responses. *Biology (Basel)* **2**: 603–628.

Falkowski, P.G. and Raven, J.A. (2013) Aquatic photosynthesis, 2nd ed. Princeton University Press.

Favorite, F. (1976) Oceanography of the Subarctic Pacific region 1960-71. *Bull Int North Pacific Comm* **33**: 1–187.

Fiala, M. and Oriol, L. (1990) Light-temperature interactions on the growth of Antarctic diatoms. *Polar Biol* **10**: 629–636.

Fritz, L., Quilliam, M.A., Wright, J.L.C., Beale, A.M., and Work, T.M. (1992) An outbreak of domoic Acid poisoning attributed to the pennate diatom *Pseudo-nitzschia australis*. *J. Phycol* **28**: 439–442.

Fukamachi, Y., Mizuta, G., Ohshima, K.I., Toyota, T., Kimura, N., and Wakatsuchi, M. (2006) Sea ice thickness in the southwestern Sea of Okhotsk revealed by a moored ice-profiling sonar. *J. Geophys. Res. Oceans* **111**:.

Fukamachi, Y., Shirasawa, K., Polomoshnov, A.M., Ohshima, K.I., Kalinin, E., Nihashi, S., et al. (2009) Direct observations of sea-ice thickness and brine rejection off Sakhalin in the Sea of Okhotsk. *Cont Shelf Res.* **29**: 1541–1548.

Galindo, V., Levasseur, M., Mundy, C.J., Gosselin, M., Scarratt, M., Papakyriakou, T., et al. (2016) Contrasted sensitivity of DMSP production to high light exposure in two Arctic under-ice blooms. *J. Exp. Mar. Biol. Ecol.***475**: 38–48.

Garrison, D.L. (1991) Antarctic Sea Ice Biota. *Integr Comp Biol* **31**: 17–34.

Garrison, D.L. (1981) Monterey Bay Phytoplankton. II. Resting Spore Cycles in Coastal Diatom Populations. *J Plankton Res* **3**: 137–156.

Garrison, D.L., Buck, K.R., and Fryxell, G.A. (1987) Algal assemblages in Antarctic pack ice and in ice-edge plankton. *J. Phycol* **23**: 564–572.

Garrison, D.L. and Close, A.R. (1993) Winter ecology of the sea ice biota in Weddell Sea pack ice. *Mar. Ecol. Prog. Ser.* **96**: 17–31.

Gemmell, B.J., Oh, G., Buskey, E.J., and Villareal, T.A. (2016) Dynamic sinking behaviour in marine phytoplankton: rapid changes in buoyancy may aid in nutrient uptake. *Proc. Royal Soc. B: Biological Sciences* **283**: 20161126.

Gilstad, M. and Sakshaug, E. (1990) Growth rates of ten diatom species from the Barents Sea at different irradiances and day lengths. *Mar. Ecol. Prog. Ser.* **64**: 169–173.

Goss, R. and Jakob, T. (2010) Regulation and function of xanthophyll cycle-dependent photoprotection in algae. *Photosynth Res* **106**: 103–122.

Goss, R. and Lepetit, B. (2015) Biodiversity of NPQ. *J. Plant Physiol.* **172**: 13–32.

Gradinger, R. and Ikävalko, J. (1998) Organism incorporation into newly forming Arctic sea ice in the Greenland Sea. *J Plankton Res* **20**: 871–886.

Granskog, M.A., Nomura, D., Müller, S., Krell, A., Toyota, T., and Hattori, H. (2015) Evidence for significant protein-like dissolved organic matter accumulation in Sea of Okhotsk sea ice. *Annals of Glaciology* **56**: 1–8.

Grant, W.S. and Horner, R.A. (1976) Growth responses to salinity variation in four Arctic ice diatoms. *J. Phycol* **12**: 180–185.

Guillard, R.R.L. (1975) Culture of Phytoplankton for Feeding Marine Invertebrates. In *Culture of Marine Invertebrate Animals*. Smith, W.L. and Chanley, M.H. (eds). Springer US, pp. 29–60.

Guillard, R.R.L. and Ryther, J.H. (1962) Studies of marine planktonic diatoms: I. *Cyclotella Nana* Hustedt, and *Detonula Confervacea* (cleve) Gran. *Can J Microbiol* **8**: 229–239.

Guiry, M.D. (2012) How many species of algae are there? *J. Phycol* **48**: 1057–1063.

Gundermann, K. and Büchel, C. (2012) Factors determining the fluorescence yield of fucoxanthin-chlorophyll complexes (FCP) involved in non-photochemical quenching in diatoms. *Biochimica et Biophysica Acta (BBA) - Bioenergetics* **1817**: 1044–1052.

Haecky, P., Jonsson, S., and Andersson, A. (1998) Influence of sea ice on the composition of the spring phytoplankton bloom in the northern Baltic Sea. *Polar Biol* **20**: 1–8.

Hamasaki, K., Ikeda, M., Ishikawa, M., Shirasawa, K., and Taguchi, S. (1998) Seasonal variability of size-fractionated chlorophyll *a* in Monbetsu Harbor, Hokkaido, northern Japan. *Plankton Biology and Ecology* **45**: 151–158.

Hancke, K., Lund-Hansen, L.C., Lamare, M.L., Pedersen, S.H., King, M.D., Andersen, P., and Sorrell,

B.K. (2018) Extreme low light requirement for algae growth underneath sea ice: A case study from station Nord, NE Greenland. *J. Geophys. Res. Oceans* **123**: 985–1000.

Hasle, G.R. and Booth, B.C. (1984) *Nitzschia cylindroformis* sp. nov., a common and abundant nanoplankton diatom of the eastern subarctic Pacific. *J Plankton Res* **6**: 493–503.

Havurinne, V. and Tyystjärvi, E. (2017) Action Spectrum of Photoinhibition in the Diatom Phaeodactylum tricornutum. *Plant Cell Physiol* **58**: 2217–2225.

Hegseth, E.N. (1992) Sub-ice algal assemblages of the Barents Sea: Species composition, chemical composition, and growth rates. *Polar Biol* **12**: 485–496.

Hernando, M., Schloss, I.R., Malanga, G., Almandoz, G.O., Ferreyra, G.A., Aguiar, M.B., and Puntarulo, S. (2015) Effects of salinity changes on coastal Antarctic phytoplankton physiology and assemblage composition. *J. Exp. Mar. Biol. Ecol.***466**: 110–119.

Hiwatari, T., Shirasawa, K., Fukamachi, Y., Nagata, R., Koizumi, T., Koshikawa, H., and Kohata, K. (2008) Vertical material flux under seasonal sea ice in the Okhotsk Sea north of Hokkaido, Japan. *Polar Sci* **2**: 41–54.

Ho, T.-Y., Quigg, A., Finkel, Z.V., Milligan, A.J., Wyman, K., Falkowski, P.G., and Morel, F.M.M. (2003) The elemental composition of some marine phytoplankton. *J. Phycol* **39**: 1145–1159.

Hoagland, K.D., Rosowski, J.R., Gretz, M.R., and Roemer, S.C. (1993) Diatom extracellular polymeric substances: function, fine structure, chemistry, and physiology. *J. Phycol* **29**: 537–566.

Hopes, A., Thomas, D.N., and Mock, T. (2017) Polar Microalgae: Functional Genomics, Physiology, and the Environment. In *Psychrophiles: From Biodiversity to Biotechnology*. Margesin, R. (ed). Cham: Springer International Publishing, pp. 305–344.

Hoppenrath, M., Beszteri, B., Drebes, G., Halliger, H., Beusekom, J.E.E.V., Janisch, S., and Wiltshire, K.H. (2007) Thalassiosira species (Bacillariophyceae, Thalassiosirales) in the North Sea at Helgoland (German Bight) and Sylt (North Frisian Wadden Sea) – a first approach to assessing diversity. *European J. Phycol* **42**: 271–288.

Horner (1985) Sea Ice Biota, CRC Press.

Horvat, C., Jones, D.R., Iams, S., Schroeder, D., Flocco, D., and Feltham, D. (2017) The frequency and extent of sub-ice phytoplankton blooms in the Arctic Ocean. *Science Advances* **3**: e1601191.

Hüner, N.P.A., Bode, R., Dahal, K., Busch, F.A., Possmayer, M., Szyszka, B., et al. (2012) Shedding some light on cold acclimation, cold adaptation, and phenotypic plasticity. *Botany* **91**: 127–136.

Ito, M., Fukamachi, Y., Ohshima, K.I., and Shirasawa, K. (2020) Observational evidence of supercooling and frazil ice formation throughout the water column in a coastal polynya in the Sea of Okhotsk. *Cont Shelf Res.* **196**: 104072.

Itoh, M. and Ohshima, K.I. (2000) Seasonal Variations of Water Masses and Sea Level in the Southwestern Part of the Okhotsk Sea. *J. Oceanogr.* **56**: 643–654.

Itoh, M., Ohshima, K.I., and Wakatsuchi, M. (2003) Distribution and formation of Okhotsk Sea Intermediate Water: An analysis of isopycnal climatological data. *J. Geophys. Res. Oceans* **108**:.

Jahnke, J. and Baumann, M. (1983) Chemical and physical effects on the shape and growth of the diatom *Biddulphia sinensis* Greville in batch cultures: A contribution to bioindication in plankton ecology. *Hydrobiol. bull.* **17**: 5–20.

Ji, R., Jin, M., and Varpe, Ø. (2013) Sea ice phenology and timing of primary production pulses in the Arctic Ocean. *Glob Change Biol* **19**: 734–741.

John, D.E., Patterson, S.S., and Paul, J.H. (2007) Phytoplankton-group specific quantitative polymerase chain reaction assays for RuBisCO mRNA transcripts in seawater. *Mar Biotechnol* **9**: 747–759.

Juhl, A.R. and Krembs, C. (2010) Effects of snow removal and algal photoacclimation on growth and export of ice algae. *Polar Biol* **33**: 1057–1065.

Kanervo, E., Tasaka, Y., Murata, N., and Aro, E.M. (1997) Membrane lipid unsaturation modulates processing of the Photosystem II reaction-center protein D1 at low temperatures. *Plant Physiology* **114**: 841–849.

Kanna, N. and Nishioka, J. (2016) Bio-availability of iron derived from subarctic first-year sea ice. *Mar Chem* **186**: 189–197.

Kanna, N., Sibano, Y., Toyota, T., and Nishioka, J. (2018) Winter iron supply processes fueling spring phytoplankton growth in a sub-polar marginal sea, the Sea of Okhotsk: Importance of sea ice and the East Sakhalin Current. *Mar Chem* **206**: 109–120.

Kanna, N., Toyota, T., and Nishioka, J. (2014) Iron and macro-nutrient concentrations in sea ice and their impact on the nutritional status of surface waters in the southern Okhotsk Sea. *Prog. Oceanogr.* **126**: 44–57.

Kasai, H. and Hirakawa, K. (2015) Seasonal changes of primary production in the southwestern Okhotsk Sea off Hokkaido, Japan during the ice-free period. *Plankton and Benthos Research* **10**: 178–186.

Kasai, H., Niimura, Y., Nagata, R., Katakura, S., and Hamaoka, S. (2014) Biomass and species composition of microalgae (ice algae) in drifting sea-ice collected in coastal waters off Mombetsu, Hokkaido, in the Okhotsk Sea.

Kashino, Y., Fujimoto, K., Akamatsu, A., Koike, H., Satoh, K., and Kudoh, S. (1998) Photosynthetic pigment composition of ice algal and phytoplankton assemblages in early spring in Saroma Ko Lagoon, Hokkaido, Japan. *Proceedings of the NIPR Symposium on Polar Biology* **11**: 22–32.

Kashiwase, H., Ohshima, K.I., and Nihashi, S. (2014) Long-term variation in sea ice production and its relation to the intermediate water in the Sea of Okhotsk. *Prog. Oceanogr.* **126**: 21–32.

Katayama, T. and Taguchi, S. (2013) Photoprotective responses of an ice algal community in Saroma-Ko Lagoon, Hokkaido, Japan. *Polar Biol* **36**: 1431–1439.

Katsumata, K., Ohshima, K.I., Kono, T., Itoh, M., Yasuda, I., Volkov, Y.N., and Wakatsuchi, M. (2004) Water exchange and tidal currents through the Bussol' Strait revealed by direct current measurements. *J. Geophys. Res. Oceans* **109**:.

Kauko, H.M., Olsen, L.M., Duarte, P., Peeken, I., Granskog, M.A., Johnsen, G., et al. (2018) Algal colonization of young Arctic sea ice in spring. *Front Mar Sci* **5**: 199.

Kikuchi-Kawanobe, K. and Kudoh, S. (1995) Species composition of ice algal assemblages in Saroma Ko Lagoon and Resolute Passage. *Proceedings of the NIPR Symposium on Polar Biology*.

Kim, S.T. (2012) A review of the Sea of Okhotsk ecosystem response to the climate with special emphasis on fish populations. *ICES J Mar Sci* **69**: 1123–1133.

Kimura, N. and Wakatsuchi, M. (1999) Processes controlling the advance and retreat of sea ice in the

Sea of Okhotsk. *J. Geophys. Res. Oceans* **104**: 11137–11150.

Krawiec, R.W. (1982) Autecology and clonal variability of the marine centric diatom Thalassiosira rotula (Bacillariophyceae) in response to light, temperature and salinity. *Mar Biol* **69**: 79–89.

Krell, A., Funck, D., Plettner, I., John, U., and Dieckmann, G. (2007) Regulation of proline metabolism under salt Stress in the psychrophilic diatom *Fragilariopsis cylindrus* (bacillariophyceae). *J. Phycol* **43**: 753–762.

Krembs, C., Eicken, H., and Deming, J.W. (2011) Exopolymer alteration of physical properties of sea ice and implications for ice habitability and biogeochemistry in a warmer Arctic. *PNAS* **108**: 3653–3658.

Krembs, C., Eicken, H., Junge, K., and Deming, J.W. (2002) High concentrations of exopolymeric substances in Arctic winter sea ice: implications for the polar ocean carbon cycle and cryoprotection of diatoms. *Deep Sea Res. Part I Oceanogr. Res. Pap.***49**: 2163–2181.

Kropuenske, L.R., Mills, M.M., van Dijken, G.L., Bailey, S., Robinson, D.H., Welschmeyer, N.A., and Arrigoa, K.R. (2009) Photophysiology in two major Southern Ocean phytoplankton taxa: Photoprotection in *Phaeocystis antarctica* and *Fragilariopsis cylindrus*. *Limnol Oceanogr* **54**: 1176–1196.

Kuczynska, P., Jemiola-Rzeminska, M., and Strzalka, K. (2015) Photosynthetic pigments in diatoms. *Mar. Drugs* **13**: 5847–5881.

Kudoh, S. (1993) Responses of microalgal primary productivity to the reduction of sea ice coverage in Lake Saroma during winter. *Bull Plankton Soc Jpn* **39**: 155–156.

Kudoh, S., Robineau, B., Suzuki, Y., Fujiyoshi, Y., and Takahashi, M. (1997) Photosynthetic acclimation and the estimation of temperate ice algal primary production in Saroma-ko Lagoon, Japan. *J Mar Syst.* **11**: 93–109.

Kulk, G., Buist, A., van de Poll, W.H., Rozema, P.D., and Buma, A.G.J. (2019) Size scaling of photophysiology and growth in four freshly isolated diatom species from Ryder Bay, western Antarctic peninsula. *J Phycol* **55**: 314–328.

Kuroda, H., Toya, Y., Watanabe, T., Nishioka, J., Hasegawa, D., Taniuchi, Y., and Kuwata, A. (2019) Influence of Coastal Oyashio water on massive spring diatom blooms in the Oyashio area of the North Pacific Ocean. *Prog. Oceanogr.* **175**: 328–344.

Lacour, T., Larivière, J., and Babin, M. (2017) Growth, Chl a content, photosynthesis, and elemental composition in polar and temperate microalgae. *Limnol Oceanogr* **62**: 43–58.

Lavaud, J. (2002) Influence of the diadinoxanthin pool size on photoprotection in the marine planktonic diatom *Phaeodactylum tricornutum*. *Plant Physio* **129**: 1398–1406.

Lavaud, J. and Lepetit, B. (2013) An explanation for the inter-species variability of the photoprotective non-photochemical chlorophyll fluorescence quenching in diatoms. *Biochim Biophys Acta Biomembr* **1827**: 294–302.

Lavaud, J., Rousseau, B., and Etienne, A.-L. (2004) General features of photoprotection by energy dissipation in planktonic diatoms (Bacillariophyceae). *J. Phycol* **40**: 130–137.

Legendre, L., Ackley, S.F., Dieckmann, G.S., Gulliksen, B., Horner, R., Hoshiai, T., et al. (1992) Ecology of sea ice biota. *Polar Biol* **12**: 429–444.

Legendre, L., Ingram, R.G., and Poulin, M. (1981) Physical control of phytoplankton production under

sea ice (Manitounuk Sound, Hudson Bay). *Can J Fish Aquat Sci* **38**: 1385–1392.

Leonov, A.V., Mogil'nikova, T.A., Pishchal'nik, V.M., and Zenkin, O.V. (2007) Characteristic of microalgae development in the Sea of Okhotsk in winter and modeling of their annual dynamics in Aniva Bay. *Water Resour* **34**: 184–194.

Lepetit, B., Volke, D., Gilbert, M., Wilhelm, C., and Goss, R. (2010) Evidence for the existence of one antenna-associated, lipid-dissolved and two protein-bound pools of diadinoxanthin cycle pigments in diatoms. *Plant Physiol* **154**: 1905–1920.

Leu, E., Mundy, C.J., Assmy, P., Campbell, K., Gabrielsen, T.M., Gosselin, M., et al. (2015) Arctic spring awakening – Steering principles behind the phenology of vernal ice algal blooms. *Prog. Oceanogr.* **139**: 151–170.

Li, G., Talmy, D., and Campbell, D.A. (2017) Diatom growth responses to photoperiod and light are predictable from diel reductant generation. *J Phycol* **53**: 95–107.

Light, B., Maykut, G.A., and Grenfell, T.C. (2003) Effects of temperature on the microstructure of first-year Arctic sea ice. *J. Geophys. Res. Oceans* **108**:.

Litchman, E. and Klausmeier, C.A. (2001) Competition of Phytoplankton under Fluctuating Light. *Am. Nat* **157**: 170–187.

Liu, H., Suzuki, K., Nishioka, J., Sohrin, R., and Nakatsuka, T. (2009) Phytoplankton growth and microzooplankton grazing in the Sea of Okhotsk during late summer of 2006. *Deep Sea Res. Part I Oceanogr. Res. Pap.* **56**: 561–570.

Lund-Hansen, L.C., Hawes, I., Sorrell, B.K., and Nielsen, M.H. (2014) Removal of snow cover inhibits spring growth of Arctic ice algae through physiological and behavioral effects. *Polar Biol* **37**: 471–481.

MacIntyre, H.L. and Cullen, J.J. (2005) Using cultures to investigate the physiological ecology of microalgae. In *Algal culturing techniques*. Amsterdam: Elsevier, pp. 287–326.

Mallick, N. and Mohn, F.H. (2000) Reactive oxygen species: response of algal cells. *J. Plant Physiol.* **157**: 183–193.

Manes, S.S. and Gradinger, R. (2009) Small scale vertical gradients of Arctic ice algal photophysiological properties. *Photosyn Res* **102**: 53–66.

Martin, A., McMinn, A., Heath, M., Hegseth, E.N., and Ryan, K.G. (2012) The physiological response to increased temperature in over-wintering sea ice algae and phytoplankton in McMurdo Sound, Antarctica and Tromsø Sound, Norway. *J. Exp. Mar. Biol. Ecol.***428**: 57–66.

Martin, S., Drucker, R., and Yamashita, K. (1998) The production of ice and dense shelf water in the Okhotsk Sea polynyas. *J. Geophys. Res. Oceans* **103**: 27771–27782.

Maxwell, D.P., Falk, S., Trick, C.G., and Huner, N. (1994) Growth at low temperature mimics high-light acclimation in Chlorella vulgaris. *Plant Physiol* **105**: 535–543.

McMinn A., Ashworth C., and Ryan K. (2005) Growth and productivity of Antarctic sea ice algae under PAR and UV irradiances. *botm* **42**: 401.

McMinn, A. and Hattori, H. (2006) Effect of time of day on the recovery from light exposure in ice algae from Saroma Ko lagoon, Hokkaido. *Polar Sci* **20**: 30–36.

McMinn, A., Hattori, H., Hirawake, T., and Iwamoto, A. (2008) Preliminary investigation of Okhotsk

Sea ice algae; taxonomic composition and photosynthetic activity. *Polar Biol* **31**: 1011–1015.

McMinn, A. and Martin, A. (2013) Dark survival in a warming world. *Proc. R. Soc. B: Biological Sciences* **280**: 20122909.

McMinn, A., Martin, A., and Ryan, K. (2010) Phytoplankton and sea ice algal biomass and physiology during the transition between winter and spring (McMurdo Sound, Antarctica). *Polar Biol* **33**: 1547–1556.

McMinn, A., Müller, M.N., Martin, A., and Ryan, K.G. (2014) The response of Antarctic Sea ice algae to changes in pH and CO_2. *PLoS One* **9**: e86984.

Medlin, L.K. and Hasle, G.R. (1990) Some Nitzschia and related diatom species from fast ice samples in the Arctic and Antarctic. *Polar Biol* **10**: 451–479.

Medlin, L.K. and Priddle, J. (1990) Polar Marine Diatoms, British Antarctic Survey, Natural Environment Research Council.

Michel, C., Legendre, L., and Taguchi, S. (1997) Coexistence of microalgal sedimentation and water column recycling in a seasonally ice-covered ecosystem (Saroma-ko Lagoon, Sea of Okhotsk, Japan). *J Mar Syst.* **11**: 133–148.

Miyake, C. (2010) Alternative electron flows (water–water cycle and cyclic electron flow around PSI) in photosynthesis: Molecular mechanisms and physiological functions. *Plant and Cell Physiol* **51**: 1951–1963.

Mock, T. and Hoch, N. (2005) Long-term temperature acclimation of photosynthesis in steady-state cultures of the polar diatom *Fragilariopsis cylindrus*. *Photosynth Res* **85**: 307–317.

Mock, T. and Valentin, K. (2004) Photosynthesis and cold acclimation: molecular evidence from a polar diatom. *J. Phycol* **40**: 732–741.

Morgan-Kiss, R.M., Priscu, J.C., Pocock, T., Gudynaite-Savitch, L., and Huner, N.P.A. (2006) Adaptation and acclimation of photosynthetic microorganisms to permanently cold environments. *Microbiol Mol Biol Rev* **70**: 222–252.

Moroshkin, K.V. (1968) Water Masses of the Sea of Okhotsk, Joint Publications Research Service.

Motylkova, I.V. and Konovalova, N.V. (2010) Seasonal dynamics of phytoplankton in a lagoon-type lake Izmenchivoye (Southeast Sakhalin). *Russ. J. Mar. Biol.* **36**: 86–92.

Mundy, C.J., Barber, D.G., and Michel, C. (2005) Variability of snow and ice thermal, physical and optical properties pertinent to sea ice algae biomass during spring. *J Mar Syst.* **58**: 107–120.

Mundy, C.J., Gosselin, M., Ehn, J., Gratton, Y., Rossnagel, A., Barber, D.G., et al. (2009) Contribution of under-ice primary production to an ice-edge upwelling phytoplankton bloom in the Canadian Beaufort Sea. *Geophys Res Lett* **36**: L17601.

Mundy, C.J., Gosselin, M., Ehn, J.K., Belzile, C., Poulin, M., Alou, E., et al. (2011) Characteristics of two distinct high-light acclimated algal communities during advanced stages of sea ice melt. *Polar Biol* **34**: 1869–1886.

Mundy, C.J., Gosselin, M., Gratton, Y., Brown, K., Galindo, V., Campbell, K., et al. (2014) Role of environmental factors on phytoplankton bloom initiation under landfast sea ice in Resolute Passage, Canada. *Mar Ecol Prog Ser* **497**: 39–49.

Mustapha, M.A. and Saitoh, S.-I. (2008) Observations of sea ice interannual variations and spring

bloom occurrences at the Japanese scallop farming area in the Okhotsk Sea using satellite imageries. *Estuar. Coast. Shelf Sci* **77**: 577–588.

Nakamura, T., Awaji, T., Hatayama, T., Akitomo, K., and Takizawa, T. (2000) Tidal Exchange through the Kuril Straits. *J Phys Oceanogr* **30**: 1622–1644.

Nelson, D.M., Tréguer, P., Brzezinski, M.A., Leynaert, A., and Quéguiner, B. (1995) Production and dissolution of biogenic silica in the ocean: Revised global estimates, comparison with regional data and relationship to biogenic sedimentation. *Global Biogeochem Cycles* **9**: 359–372.

Nelson, N. and Yocum, C.F. (2006) Structure and Function of Photosystems I and II. *Annu. Rev. Plant Biol.* **57**: 521–565.

Ni, G., Zimbalatti, G., Murphy, C.D., Barnett, A.B., Arsenault, C.M., Li, G., et al. (2017) Arctic Micromonas uses protein pools and non-photochemical quenching to cope with temperature restrictions on Photosystem II protein turnover. *Photosynth Res* **131**: 203–220.

Nicolaus, M., Katlein, C., Maslanik, J., and Hendricks, S. (2012) Changes in Arctic sea ice result in increasing light transmittance and absorption. *Geophys Res Lett* **39**: L24501.

Nihashi, S., Kurtz, N.T., Markus, T., Ohshima, K.I., Tateyama, K., and Toyota, T. (2018) Estimation of sea-ice thickness and volume in the Sea of Okhotsk based on ICESat data. *Ann. Glaciol.* **59**: 101–111.

Nihashi, S., Ohshima, K.I., Tamura, T., Fukamachi, Y., and Saitoh, S. (2009) Thickness and production of sea ice in the Okhotsk Sea coastal polynyas from AMSR-E. *J. Geophys. Res. Oceans* **114**:.

Nishioka, J., Mitsudera, H., Yasuda, I., Liu, H., Nakatsuka, T., and Volkov, Y.N. (2014) Biogeochemical and physical processes in the Sea of Okhotsk and the linkage to the Pacific Ocean. *Prog. Oceanogr* **126**: 1–7.

Nishioka, J., Ono, T., Saito, H., Nakatsuka, T., Takeda, S., Yoshimura, T., et al. (2007) Iron supply to the western subarctic Pacific: Importance of iron export from the Sea of Okhotsk. *J Geophys Res* **112**: C10012.

Nomura, D., Takatsuka, T., Ishikawa, M., Kawamura, T., Shirasawa, K., and Yoshikawa-Inoue, H. (2009) Transport of chemical components in sea ice and under-ice water during melting in the seasonally ice-covered Saroma-ko Lagoon, Hokkaido, Japan. *Estuar. Coast. Shelf Sci* **81**: 201–209.

Notz, D. and Worster, M.G. (2009) Desalination processes of sea ice revisited. *J. Geophys. Res. Oceans* **114**:.

Obrezkova, M.S., Kolesnik, A.N., and Semiletov, I.P. (2014) The diatom distribution in the surface sediments of the Eastern Arctic seas of Russia. *Russ. J. Mar. Biol.* **40**: 465–472.

Oguma, S., Ono, T., Kusaka, A., Kasai, H., Kawasaki, Y., and Azumaya, T. (2008) Isotopic tracers for water masses in the coastal region of eastern Hokkaido. *J Oceanogr* **64**: 525–539.

Ohshima, K.I., Mizuta, G., Itoh, M., Fukamachi, Y., Watanabe, T., Nabae, Y., et al. (2001) Winter Oceanographic Conditions in the Southwestern Part of the Okhotsk Sea and Their Relation to Sea Ice. *J. Oceanogr.* **57**: 451–460.

Ohshima, K.I., Nakanowatari, T., Riser, S., Volkov, Y., and Wakatsuchi, M. (2014) Freshening and dense shelf water reduction in the Okhotsk Sea linked with sea ice decline. *Res. Oceans* **126**: 71–79.

Ohshima, K.I., Nihashi, S., Hashiya, E., and Watanabe, T. (2006) Interannual variability of sea ice area

in the Sea of Okhotsk: Importance of surface heat flux in fall. *Journal of the Meteorological Society of Japan Ser II* **84**: 907–919.

Ohshima, K.I., Riser, S.C., and Wakatsuchi, M. (2005) Mixed layer evolution in the Sea of Okhotsk observed with profiling floats and its relation to sea ice formation. *Geophys. Res. Lett.* **32**:.

Ohshima, K.I., Wakatsuchi, M., Fukamachi, Y., and Mizuta, G. (2002) Near-surface circulation and tidal currents of the Okhotsk Sea observed with satellite-tracked drifters. *J. Geophys. Res. Oceans* **107**: 16-1-16–18.

Ohtani, K. (1989) The role of the Sea of Okhotsk on the formation of the Oyashio Water. *Umi to Sora* **65**: 63–83.

Ohwada, M. (1956) Diatom communities in the Okhotsk Sea, principally on the west coast of Kamchatka, spring to summer 1955. *Journal of the Oceanographical Society of Japan* **13**: 29–34.

Okolodkov, Y.B. (1992) Cryopelagic flora of the Chukchi, East Siberian and Laptev seas. Citeseer, pp. 28–43.

Olaizola, M., Roche, J.L., Kolber, Z., and Falkowski, P.G. (1994) Non-photochemical fluorescence quenching and the diadinoxanthin cycle in a marine diatom. *Photosynth Res* **41**: 357–370.

Olsen, L.M., Laney, S.R., Duarte, P., Kauko, H.M., Fernández-Méndez, M., Mundy, C.J., et al. (2017) The seeding of ice algal blooms in Arctic pack ice: The multiyear ice seed repository hypothesis. *J Geophys Res Biogeosci* **122**: 2016JG003668.

Öquist, G. (1983) Effects of low temperature on photosynthesis. *Plant, Cell & Environ* **6**: 281–300.

Orlova, T.Yu., Selina, M.S., and Stonik, I.V. (2004) Species Structure of Plankton Microalgae on the Coast of the Sea of Okhotsk on Sakhalin Island. *Russ. J. Mar. Biol.* **30**: 77–86.

Owens, T.G., Falkowski, P.G., and Whitledge, T.E. (1980) Diel periodicity in cellular chlorophyll content in marine diatoms. *Mar Biol* **59**: 71–77.

Owens, T.G. and Falkowskit, P.G. (1982) Enzymatic degradation of chlorophyll *a* by marine phytoplankton in vitro. *Phytochem* **21**: 979–984.

Paasche, E. (1975) Growth of the plankton diatom *Thalassiosira nordenskioeldii* Cleve at low silicate concentrations. *J. Exp. Mar. Biol. Ecol.***18**: 173–183.

Park, J.S., Jung, S.W., Lee, S.D., Yun, S.M., and Lee, J.H. (2016) Species diversity of the genus *Thalassiosira* (Thalassiosirales, Bacillariophyta) in South Korea and its biogeographical distribution in the world. *Phycologia*.

Park, S., Jung, G., Hwang, Y., and Jin, E. (2010) Dynamic response of the transcriptome of a psychrophilic diatom, Chaetoceros neogracile, to high irradiance. *Planta* **231**: 349.

Peck, L.S., Convey, P., and Barnes, D.K.A. (2006) Environmental constraints on life histories in Antarctic ecosystems: tempos, timings and predictability. *Biological Reviews* **81**: 75–109.

Petrou, K., Hill, R., Brown, C.M., Campbell, D.A., Doblin, M.A., and Ralph, P.J. (2010) Rapid photoprotection in sea-ice diatoms from the East Antarctic pack ice. *Limnol Oceanogr* **55**: 1400–1407.

Petrou, K., Hill, R., Doblin, M.A., McMinn, A., Johnson, R., Wright, S.W., and Ralph, P.J. (2011) Photoprotection of sea-ice microalgal communities from the east Antarctic pack ice. *J. Phycol* **47**: 77–86.

Poulin, M. (1990) Sea ice diatoms (Bacillariophyceae) of the Canadian Arctic. I. The genus Stenoneis. *J. Phycol* **26**: 156–167.

Poulin, M., Daugbjerg, N., Gradinger, R., Ilyash, L., Ratkova, T., and Quillfeldt, C. von (2011) The pan-Arctic biodiversity of marine pelagic and sea-ice unicellular eukaryotes: a first-attempt assessment. *Mar Biodiv* **41**: 13–28.

Preller, R.H. and Hogan, P.J. (1998) Oceanography of the Sea of Okhotsk and the Japan/East Seas. In *The Sea*. John Wiley and Sons, Inc., pp. 429–481.

Qasim, S.Z., Bhattathiri, P.M.A., and Devassy, V.P. (1972) The influence of salinity on the rate of photosynthesis and abundance of some tropical phytoplankton. *Mar.Biol.* **12**: 200–206.

von Quillfeldt, C.H., Ambrose, W.G., and Clough, L.M. (2003) High number of diatom species in first-year ice from the Chukchi Sea. *Polar Biol* **26**: 806–818.

Rajanahally, M.A., Sim, D., Ryan, K.G., and Convey, P. (2014) Can bottom ice algae tolerate irradiance and temperature changes? *J. Exp. Mar. Biol. Ecol.***461**: 516–527.

Ralph, P.J., Ryan, K.G., Martin, A., and Fenton, G. (2007) Melting out of sea ice causes greater photosynthetic stress in algae than freezing in1. *J. Phycol* **43**: 948–956.

Raven, J.A., Evans, M.C.W., and Korb, R.E. (1999) The role of trace metals in photosynthetic electron transport in O2-evolving organisms. *Photosyn Res* **60**: 111–150.

Reeves, S., McMinn, A., and Martin, A. (2011) The effect of prolonged darkness on the growth, recovery and survival of Antarctic sea ice diatoms. *Polar Biol* **34**: 1019–1032.

Rijstenbil, J.W. (1987) Phytoplankton composition of stagnant and tidal ecosystems in relation to salinity, nutrients, light and turbulence. *Neth. J. Sea Res.* **21**: 113–123.

Rijstenbil, J.W. (2005) UV- and salinity-induced oxidative effects in the marine diatom Cylindrotheca closterium during simulated emersion. *Mar. Biol.* **147**: 1063–1073.

Rijstenbil, J.W., Wijnholds, J.A., and Sinke, J.J. (1989) Implications of salinity fluctuation for growth and nitrogen metabolism of the marine diatom *Ditylum brightwellii* in comparison with *Skeletonema costatum*. *Mar Biol* **101**: 131–141.

Roy, S., Llewellyn, C.A., Egeland, E.S., and Johnsen, G. (2011) Phytoplankton Pigments: Characterization, Chemotaxonomy and Applications in Oceanography, Cambridge University Press.

Różańska, M., Gosselin, M., Poulin, M., Wiktor, J.M., and Michel, C. (2009) Influence of environmental factors on the development of bottom ice protist communities during the winter–spring transition. *Mar. Ecol. Prog. Ser.* **386**: 43–59.

Ruban, A., Lavaud, J., Rousseau, B., Guglielmi, G., Horton, P., and Etienne, A.-L. (2004) The super-excess energy dissipation in diatom algae: comparative analysis with higher plants. *Photosyn Res* **82**: 165.

Ruban, A.V. (2017) Quantifying the efficiency of photoprotection. *Philos Trans R Soc Lond B Biol Sci* **372**: 20160393.

Ryan, K.G., Tay, M.L., Martin, A., McMinn, A., and Davy, S.K. (2011) Chlorophyll fluorescence imaging analysis of the responses of Antarctic bottom-ice algae to light and salinity during melting. *J. Exp. Mar. Biol. Ecol.* **399**: 156–161.

Sakamoto, K., Tsujino, H., Nishikawa, S., Nakano, H., and Motoi, T. (2010) Dynamics of the Coastal Oyashio and Its Seasonal Variation in a High-Resolution Western North Pacific Ocean Model. *J Phys Oceanogr* **40**: 1283–1301.

Sakshaug, E. (2004) Primary and Secondary Production in the Arctic Seas. In *The Organic Carbon Cycle in the Arctic Ocean*. Springer, Berlin, Heidelberg, pp. 57–81.

Schumann, A., Goss, R., Jakob, T., and Wilhelm, C. (2007) Investigation of the quenching efficiency of diatoxanthin in cells of *Phaeodactylum tricornutum* (Bacillariophyceae) with different pool sizes of xanthophyll cycle pigments. *Phycologia* **46**: 113–117.

Sea of Okhotsk | Russian Far East | Heritage Expeditions.

Selz, V., Laney, S., Arnsten, A.E., Lewis, K.M., Lowry, K.E., Joy-Warren, H.L., et al. (2018) Ice algal communities in the Chukchi and Beaufort Seas in spring and early summer: Composition, distribution, and coupling with phytoplankton assemblages. *Limnol. Oceanogr.* **63**: 1109–1133.

Shcherbina, A.Y., Talley, L.D., and Rudnick, D.L. (2003) Direct observations of North Pacific ventilation: Brine rejection in the Okhotsk Sea. *Science* **302**: 1952–1955.

Shibanuma, S., Kajihara, M., and Miyake, H. (1995) Water characteristics in Lake Saroma. *Aquacultural Oceanography* **59**: 1–9.

Shikanai, T. (2014) Central role of cyclic electron transport around photosystem I in the regulation of photosynthesis. *Curr. Opin. Biotechnol.* **26**: 25–30.

Shinada, A., Shiga, N., and Ban, S. (1999) Structure and magnitude of diatom spring bloom in Funka Bay, southwestern Hokkaido, Japan, as influenced by the intrusion of Coastal Oyashio Water. *Plankton Benthos Res* **46**: 22–29.

Shiomoto, A. (1997) Size-Fractionated Chlorophyll a Concentration and Primary Production in the Okhotsk Sea in October and November 1993, with Special Reference to the Influence of Dichothermal Water. *J. Oceanogr.* **53**: 601–610.

Shiomoto, A., Asakuma, K., Hoon, H.-D., Sakaguchi, K., and Maekawa, K. (2012) An early spring bloom of large diatoms in the ice-covered Saroma-ko Lagoon, Hokkaido, Japan. J. Mar. Biolog. Assoc. U.K. 92: 29–37.

Shuntov, V.P. (2001) New data about seasonal distribution and migrations of whales and dolphins in the Sea of Okhotsk. *Russ. J. Mar. Biol.* **27**: 201–208.

Simizu, D. and Ohshima, K.I. (2006) A model simulation on the circulation in the Sea of Okhotsk and the East Sakhalin Current. *J. Geophys. Res. Oceans* **111**:.

Smayda, T.J. (1969) Experimental observations on the influence of temperature, light, and salinity on cell division of the marine diatom, Detonula confervacea (Cleve) Gran. *J Phycol* **5**: 150–157.

Smetacek, V. and Nicol, S. (2005) Polar ocean ecosystems in a changing world. *Nature* **437**: 362–368.

Smetacek, V.S. (1985) Role of sinking in diatom life-history cycles: ecological, evolutionary and geological significance. *Mar Biol* **84**: 239–251.

Smirnova, L.T. (1959) Phytoplankton in the Okhotsk Sea and Kuril Island region. *Trudy Inst Okeanol Akad Nauk SSSR* 3–51.

Sorokin, Y.I. and Sorokin, P.Y. (2002) Microplankton and primary production in the Sea of Okhotsk in summer 1994. *J Plankton Res* **24**: 453–470.

Sorokin, Y.I. and Sorokin, P.Y. (1999) Production in the Sea of Okhotsk. *J Plankton Res* **21**: 201–230.

Stroeve, J. and Notz, D. (2018) Changing state of Arctic sea ice across all seasons. *Environ Res Lett* **13**: 103001.

Strzepek, R.F. and Harrison, P.J. (2004) Photosynthetic architecture differs in coastal and oceanic diatoms. *Nature* **431**: 689–692.

Sugie, K., Nishioka, J., Kuma, K., Volkov, Y.N., and Nakatsuka, T. (2013) Availability of particulate Fe to phytoplankton in the Sea of Okhotsk. *Mar Chem* **152**: 20–31.

Sugimoto, K., Fukuda, H., Baki, M.A., and Koike, I. (2007) Bacterial contributions to formation of transparent exopolymer particles (TEP) and seasonal trends in coastal waters of Sagami Bay, Japan. *Aquat Microb Ecol* **46**: 31–41.

Suzuki, K., Hattori-Saito, A., Sekiguchi, Y., Nishioka, J., Shigemitsu, M., Isada, T., et al. (2014) Spatial variability in iron nutritional status of large diatoms in the Sea of Okhotsk with special reference to the Amur River discharge. *Biogeosciences* **11**: 2503–2517.

Suzuki, K., Kamimura, A., and Hooker, S.B. (2015) Rapid and highly sensitive analysis of chlorophylls and carotenoids from marine phytoplankton using ultra-high performance liquid chromatography (UHPLC) with the first derivative spectrum chromatogram (FDSC) technique. *Mar Chem* **176**: 96–109.

Suzuki, K., Kuwata, A., Yoshie, N., Shibata, A., Kawanobe, K., and Saito, H. (2011) Population dynamics of phytoplankton, heterotrophic bacteria, and viruses during the spring bloom in the western subarctic Pacific. *Deep Sea Res. Part I Oceanogr. Res. Pap.* **58**: 575–589.

Szymanski, A. and Gradinger, R. (2016) The diversity, abundance and fate of ice algae and phytoplankton in the Bering Sea. *Polar Biol* **39**: 309–325.

Tachibana, Y., Oshima, K., and Ogi, M. (2008) Seasonal and interannual variations of Amur River discharge and their relationships to large-scale atmospheric patterns and moisture fluxes. *J. Geophys. Res. Atmos* **113**:.

Taguchi, S., Satoh, F., Hamaoka, S., Ikeda, M., Ishikawa, M., and Shirasawa, K. (2000) Effect of ice algal community on the increase of chlorophyll a concentration during spring in coastal water of the Sea of Okhotsk. *Polar Sci* **13**: 1–14.

Taguchi, S., Smith, R.E.H., and Shirasawa, K. (1997) Effect of silicate enrichment on ice algae at low salinity in Saroma-ko Lagoon, Hokkaido, Japan. *J Mar Syst.* **11**: 45–52.

Takahashi, K. (1998) The Bering and Okhotsk Seas: modern and past paleoceanographic changes and gateway impact. *J. Asian Earth Sci.* **16**: 49–58.

Takeuchi, T. and Fujiyoshi, Y. (1989) Characteristics of the winter water currents under sea ice cover in Saroma Lagoon. *Coastal Engineering Committee* **36**: 834–838.

Takizawa, T. (1982) Characteristics of the Sôya Warm Current in the Okhotsk Sea. *Journal of the Oceanographical Society of Japan* **38**: 281–292.

Talley, L.D. (1991) An Okhotsk Sea water anomaly: implications for ventilation in the North Pacific. *Deep Sea Res. Part I Oceanogr. Res. Pap.* **38**: S171–S190.

Talley, L.D. and Nagata, Y. (1995) The Okhotsk Sea and Oyashio Region, Sidney, British Columbia: North Pacific Marine Science Organization (PICES).

Tedesco, L., Vichi, M., and Scoccimarro, E. (2019) Sea-ice algal phenology in a warmer Arctic. *Sci Adv* **5**: eaav4830.

Tedesco, L., Vichi, M., and Thomas, D.N. (2012) Process studies on the ecological coupling between sea ice algae and phytoplankton. *Ecol Model* **226**: 120–138.

Thomas, D.N. and Dieckmann, G.S. (2002) Antarctic Sea Ice--a Habitat for Extremophiles. *Science* **295**: 641–644.

Thomas, M.K., Kremer, C.T., Klausmeier, C.A., and Litchman, E. (2012) A global pattern of thermal adaptation in marine phytoplankton. *Science* **338**: 1085–1088.

Tomas, C.R. (1997) Identifying Marine Phytoplankton, Elsevier.

Torstensson, A., Hedblom, M., Andersson, J., Andersson, M.X., and Wulff, A. (2013) Synergism between elevated pCO_2 and temperature on the Antarctic sea ice diatom *Nitzschia lecointei*. *Biogeosciences* **10**: 6391–6401.

Toyota, T., Kawamura, T., Ohshima, K.I., Shimoda, H., and Wakatsuchi, M. (2004) Thickness distribution, texture and stratigraphy, and a simple probabilistic model for dynamical thickening of sea ice in the southern Sea of Okhotsk. *J. Geophys. Res. Oceans* **109**:.

Toyota, T., Takatsuji, S., Tateyama, K., Naoki, K., and Ohshima, K.I. (2007) Properties of sea ice and overlying snow in the Southern Sea of Okhotsk. *J Oceanogr* **63**: 393–411.

Uehara, H., Kruts, A.A., Mitsudera, H., Nakamura, T., Volkov, Y.N., and Wakatsuchi, M. (2012) Interannual variations of Dense Shelf Water in the Sea of Okhotsk affected by oceanic freshwater transport in the North Pacific subpolar gyre. *AGU Fall Meeting Abstracts* **33**: OS33C-1836.

Underwood, G.J.C., Phillips, J., and Saunders, K. (1998) Distribution of estuarine benthic diatom species along salinity and nutrient gradients. *Eur. J. Phycol* **33**: 173–183.

Vancoppenolle, M., Goosse, H., Montety, A. de, Fichefet, T., Tremblay, B., and Tison, J.-L. (2010) Modeling brine and nutrient dynamics in Antarctic sea ice: The case of dissolved silica. *J. Geophys. Res. Oceans* **115**:.

Vancoppenolle, M., Meiners, K.M., Michel, C., Bopp, L., Brabant, F., Carnat, G., et al. (2013) Role of sea ice in global biogeochemical cycles: emerging views and challenges. *Quaternary Science Reviews* **79**: 207–230.

Vinyard, D.J., Ananyev, G.M., and Charles Dismukes, G. (2013) Photosystem II: The Reaction Center of Oxygenic Photosynthesis. *Annu. Rev. Biochem.* **82**: 577–606.

Wagner, H., Jakob, T., Lavaud, J., and Wilhelm, C. (2016) Photosystem II cycle activity and alternative electron transport in the diatom Phaeodactylum tricornutum under dynamic light conditions and nitrogen limitation. *Photosyn Res* **128**: 151–161.

Waite, A.M., Thompson, P.A., and Harrison, P.J. (1992) Does energy control the sinking rates of marine diatoms? *Limnol. Oceanogr.* **37**: 468–477.

Wells, L.E. and Deming, J.W. (2006) Modelled and measured dynamics of viruses in Arctic winter sea-ice brines. *Environ. Microbiol.* **8**: 1115–1121.

Wilhelm, C., Jungandreas, A., Jakob, T., and Goss, R. (2014) Light acclimation in diatoms: From phenomenology to mechanisms. *Mar Genom* **16**: 5–15.

Wongpan, P., Hughes, K.G., Langhorne, P.J., and Smith, I.J. (2018) Brine Convection, Temperature Fluctuations, and Permeability in Winter Antarctic Land-Fast Sea Ice. *J. Geophys. Res. Oceans* **123**: *216–230*.

Yan, D., Endo, H., and Suzuki, K. (2019) Increased temperature benefits growth and photosynthetic performance of the sea ice diatom *Nitzschia* cf. *neglecta* (Bacillariophyceae) isolated from Saroma Lagoon, Hokkaido, Japan. *J. Phycol* **55**: 700–713.

Yang, J. and Honjo, S. (1996) Modeling the near-freezing dichothermal layer in the Sea of Okhotsk and its interannual variations. *J. Geophys. Res. Oceans* **101**: 16421–16433.

Yoshida, K., Endo, H., Lawrenz, E., Isada, T., Hooker, S.B., Prášil, O., and Suzuki, K. (2018) Community composition and photophysiology of phytoplankton assemblages in coastal Oyashio waters of the western North Pacific during early spring. *Estuar. Coast. Shelf Sci.* **212**: 80–94.

Yoshida, K., Seger, A., Kennedy, F., McMinn, A., and Suzuki, K. (2020) Freezing, melting and light stress on the photophysiology of ice algae: ex situ incubation of the ice algal diatom *Fragilariopsis cylindrus* (Bacillariophyceae) using an ice tank. *J. Phycol* (in press)

Young, J.N., Goldman, J.A.L., Kranz, S.A., Tortell, P.D., and Morel, F.M.M. (2015) Slow carboxylation of Rubisco constrains the rate of carbon fixation during Antarctic phytoplankton blooms. *New Phytol* **205**: 172–181.

Zhang, Chang.I., Radchenko, V., Sugimoto, T., and Hyun, S.M. (2006) Interdisciplinary physical and biological processes of the Sea of Okhotsk and the Japan/East Sea. In *The Global Coastal Ocean: Interdisciplinary Regional Studies and Syntheses, Pan-regional syntheses and the Coasts of North and South America and Asia*. Harvard University Press.

Zhang, Q., Gradinger, R.R., and Spindler, M. (1999) Experimental study on the effect of salinity on growth rates of Arctic-sea-ice algae from the Greenland Sea.

Response to comments

●実験詳細について

Chapter 2

１．Chapter2 のオホーツク海の実験について。サンプルを現場で採取してから持ち帰るまでに−5 度で保管している。この保存期間中は海氷から海水も抜けて、−5 度の低温にさらされている。保管中にダメージがないのか？そのダメージの大きさが Centric と pennate で違いはないのか？実験設定の保管条件の妥当性について教えて欲しい。

About the Okhotsk Sea experiment in Chapter 2. The samples are stored at -5 degrees from the sampling site until experiment. At this storage condition, the sea ice was dried and is exposed to low temperatures -5 degrees. Is there no damage on diatom at -5 degrees and dry condition during storage? Is there no difference in the magnitude of the damage between Centric and pennate? Please explain about the validity of storage conditions.

For the storage of sea ice samples with ice algae, the temperature used for storage cannot be too high or too low. High temperatures may result in sea ice to melt and more biological activities of all microorganisms inside the sea ice. Biological activities are suppressed under very low temperatures, while this may also cause more cell death. Because lower temperatures result in significant decreases in the brine volume and thus increases in brine salinity. Some organisms will die due to the very high brine salinity. The temperature of –5 °C was used for two reasons. The first reason is according to phase equations of sea ice, the threshold for fluid permeability in sea ice occurs when the porosity approaches 5%, which occurs at a temperature of about –5 °C for sea ice with a bulk salinity of 5. The other reason is it was similar to the ice temperature at the top part of the sea ice measured in the field. So ice algal cells were expected to survive at such a temperature. In my experience, pennate diatoms are more tolerant to storage in the dark. There would be a larger difference in the number of dead cells between the centric and pennate diatoms if the period of storage becomes longer.

２．*rcbL* の測定は pennate と centric を分けて測定していないと思うが正しいか？rcbL の増加は pennate と centric を分けて確認はしていないが、*rcbL* の増加が、融解期の *Thalassiosira* の RubisCO の合成に伴う osmoprotection と解釈できる理由はなぜ？pennate も osmoprotection 機能を働かせていたとは考えないのか？

I think that *rcbL* is not measured separately for pennate and centric. Is this correct?

Although the increase in rcbL has not been confirmed separately for pennate and centric, why is it possible to interpret the increase in rcbL as osmoprotection response with the synthesis of RubisCO in *Thalassiosira* during the melting phase? Don't you think that pennate also worked the osmoprotection function?

Yes, *rbcL* was not separately measured. As you kindly pointed out, pennate diatoms also worked for osmoprotection. While according the community composition data, most of the

diatoms in the water samples were *Thalassiosira*. So the physiological data mainly reflects the physiological status of *Thalassiosira*.

3.５０マイクロモル photons m-2S-1 は現場の光条件と比べてどの程どの光量なのか？

How much light is 50 micromole photons $m^{-2}s^{-1}$ compared to the light conditions at the site?

I'm sorry that I don't have the light condition data in the field. In my experience, 50 μmol photons m^{-2} s^{-1} is a typical low light condition for diatom cultures.

4. Fig. 2-2 では Centric の dead cell %は、sea ice melt period より non-sea-ice period の方が３倍大きい（0.5→1.68）。なぜ増加したのか？

In Fig. 2-2, the centric dead cell% is 3 times larger in the non-sea-ice period than in the sea ice melt period (0.5→1.68). Why did it increase?

I'm not sure about this. One possibility is that some of the centric diatoms became senescent during the incubation. And their lives have come to an end.

５. Light microscopy analysis (LM)と metabarcording を比較すると、例えば *Thalassiosira* 種の優先率は LM で 10%と metabarcording で 0.3%など大きな違いがある。この違いはどのような要因によって生じているのか？

Comparing light microscopy analysis and metabarcording, there is a big difference in species abundant, for example, that the priority of *Thalassiosira* species is 10% in LM and 0.3% in metabarcording. What factors make this difference?

There are many processes until we get the final result of the metabarcoding. And all of the processes included may introduce some biases into the final results. The mismatch between metabarcoding and LM could be resulted from the following reasons. (a) We used the same pair of primer to amplify the 18S for all species inside the sample. The amplification efficiency of this pair primer for different species is different. This means the 18S of some species could be easily amplified while others cannot. (b) The number of the 18S gene copy in each species is different. Some species have more 18S while others have fewer 18S. (c) Some species are not included in the 18S database. And some of 18S in the database are wrongly annotated. For (a) and (b), the species with a larger copy number of the 18S gene and those with the 18S that are more easily amplified during the PCR amplification would appear more abundant in the final result.

６． なぜ pennate は ice melt の培地でも増殖速度が 0.05 と、極域のほかの報告と比べて低いのか？何かオホーツク海特有の条件があるのか？

After complete ice melt, pennate diatom has only very low growth rate as 0.05, this rate is significantly lower than reported polar region pennate diatom in same condition. What is the reason for the Okhotsk pennate diatom cannot grow in SW?

Pennate diatoms with large cell sizes such as *Navicula* and *Nitzschia* usually grew slowly. And their ecology is not well-known. The growth rate of diatoms is largely affected by temperature and light intensity. In this study, we used a low temperature and a low light intensity for culture. So the growth is limited by the low temperature and low light conditions. And the acclimation of pennate diatoms to salinity changes might need more time and they are still on the way of recovering.

７．In Fig 2.10, *rcbL* は実験開始後 10h まで急上昇し、その後減少する。Salinity は 10h までは 32.5-31 程度だが、その後 30h までに急減少する。もし *rcbL* の増加が osmotic stress への対応なら、より後半で増加しても良いと思うが、データはそうなっていない。なぜ？

In Fig 2.10, *rcbL* increased from 0 to 10 hours and then decreases. From 0 to 10 hours, salinity is around 32.5-31 until 10h, but then sharply decreases by 30h (decreased sharply in 10-25h). If the increase in *rcbL* responds to osmotic stress, it may increase in the latter half (from 10-25h), but the data do not. why?

Because changing in the environmental factors is a kind of a shock. There is usually a lag phase before the cells can grow normally after they are exposed to such an environmental shock. During this period, they will adjust their metabolism to acclimate to the changes. Therefore, the first a few hours after being exposed is usually very important. And the salinity shown in the figure is the salinity of the seawater in the beakers, which has mixed before sampling. When sea ice melts, the changes in the salinity of the microenvironment surrounding algal cells could be larger than the apparent salinity changes of the seawater in the beakers. Because sea ice itself has a very low salinity and the flushing of the melted sea ice will significantly decrease the salinity surrounding algal cells.

Chapter 3

1.サロマ湖の実験では光と温度に対しての耐性を調べて、pennate には photoprotection 機能が働き、高水温での増殖を確認しているが、海氷融解を想定しているのであれば、塩分も複合的に試験する必要がある。しかし塩分は natural sweater の F2 培地。この点、Chapter 2 と複合して考えた場合、pennate には photoprotection や水温耐性に対する塩分の影響に関してどのような情報が得られたと考えられるのか？

In the experiment of Lake Saroma, you used natural seawater for F/2 medium. The influence to light and temperature was investigated, and you confirmed that the photoprotection function works on the pennate and they grew at high water temperature. But you have not check salinity influence in Chapter 3 experiment. If sea ice melting is assumed to chapter 3 experiment condition, do you think you could be obtained same result on photoprotection and water temperature tolerance in pennate?

In ecology, the tolerance of a given environmental factor will decrease if the organism is

suffering from stress caused by other environmental factors. So if the salinity change is added, I think the algal cells need a longer time for the photoacclimation. Cells under such conditions will be damaged more easily.

２．４５０マイクロモル photons m^{-2} s^{-1} は現場の光条件と比べてどの程どの光量なのか？Chapter 3 の実験では 50 マイクロモル photons m^{-2} s^{-1} なのはなぜ？

How much light is 450 micromole photons m^{-2} s^{-1} compared to the light conditions at the site? Why the light is 50 micromole photons m^{-2} s^{-1} in Okhotsk expt.

In the experiment, we wanted to use a light intensity that is high enough to cause photoinhibition. The intensity of 450 μmol photons m^{-2} s^{-1} was the highest intensity we can get. And it was enough to cause photoinhibition according to the results.

３．Fig. 3.6. Expose 実験の 2 度の条件では、PPC は速やかに減少する。10 度だと PPC は高いままで維持。実際の現場での融解期の水温を考えると photoprotection 機能は働かないのでは？

Fig. 3.6. Temperature was likely to be the main cause of variations in cellular pigment content with changing light conditions. Under the 2 degree conditions of the Expose experiment, PPC decreases rapidly. At 10 degrees, PPC remains high. Please explain again what PPC decreasing mean, how relevant to Ddx-Dtx cycle?

The photoprotection function may not work considering the actual water temperature during the melting period. How do you think?

PPC decreased in the context that all pigments decreased. The decrease in the total amount of pigments could also be an attempt to fight against photodamage. The increase of NPQ during the exposure suggest that algal cells succeeded at the lower temperature in photoprotection though there was a loss of PPC.

●全般について

1.本研究では Chapter 2 と Chapter 3 を統合すると、Centric は osmotic protection が確認され Pennate では photoprotection と温度耐性があり、osmotic 耐性は低いと確認されたと考えられる。Seeding effect を考える際には、Centric が光や水温への耐性をもつのかは確認されているのか？Chapter 2 の PPC の色素の結果から言えることを説明してください。

Results from Chapter 2 and Chapter 3, Centric was confirmed to have osmotic protection, and Pennate was confirmed to have photoprotective function and can grow in higher temperature. But pennate do not have osmotic protection function.

When considering the seeding effect, you need to confirm that Centric have photoprotection and water temperature tolerance. Did you have the data for this point, could you explain

again? Could you explain again about your result of PPC (photo protective carotenoids) pigment data from chapter 2 experiment (Fig. 2.8)? (Ddx-Dtx cycle work?)

It is very likely that centrics especially *Thalassiosira* also have effective photoprotective strategies. Because they can form bloom in open waters during the spring time. At that time the light intensity in the surface layer can reach 2000 µmol photons m^{-2} s^{-1} at noon. If they don't have effective photoprotective strategies they cannot bloom under such light conditions. Fig 2.8 shows that PPC was not very abundant in algal cells during the incubation. This is because the light used for the incubation was only 50 µmol photons m^{-2} s^{-1}. This is a relatively low light condition for the growth of most phytoplankton and won't cause photoinhibition.

2. Seeding effect を考える際に、光、水温、塩分への耐性以外に、浮力を持つ必要がある。植物プランクトンの浮力は、形態学的な形状、栄養状態、生理状態によって変わってくることが知られているが、融解後のアイスアルジーについての浮力に関してはどのような情報を持っていますか？

When considering the seeding effect, it is necessary to have buoyancy in addition to protection from light, water temperature, and salt damage. It is known that the buoyancy of phytoplankton varies depending on its morphological shape, nutrient condition and physiological condition. What information do you have regarding buoyancy of ice algae after ice melt for centric and pennate diatoms?

The seeding of ice algae is strongly dependent on the survival and sedimentation of the algae cells. Your study show *Thalassiosira* can physiologically survive after ice melt but not show that they can avoid sedimentation. Do you have some information that *Thalassiosira* can avoid sedimentation? And that reason?

Thalassiosira is a common taxon of phytoplankton so theoretically they should always be in the water column. Cells sink when they become senescent. *Thalassiosira* cells have a morphology that can keep themselves staying in the water column. They are always in chains and the material used as storage is oil. Those characteristics increase the floating capacity of algal cells. The sedimentation is also adjusted by physiology that is mentioned in the discussion of Chapter2.

3. また今後、Seeding effect の実態を明らかにしていくためにはどのような研究が必要と考えているか？

I would like to ask you about your future study. Addition to this thesis research, what kind of research do you need for clarifying the actual state of the seeding effect of ice algae for spring phytoplankton bloom in natural condition?

I have isolated some representative centric diatom species living in the Okhotsk sea ice. I'm considering using those isolates to do some incubation experiments. I would like to see the growth and photophysiological changes under changing salinities. And also I want to know

the bloom in the field. More sea ice and seawater samples from the Sea of the Okhotsk would be needed in order to understand the changes in the composition of the communities.

4. なぜアイスアルジーの主な優占種は一般的に pannate なのか？なぜオホーツクの海氷内には Centric が多かったのか？Yan さんの研究からの示唆は？

Previous studies indicated that, Pennate diatoms with large cell size usually contribute more to ice algal communities than centric diatom. Why can be Pennate the main dominant species of ice algae? Why was the centric main dominant species of your ice? If Pennate is likely to remain on sea ice, is it necessary to tolerate the high salinity of brine? What are your suggestions from Yan's research?

Diatoms account for about 50 to 75% of all protist species occurring with ice. Currently 731 species have been observed in Arctic sea ice. Most studies used light microscope to quantify ice algae. Diatoms are easy to see and identify under a light microscope. And as shown in this study, if cells suffered from melting stress, they might have already exploded before they can be identified. Diatoms have silica cell walls that provide protection against physical damage they may encounter in sea ice. Most cells live and grow at the bottom of sea ice where the living conditions are relatively milder than the upper parts. Benthic pennate diatoms like environments that provide them a surface to glide on. Sea ice is a good habitat for those pennate diatoms. In addition, pennate diatoms always secrete some materials in order to live better in sea ice, such as polysaccharide-rich extracellular polymeric substances (EPS) and anti-freeze proteins. When sea ice melts, most of the pennate diatoms sink quickly out of the low salinity layer beneath the melting sea ice. And they will recover soon where there is no salt stress and live and grow at the bottom until they are incorporated into sea ice again. Vegetative growth of them is restricted to a short period, but benthic survival of ensures that those species will continue in an area.

Thalassiosira is a common and important marine planktonic diatom in the Arctic and subarctic. They are also commonly found in the Arctic sea ice, and form dense blooms in water. In the Sea of Okhotsk, *Thalassiosira* usually forms bloom after ice retreats when the water temperature is still very low in coastal waters. *Thalassiosira* lives as part of the planktonic community in all seasons throughout the year. So they are always found in seawater, though they are not abundant all the time. *Thalassiosira* in sea ice possibly come from the northern shelf waters near Russia and the eastern coastal waters off Sakhalin. Because the cell size of *Thalassiosira* we found in the Sea of Okhotsk is large, they need more nutrients for growth. So theoretically they should prefer the nutrient-rich coastal waters. And as ice algae, low temperatures are needed in order to survive so they can survive in the cold waters in the northern part. Another origin is the sediment. Because some *Thalassiosira* can form resting spores and stay in sediments until being swirled up to germinate. The cells are incorporated into sea ice through underwater interaction with frazil ice and/or flooding of sea ice floes.

5. オホーツク海のアイスアルジーの種類に関してどの程度情報をもっているか？毎年同じような種類が出現するのか？エリアによる違いなどどの程度わかっているのか？

How much information do you have about the types of ice algae in the Sea of Okhotsk? Is similar species appear every year? Is the species differences between areas?

The ice algae data of 2019 has been fully analysed. I also took DNA samples of a sea ice sample taken in 2018 and 2019 but I haven't analyzed it yet. I checked the ice algal community of one station taken during the *Soya* cruise of 2018 under LM. The species found were a mixture of centrics and pennates. Pennates had larger abundance and was more diverse. I couldn't identify most of them due to a lack of knowledge. I think most of the species occurred in both years. There is a difference in the communities found in different regions according to the results of statistics. While the ice samples were taken within a very small area and the number of the sample is too few. So I cannot say too much about it.

1) Definition of ice algae

In the text, there appears various expressions regarding ice algae, such as “ice algal diatoms”, “ice diatoms”, and “ice algae” (P18-19). Are there any differences among them? Or do they mean the same thing? If they are used to mean the same thing, it would be more readable to unify the terminology.

“Ice algal diatoms” and “ice diatoms” are the same. “Ice algal diatoms” has been altered to “ice diatoms”. Algae contains various types of organisms and diatoms are only part of them.

2) The mechanism of the seeding effect

I think the seeding effect is one of the key words in this study. But I could not understand well what is really happening during the seeding. To my understanding, the word “seeding” is originally used for fine particles to a solution to induce crystallization. Such a tiny particle acts as a nucleus upon which the new crystal grows. In the case of this study, tiny ice algae can act as nuclei for the growth of phytoplankton. Is that right? If so, I would like to know how ice algae contribute to the growth of phytoplankton.

The cells in the phytoplankton bloom come from sea ice. They were ice algae and then they become phytoplankton. The growth of the phytoplankton means they increase the cell number in the population. In other words, the phytoplankton bloom is seeded from ice algae. Ice algae can act as seeding populations.

3) The relevance of Chapter 3 to the whole scenario of this study

If I understand correctly, the pennate diatoms do not contribute to the spring bloom in the Sea of Okhotsk. On the other hand, the focus of study in Chapter 3 seem to be put on the properties of pennate diatoms. Can I think the results obtained in this chapter, such as the tolerance to higher temperature, are applicable to the centric diatoms? I guess the study in this chapter might have done independently from Chapter 2. Even so, it might be desirable to mention the relevance to the whole scenario of this study.

It is very likely that centrics especially *Thalassiosira* can tolerate higher temperatures and that they have effective photoprotective strategies. Because they can form bloom in open waters during the spring time. At that time the light intensity in the surface layer can reach 2000 μmol photons m^{-2} s^{-1} at noon.

4) The applicability of the results to other ice-covered seas in the world

It is stated in Chapter 2 that the ice algal community in the Sea of Okhotsk is unique in that the centric diatoms like *Thalassiosira* are abundant in contrast with other ice-covered seas and they play an important role in the spring bloom due to its wide tolerance to the change in salinity. It is interesting. But it was also pointed out by other studies that abundant iron entrapped in sea ice may contribute to the spring bloom significantly when released to the ocean in the melting season. My questions are:

+ why *Thalassiosira* is abundant in the Sea of Okhotsk? Where is the origin?

+ which do you think is more important to the spring bloom, *Thalassiosira* or iron?

+ is it possible to separate these effects by comparing the results obtained in the other ice-covered seas? Although *Thalassiosira* is not so abundant in the other ice-covered seas as in the Sea of Okhotsk, the abundance of iron within sea ice seems to be common in the ice-covered seas.

Thalassiosira is a common and important marine planktonic diatom in the Arctic and subarctic. They are also commonly found in the Arctic sea ice, and form dense blooms in water. In the Sea of Okhotsk, *Thalassiosira* usually forms bloom after ice retreats when the water temperature is still very low in coastal waters. *Thalassiosira* lives as part of the planktonic community in all seasons throughout the year. So they are always found in seawater, though they are not abundant all the time. *Thalassiosira* in sea ice possibly come from the northern shelf waters near Russia and the eastern coastal waters off Sakhalin. Because the cell size of *Thalassiosira* we found in the Sea of Okhotsk is large, they need more nutrients for growth. So theoretically they should prefer the nutrient-rich coastal waters. And as ice algae, low temperatures are needed in order to survive so they can survive in the cold waters in the northern part. Another origin is the sediment. Because some *Thalassiosira* can form resting spores and stay in sediments until being swirled up to germinate. The cells are incorporated into sea ice through underwater interaction with frazil ice and/or flooding of sea ice floes.

Usually we don't compare organisms and chemical parameters. Which one is more important depends on the species that form the bloom. *Thalassiosira* that form bloom in the Sea of Okhotsk are usually those taxa with large cell sizes. A large amount of nutrients would thus be needed to support the growth of such diatoms. And for the bloom of those species, I think high iron concentrations should be necessary. In this situation *Thalassiosira* and iron would be equally important for the bloom. If the *Thalassiosira* species that form the bloom doesn't need much iron to support those growth, e.g. very small cells, then iron would not be that important.

It is possible to separate the effect of *Thalassiosira* and iron by comparing the result of the natural community with or without the addition of inhibitors that can inhibit the use of iron of diatom cells and see what species will bloom.

5) What kind of seawater did you use? I mean, did you filter out the biological activities from the seawater? I ask you because it might be important for your experiment.

The seawater used was the sea water collected from the surface of the Sea of Okhotsk during the *Soya* cruise. The seawater was filtered through 0.7 μm pore size filters and sterilized at 121 °C for 20 min before use. So there was no living organisms inside the seawater.

"Growth rates" (P58L20)

I understand growth rates are defined by the increase in number, not by size.

Is that correct? If so, why cell size does not matter?

For microorganisms the growth rate is calculated as the growth rate of the population that is consisted of this organism. The cell size of the diatoms and other phytoplankton is usually very small and cell sizes usually won't change much during their whole life. Especially for diatoms because their cell wall is made of Si and the cell size remains the same if they don't undergo reproductive processes.

"We believe that these findings can apply to some other species in Saroma Lagoon"

(P70L4 from bottom)

Why do you think so? Do you have any evidence about this?

Saroma Lagoon is very shallow and light can penetrate to the bottom part of the lagoon. So there should be many diatoms living on the sediments of this lagoon. Those may have something in common that they may have similar living strategies.